Concealed Weapon Detection

A microwave imaging approach

MASTER OF SCIENCE THESIS

Leonardo Carrer

Thesis Supervisor: Prof. Dsc. A. G. Yarovoy

May 29, 2012

Delft University of Technology

Faculty of Electrical Engineering, Mathematics and Computer Science (EEMCS)

The undersigned hereby certify that they have read and recommend to the Faculty of Electrical Engineering, Mathematics and Computer Science (EEMCS) for acceptance a thesis entitled '**Concealed Weapon Detection: A microwave imaging approach**' by **Leonardo Carrer** in partial fulllment of the requirements for the degree of Master of Science in Electrical Engineering: Telecommunications Track

Dated: May 29, 2010

Commitee members:

Prof. Dsc. A. Yarovoy

Dr. Ir. B. J. Kooij

Dr. Ir. R. F. Remis

Dr. T. Sakamoto

Abstract

In the last years, there has been a renewed interest in security applications designed to detect potentially dangerous concealed object carried by an individual. In particular automatic detection and classification of concealed weapons is a fundamental part of every surveillance system.

Until now merely all the research in image processing for Concealed Weapon Detection has been focused on millimeter wave imagers and X-ray imagers with very little work done in the microwave range.

The main objective of this thesis is to develop robust novel image processing algorithms for detection and classification of concealed weapon.

In particular, the developed algorithms are specifically tailored to work with microwave radar images. The algorithms shall also perform efficiently with a low false alarm rate in a reduced contrast envinroment such as the one of microwave images.

Depolarization Analysis and SIFT Analysis which are two novel algorithms for concealed weapon detection and classification in the field of 3D high resolution microwave radar imaging are presented in this thesis research project.

Keywords– Concealed Weapon Detection, 3D high-resolution microwave images, Depolarization, SIFT, image processing, PCA, Phase Symmetry

Acknowledgments

In this page I would like to say thank you to a number of people who supported me while preparing this Thesis work.

First I want to thank my Supervisor Prof. A. Yarovoy for the nice advices he has given me regarding my work and for the freedom that he allowed me to have in developing it. Secondly, I'm extremely grateful to P.Aubry for its invaluable help in the measurement campaign and for his patience in answering all my technical questions during this months.

Even if I am not going to list all of them in this little page, I would like to to say thank you (grazieee!) to all my beloved friends in Rome for supporting me throughout the years in good and bad times and without whom I would never been able to arrive at this point. I would also like to say thanks to all my friends here in Delft for the amazing time I have spent with them which made my life happier. A special thanks goes to Gustavo and Mark for reading and correcting my Thesis.

Finally I would like to thank my family for their unconditional love and for supporting me in all my decisions.

Leonardo Carrer

Delft, The Netherlands

16/05/2012

Contents

List of Figures

List of Tables

1. Introduction

"*The tongue can conceal the truth, but the eyes never!*"

The Master and Margarita,M.Bulgakov

1.1. Overview

In the last fifteen years, and in particular after 11th Sept. 2001, there has been a renewed interest in security applications designed to detect potentially dangerous concealed objects. It is a common experience in everyone's life to go through a portal type metal detector at the airport or when entering sensitive buildings. Despite the fact that portal type metal detectors screening approach is successful and widely used around the world it has some major flaws and in particular it cannot detect dielectric weapons (e.g. ceramic knifes) , explosives, inflammables and it may fail to detect very small items such as rounds of ammunition [1] . On top of that, it cannot discriminate between innocuous items (e.g. keys) and dangerous objects. Furthermore, in order to be screened, people have to go one by one through a gate, creating longer queues in places such as airports. This also implies that it is not possible to perform security screenings in crowded situation such as public gatherings. Nevertheless a wide area metal detector is currently being developed which allows to locate concealed metal weapons in a crowd [2] .In order to overcome

these limitations, a wide choice of valid concealed weapon detection systems(CWDS) alternatives to metal detectors have been developed in the last twenty years. CWDS can be classified accordingly to five parameters [3] :

1. Form of detected energy: It specifies the type of energy source collected and/or emitted by the CWDS. It can be Electromagnetic or Acoustic.

2. Type of Illumination: It can be passive or active. Passive systems do not radiate any form of energy and they simply measure the energy that is naturally emitted or reflected by the target. Active illumination systems, on the other hand, stimulate the environment by emitting in a controlled way EM or acoustic energy which interacts with the target and , as a result of this interaction, it is partly scattered back to the active system sensors.

3. Proximity: Defines the operational range of the CWDS. Some devices are able to detected dangerous items carried by an individual from a standoff distance (e.g. MM wave radar detectors) while other requires the detection system to be placed near the person (e.g. walk-through metal detector) . A proximity distance is considered near if it is less than one meter.

4. Portability: Describes how easy is to transport the CWDS from one location to another and if it can be hand held. There is a substantial difference between a body cavity imager which is a really large devices that cannot be moved and a metal detector which in some versions can be hand held and can operate on batteries.

5. Operating frequency range: This usually affects the resolution,operational range (i.e. proximity) , and material penetrating properties of the system.

The systems marked as imagers in Table 1.1 are not only capable of detecting concealed weapon but also, each one to a different extent depending on the operating

Description	Frequency range	Illumination	Proximity	Portability	Energy
Acoustic object detector	2 Hz to 1 Mhz	active	far	yes	Acoustic
Metal object detector	Up to 5 Mhz	active	near	yes	Magnetic
Body cavity imager	Up to 400 Mhz	active	near	no	Magnetic
EM resonance	200 Mhz to 2 Ghz	active	far	yes	EM wave
Microwave imager	3 to 30 Ghz	active	far	yes	EM wave
MM-wave imager	30 Ghz to 300 Ghz	active/passive	far	yes	EM wave
THz wave imager	300 Ghz to 300 Thz	active	far	yes	EM wave
IR imager	1 to 400 Thz	passive	far	yes	EM wave
X-ray imager	30 Phz to 30 Ehz	active	far	yes	EM wave

Table 1.1.: An overview of the more important CWDS technologies. Data retrieved from [3, 5] .

frequencies, to see through clothing and walls and to provide an image of the target and the concealed objects if there is any present [4] . Typical frequency range where concealed weapon detection imagers operate are Microwave, MMW (i.e. millimiter waves) , Thz, IR (infrared) and X-ray.

1.2. State of the art

Considering the previous discussed classification let us focus in the frequency range that goes from the microwave imagers to the X-ray imagers and discuss properties and up to date, according to research, capabilities of these imagers:

- Thz imaging is an attractive technique for CWD due to its really high spatial resolution and harmlessness to human body [6] . Furthermore many dangerous materials possess an unique signature in the Thz spectrum which allows spectral identification of them. On the other side operational range of Thz imaging systems is limited due to atmospheric attenuation [7]. The system resolution of a Thz imager is such that anatomical details of the human body are revealed causing privacy concerns. An example of a Thz CWDS produced

image is shown in Figure 1.1.

- X-ray imaging provides the best quality images but it radiates ionizing radiation which is harmful for human body therefore it still remains the best option for screening objects[8] (e.g, suspicious luggages) .
- Infrared imagers are known for its use as a night vision technology rather than CWDS. This is due to the fact that IR sensors do not have a small enough wavelength to penetrate through clothes therefore making the system not reliable for CWD.For the particular property of allowing night vision it can be combined with other CWDS such as MM wave imaging to give better results[9].
- Millimiter wave imagers can as well penetrate many optical opaque materials despite the relatively long wavelength using very low power which eliminates the ionizing radiation harmness problem which affects the X-ray imaging systems [12]. The resolution of a MM wave system is still really good and privacy concerns are still valid.An example of an algorithm developed for overcoming the privacy problem is shown in [11]. An example of a MM wave CDWS produced image is shown in Figure 1.3.

Figure 1.1.: 350 Ghz image of a Glock 17 9-mm gun.Image from [13].

- Microwave imagers properties are quite similar to the ones of a MM wave

one. A microwave CWDS differs from the millimiter one by using a lower operation frequency which in turns give a lower cross-range resolution, which is still sufficient for CWD detection, without breaching personal privacy and a comparable down range resolution[14]. On top of that microwave CWDS are cheaper than MM wave ones and are easier to integrate.

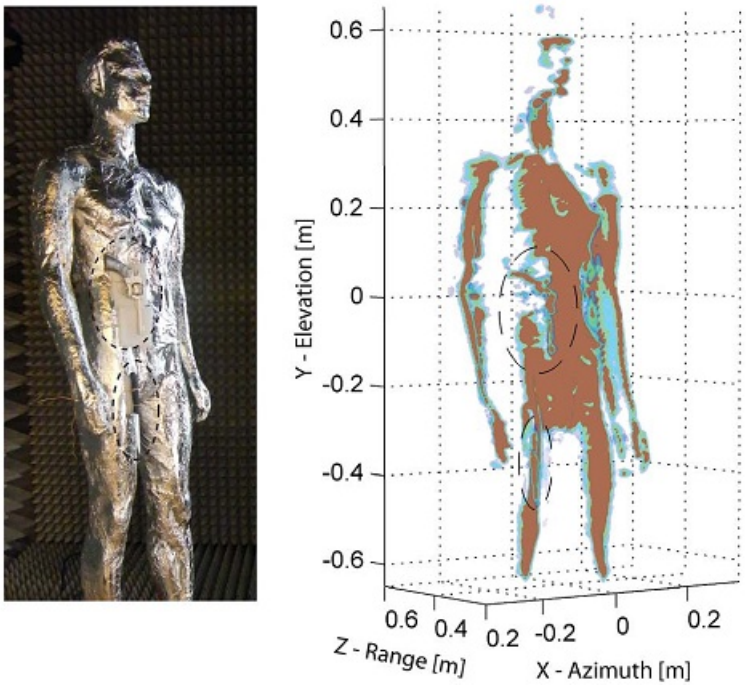

Figure 1.2.: Mannequin under test(left) and microwave image of it (right) . Image from [14].

Nevertheless all these systems require the intervention of a trained human operator to visually inspect the output of the CWDS (i.e. an image) in order to highlight and classify any possible threat.

Figure 1.3.: Optical (left) and 110-112 Ghz image (MM wave on the right) of a clothed mannequin with a concealed Glock-17 handgun. Image from [13].

Due to the fact that,as already said, these imaging systems can see through clothes and usually produce an image that looks like an optical one it is clear that this *modus operandi* arises privacy concerns and also reliability issues since the operator may not notice a dangerous item or give a false alarm.To overcome these problems, digital image processing techniques are fundamental to improve both privacy (e.g.an image of a person can be replaced by a silouette while still pointing out the location of the dangerous object on the body) and detection by introducing an automated concealed weapon detection and classification algorithms.

1.2.1. Imaging processing for CWD

A typical image processing architecture (see Figure 1.4) tailored for concealed weapon detection is composed by a preprocessing unit and a facultative automatic weapon detection one [15]. The preprocessing unit has the task to remove noise (e.g. removal of artifacts) and enhance some characteristics of the image (e.g. weapons) useful for detection. A popular approach in recent literature for denoising/enhancing a concealed weapon image it is based on wavelet transform methods usually combined

with edge detection [16, 17]. Moreover, if the CWDS has more than one sensor, the images produced by the different sensors need to be combined in a smart way and this is done by the fusion sub-unit which it may also record multiple versions of the image. Two fusion algorithms are described in [18] where a MM wave image is combined with a gray scale optical image and in a second case an infrared image is combined with a color optical image. The infrared or MM wave image provides the position of the concealed weapon while the visual image can provide personal identification. An example is given in Figure 1.5. After preprocessing, the enhanced

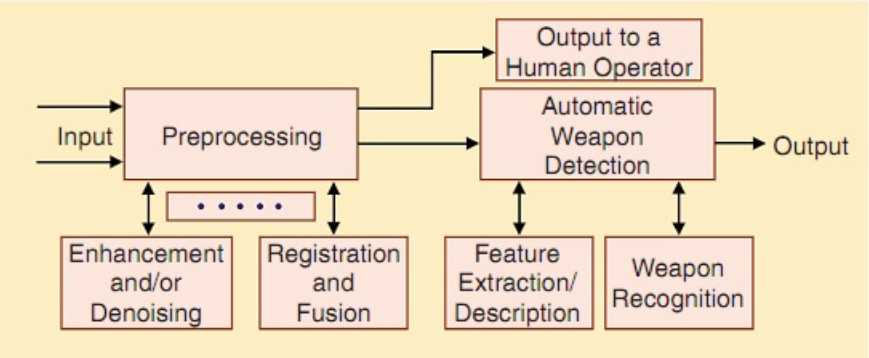

Figure 1.4.: Block diagram of a typical image processing architecture for CWD. Image from [15].

image can be sent directly to the output in order to be checked by a trained operator or can be transmitted to the automatic detection unit for further processing. In this unit several operations need to take place in order to detect and classify objects. First, the enhanced image need to be segmented to allow the extraction of weapons from it. Subsequently, each image segment is processed in order to extract meaningful features that will allow classification. Algorithms for processing image segments need to take into account that the potential dangerous items are not always in the same position (i.e. they can be rotated,scaled and translated) . In accordance with this, it is natural that a feature extraction algorithm has to rely on a mathematical shape descriptor of the object that describes it uniquely which also

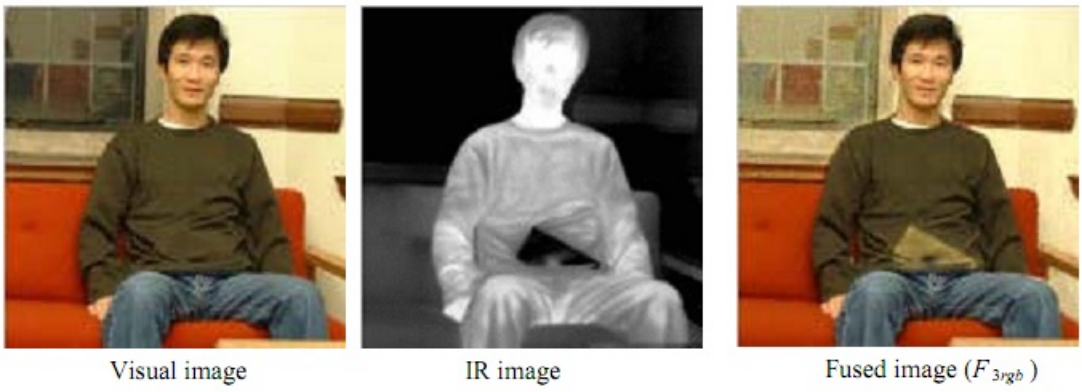

Figure 1.5.: An image fusion approach to CWD. Here an optical image is combined with an Infra red image. The combination of the two images produces an improved fused image where both the identity of the subject and the concealed weapon are highlighted. Images from [18].

it has to be invariant to the position of the object. A popular approach is based on taking a spatial Fourier transform of each segment. This is based on the assumption that, on average, man made objects produce a different spatial fourier transform than natural occuring object and exhibit certain directional pattern in the spatial fourier domain [19, 20]. An example of this is shown in Figure 1.6. Three shape descriptors commonly used are circularity,Fourier descriptors and moments which are presented in [21]. These shape descriptors are invariant,each one to a different extent depending on the descriptor,to a change in the position of the object. After mapping each segment of the image into a mathematical descriptor a further step is required in order to verify if that particular segment contains a dangerous object (i.e. weapon recognition and classification). The mapping from a mathematical descriptor back to a correspondent object is usually performed by a Neural Network or by Euclidean distance between the feature vectors. The entire procedure is shown in Figure 1.7. Three others weapon recognition algorithms are described in [22]. The first approach described in the paper is an edge dection combined with pattern recognition algorithm which has been employed to determine the presence

of a concealed gun. This approach turned out to reveal the existence of the gun but the processing time was too long and too many false alarms were generated. Second approach based on Daubechies transforms gave inconclusive results while the third approach based on SIFT algorithm appears to be promising but further investigations are required according to the author.Finally the processed image is sent to the output where the dangerous object is automatically pointed out.

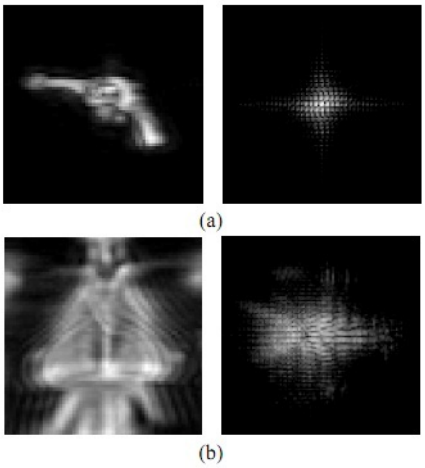

Figure 1.6.: An example on how an object can be mapped to a mathematical shape descriptor. In this case the spatial frequency distribution of a revolver (a) is different from the one produced by the chest of the human body (b) . This property can be exploited to classify objects. Images from [20] .

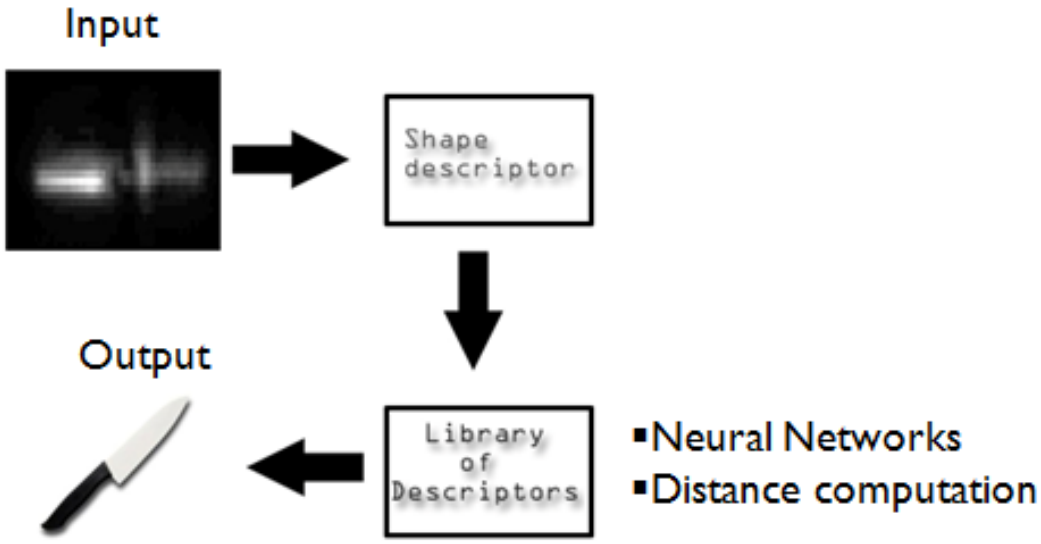

Figure 1.7.: A common object recognition procedure

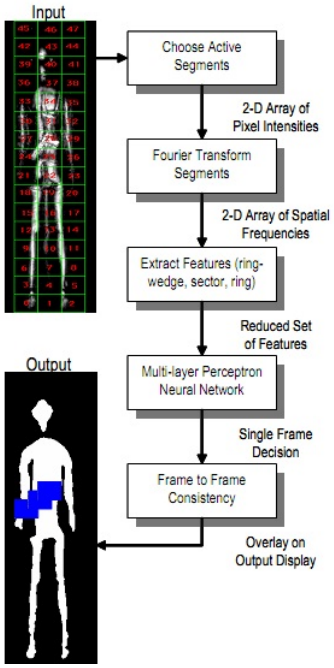

Figure 1.8.: Block diagram for the automatic weapon detection algorithm described in [19].

1.3. Research objective

Until now merely all the research in image processing for CWD has been focused on MM wave imagers and X-ray imagers with very little work done in the microwave range. The main objective of this thesis is to develop robust novel image processing algorithms for detection and classification of concealed weapon. In particular, the developed algorithms are specifically tailored to work with microwave images. The algorithm shall be able to efficiently detect and classify different objects with:

- Different shapes
- Different materials: The objects can be made of metal such as guns and keys or can be made of dielectric such as ceramic knifes and mobile phones.
- Different positions: The same object may have a different scale, position, 3D orientation or a combination of those geometric transformations.

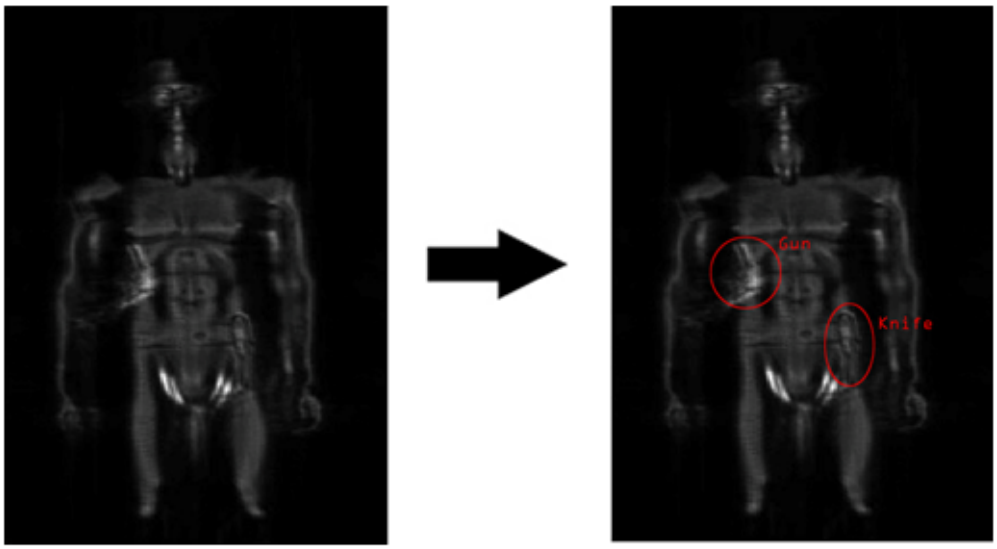

Figure 1.9.: Target output (on the right) of the CWD algorithm for a specific input (left image) .

The algorithms shall perform efficiently with a low false alarm rate in a reduced contrast envinroment such as the one of microwave images. The ideal target output of the algorithms ,for an input image, shall be a dot pointing out the position of the object and an associated text specifying which kind of object is as in Figure 1.9. Moreover, the possibility to port the developed algorithms to other frequency ranges produced images (e.g. MM wave imagers) shall be made possible.

1.3.1. Approach and feasibility

In subsection 1.2.1 the importance of shape descriptors in CWD has been discussed. In order to make reliable detection in the microwave imaging environment a robust shape descriptor with invariant properties to geometric transformations shall be formulated. In this thesis two different approaches with such a requirement are described. First approach is called Depolarization analysis. In this method polarization properties of the waves scattered by objects and symmetry considerations of the image are exploited in order to provide reliable detection of objects. Second approach is an adaptation of the SIFT algorithm that is widely used to detect and classify objects by mathematical features matching in the optical images to the microwave images. Both approaches will be first described in their working principles and then the individual feasibility of the approaches will be tested by MATLAB simulations.

1.4. Thesis outline

The Thesis has the following outline. Chapter 2, after an introduction to shape descriptors, is mainly devoted to the analysis and synthesis of new shape descriptors for microwave radar imaging for concealed weapon detection. Chapter 3 and chapter

4 are then dedicated to the design of two new robust concealed weapon detection methods based on the content of chapter 2. The first novel algorithm, which is proposed in chapter 3, is Depolarization Analysis while chapter 4 is dedicated to SIFT analysis. After introducing the working principles of both algorithms, in chapter 5 results and a comparison of the two methods will be discussed. Finally, in chapter 6 conclusions will be presented.

Acknowledgment

This research was partly supported by the EU within the framework of FP7 project ATOM FP7-AAT-2008 -RTD-1 and the results obtained in this thesis are used in the official deliverable of the project.

Bibliography

[1] N. G. Paulter, "Users' Guide for Hand-Held and Walk-Through Metal Detectors", NIJ Guide 600-00, NCJ 184433, Office of Science and Technology, U.S. Department of Justice, Washington, DC 20531, January 2001.

[2] C. V. Nelson, "Wide-Area Metal Detection System for Crowd Screening," in Proc. SPIE AeroSense 2003 Conf, Sensors and Command, Control,Communication, and Intelligence (C3T) Technologies for Homeland Defense and Law Enforcemnt II, Orlando, FL (22-25 Apr 2003).

[3] N.G. Paulter, Guide to the technologies of concealed weapon imaging and detection, NIJ Guide 602-00, 2001

[4] Nicholas C. Currie, Fred J. Demma, David D. Ferris, Jr., Robert W. McMillan, Vincent C. Vannicola and Michael C. Wicks, "Survey of state-of-the-art technology in remote concealed weapon detection", Proc. SPIE 2567, 124 (1995)

[5] A. Agurto, Y. Li, G. Tian, N. Bowring, and S. Lockwood, A review of concealed weapon detection and research in perspective, in Proc. IEEE Int. Conf. MonE02 Networking, Sensing and Control, 2007, pp. 443448.

[6] Michael C. Kemp, P. F. Taday, Bryan E. Cole, J. A. Cluff, Anthony J. Fitzgerald and William R. Tribe, "Security applications of terahertz technology", Proc. SPIE 5070, 44 (2003)

[7] R. W.McMillan, "Terahertz imaging, milimeter-wave radar", Alabama, USA, 2004.

[8] Zentai, G. ; Partain, L. , Development of a high resolution, portable x-ray imager for security applications ,Imaging Systems and Techniques, IEEE,2007. IST '07.

[9] M. A. Slamani, P. K. Varshney, R. M. Rao, M. G. Alford, D. Ferris, "An Integrated Platform for the Enhancement of Concealed Weapon Detection Sensors," Proceedings of the SPIE's International Symposium on Enabling Technologies for Law Enforcement and Security, 3575-10, Boston, Massachusetts, November 3-5, 1998.

[11] P. E. Keller, D. L. McMakin, D. M. Sheen, A. D. McKinnon, and J. W. Summet, Privacy algorithm for cylindrical holographic weapons surveillance system, IEEE Aerospace and Electronic Systems Magazine, vol. 15, no. 2, pp. 1724, Feb. 2000.

[12] D. M. Sheen, D. L. McMakin, and T. E. Hall, Near eld imaging at microwave and millimeterwave frequencies, in IEEEMTT-S Int. Dig., 2007, pp. 16931696.

[13] David M. Sheen, Douglas L. McMakin, and Thomas E. Hall,Three-Dimensional Millimeter-Wave Imaging for Concealed Weapon Detection,IEEE transactions on microwave theory and techniques, vol. 49, no. 9, september 2001.

[14] Xiaodong Zhuge and Alexander G.Yarovoy. Sparse Aperture MIMO- SAR-Based UWB Imaging System for Concealed Weapon Detection,IEEE Transactions on Geoscience and Remote Sensing, 2011, 49(1):509-518.

[15] H.M. Chen, S. Lee, R.M. Rao, M.A. Slamini, P.K. Varshney, "Imaging for concealed weapon detection a tutorial overview of development in imaging sensors and processing," IEEE signal processing mag., vol. 22, no. 2, pp. 52-61, March 2005

[16] Wei Liu; Zhengming Ma; , "Wavelet Image Threshold Denoising Based on Edge Detection," Computational Engineering in Systems Applications, IMACS Multiconference on , vol.1, no., pp.72-78, 4-6 Oct. 2006

[17] Seungsin Lee; Rao, R.; Slamani, M.-A.; , "Noise reduction and object enhancement in passive millimeter wave concealed weapon detection," Image Processing. 2002. Proceedings. 2002 International Conference on , vol.1, no., pp. I-509- I-512 vol.1, 2002 doi: 10.1109/ICIP.2002.1038072

[18] Wang Yajie; Lu Mowu; , "Image Fusion Based Concealed Weapon Detection," Computational Intelligence and Software Engineering, 2009. CiSE 2009. International Conference on , pp.1-4, 11-13 Dec. 2009

[19] Keller, P.E.; McMakin, D.L.; Hall, T.E.; Sheen, D.M.; , "Use of a Neural Network to Identify Man-made Structure in Millimeter-Wave Images for Security Screening Applications," Neural Networks, 2006. IJCNN '06. International Joint Conference on , pp.2009-2014,

[20] X.Zhuge ,A.Yarovoy,Automatic Target Recognition in Ultra-Wideband 3-D images for Concealed Weapon Detection

[21] M.A. Slamani, D.D. Ferris, Shape descriptors based detection of concealed weapons in millimeter-wave data, in Proc. SPIE AeroSense 2001, Optical Pattern Recognition XII, pp. 43874419, Orlando, FL, 16-20 Apr. 2001, pp. 43874419

[22] Richard Gesick, Caner Saritac, and Chih-Cheng Hung. 2009. Automatic image analysis process for the detection of concealed weapons. In Proceedings of the 5th Annual Workshop on Cyber Security and Information Intelligence Research: Cyber Security and Information Intelligence Challenges and Strategies (CSIIRW '09), Frederick Sheldon, Greg Peterson, Axel Krings, Robert Abercrombie, and Ali Mili (Eds.). ACM, New York, NY, USA, , Article 20 , 4 pages.

2. Shape Descriptors

"*Well, but reflect; have we not several times acknowledged that names rightly given are the likeness and images of the things which they name*?"

Socrates

2.1. Overview

Shape descriptors have been introduced in section 1.2. This chapter deepens the knowledge on shape descriptors and introduces new ones specifically tailored for microwave imaging radar concealed weapon detection. In section 2.2 an introduction to the topic is presented. After the introduction, in section 2.3, section 2.4 and section 2.6 three new shape descriptors named respectively Polarization Angle, Feature Angle and SIFT descriptor, which will be used in the design part of this thesis, are proposed. In section 2.5 the Polarization Angle and Feature Angle are combined together into a new shape descriptor called Depolarization Angle. These shape descriptors exploit polarimetric and structural properties of the image to detect and classify objects. Moreover, in section 2.7 mathematical tools such as segmentation and histogram thresholding are introduced in order to enhance the detection perfomances of the shape descriptors described in this thesis. Finally, section 2.8 contains

the conclusion for this chapter. The novel shape descriptors are then employed to design a new robust concealed weapon detection algorithms which will be described in chapter 3 and 4.

2.2. Introduction to Shape Descriptors

Shape descriptors are fundamental quantities in CWD since they allow us to represent an object via a mathematical quantity. In particular, shape descriptors are mathematical functions which are applied to an image and produce numerical values which are representative of a particular characteristic of that image. These numerical values can then be processed in order to provide some information about the objects which are concealed.

Two dimensional shape descriptors can be divided according to the following classification[1]:

- External representation: It makes use of the boundary and its features to describe the object. For example, the boundary can be described by features such as its lenght, the orientation of the straight line joining its extreme points or the number of concavities in the boundary.
- Internal representation: It makes use of the description of the region occupied by the object on the image plane. An example of an internal shape descriptor is compactness/circularity described by the equation $C = P^2/A$ where P is the length on the region perimeter and A is the area of the region. Compactness is a dimensionless quantity providing a measure of contour complexity versus area enclosed of the target. In addition to that, it is insensitive to rotation, scale and translation of the object which is a really important quality for a shape descriptor when applied to concealed weapon detection.

Shape representation schemes must have certain desiderable properties:

- Uniqueness: Each object must have a unique representation.
- Completeness: Each object must have an unambiguous representation.
- Invariance under geometrical transformations: Invariance under translation, scaling and rotation is very important in concealed weapon detection applications.
- Abstraction from details: Ability of the shape descriptor of representing the basic features of a shape and to abstract from details. This property is directly related to the noise robustness of the representation.

So far a classification and the main properties expected from a shape descriptors have been introduced. The next sections of this chapter are dedicated to introducing new shape descriptors for concealed weapon detection in radar microwave imaging.

2.3. Polarization

Polarization is a property of microwaves that describes the orientation of the electric field vector. The main phenomena which affect the polarization of a wave are reflection and diffraction. In particular these phenomena, which are caused by the interaction of an electromagnetic field with the objects, play an important role in CWD since it is mainly due to them that the radar is able to reconstruct an image of the target. Different materials have different properties with respect to the above described phenomena. To give an example of reflection, metallic materials totally reflect microwaves while non-metallic materials such as glass and some plastics are mostly transparent to microwaves. The interaction between these materials and the wave can induce a change in the polarization characteristics of the radiated wave. There are three types of reflection which can affect polarization[2]:

- Specular Reflection: A smooth surface acts like a mirror for the incident radar pulse. Most of the incident radar energy is reflected away according to the law of specular reflection. Very little energy is scattered back to the radar sensor. This kind of reflection do not produce considerable change of polarization
- Diffused Reflection: A rough surface reflects the incident radar pulse in all directions. Part of the radar energy is scattered back to the radar sensor. The amount of energy backscattered depends on the properties of the target.
- Corner Reflection: When two smooth surfaces form a right angle facing the radar beam, the beam bounces twice off the surfaces and most of the radar energy is reflected back to the radar sensor.

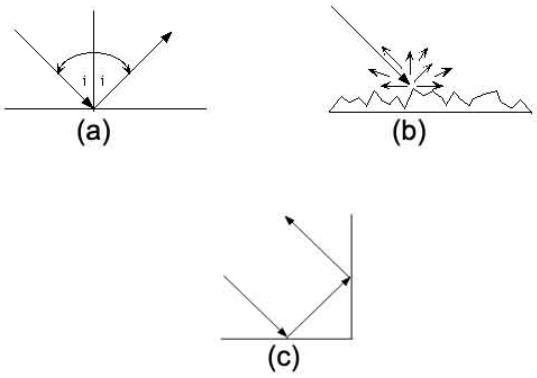

Figure 2.1.: (a) Specular Reflection (b) Diffused reflection (c) Corner Reflector

Microwaves scattering works in the following way. The interaction between a microwave field and an atom will have the effect of exciting the atom electrons. By this interaction the atom will produce its own electromagnetic field at the same frequency of the incoming wave. The EM field produced by the atom is radiated in all directions and it excites the electrons of other atoms in its surrounding which,

in turn, are reradiating the EM field. The process of absorbing and reradiating the incoming microwaves by the atoms has the effect of scattering the EM field about the medium. Scattering is very likely to produce changes in the polarization of the radiated wave by the radar depending on the material and shape of the object.

From the above considerations it is possible to infer that each object interacts with the radiated electromagnetic field in its own peculiar way due to its specific material and shape. This interaction can cause a change in the polarization of the wave transmitted by the radar.

Typical objects employed in CWD have complex shapes and *a priori* knowledge of their specific interaction with the electromagnetic field radiated by the antenna is not known but general considerations can be done. In particular, diffraction refers to various phenomena which occur when a wave encounters an obstacle that may induce a strong polarization change in the radiated field. What is known is that objects employed in CWD present many edges which can cause diffraction thus polarization changes. By focusing on this very general consideration the goal is to find a mathematical quantity (i.e. a shape descriptor) able to describe objects by highlighting the polarization changes from the rest of the image due to edge interaction.

A new shape descriptor called Polarization Angle which exploits polarimetric properties of the image will be introduced in the next section.

2.3.1. PCA and Polarization Angle

Let us define x_{hh} and x_{vv} as the pixel intensity which are normalized between 0 and 1 received by the radar when it is respectively radiating and receiving in horizontal

and vertical polarization. Each 2D[1] microwave radar image is composed of many pixels. For each pixel in the image we define the covariance matrix:

$$\mathbf{C} = \begin{bmatrix} x_{hh} \\ x_{vv} \end{bmatrix} \begin{bmatrix} x_{hh} & x_{vv} \end{bmatrix} = \begin{bmatrix} x_{hh}^2 & x_{hh}x_{vv} \\ x_{hh}x_{vv} & x_{vv}^2 \end{bmatrix}$$

$\mathbf{C}$ is a real and symmetric matrix with the following real eigenvalues:

$$\lambda_{1,2} = \frac{x_{hh}^2 + x_{vv}^2 \pm \sqrt{(x_{hh}^2 - x_{vv}^2)^2 + 4(x_{hh}x_{vv})^2}}{2} \tag{2.1}$$

Equation (1) leads to the conclusion that $\lambda_1 = x_{hh}^2 + x_{vv}^2$ and $\lambda_2 = 0$.

By solving the equation $(\mathbf{C} - \lambda\mathbf{I})\mathbf{X} = \mathbf{0}$ for each eigenvalue the two correspondent eigenvectors $\mathbf{X_1} = \begin{bmatrix} x_{11} \\ x_{12} \end{bmatrix} = x_{11}\begin{bmatrix} 1 & \frac{x_{vv}}{x_{hh}} \end{bmatrix}^T$ and $\mathbf{X_2} = \begin{bmatrix} x_{21} \\ x_{22} \end{bmatrix} = x_{22}\begin{bmatrix} -\frac{x_{vv}}{x_{hh}} & 1 \end{bmatrix}^T$ of the covariance matrix are computed. From the previous equations it is possible to demonstrate that $x_{12} = -x_{21}$ and $x_{11} = x_{22}$. Requiring that $\mathbf{X}_1^T\mathbf{X}_1 = 1$ and $\mathbf{X_2}^T\mathbf{X_2} = 1$ we obtain $x_{11} = \pm\frac{x_{hh}}{\sqrt{x_{hh}^2+x_{vv}^2}}$ and $x_{22} = \pm\frac{x_{hh}}{\sqrt{x_{hh}^2+x_{vv}^2}}$.

In this bidimensional case, by choosing $x_{11} > 0$, the eigenvectors of the covariance matrix $\mathbf{C}$ form the following matrix:

$$\mathbf{T} = [\mathbf{X_1}, \mathbf{X_2}] = \frac{x_{hh}}{\sqrt{x_{hh}^2 + x_{vv}^2}} \begin{bmatrix} 1 & -\frac{x_{vv}}{x_{hh}} \\ \frac{x_{vv}}{x_{hh}} & 1 \end{bmatrix} = \begin{bmatrix} \frac{x_{hh}}{\sqrt{x_{hh}^2+x_{vv}^2}} & -\frac{x_{vv}}{\sqrt{x_{hh}^2+x_{vv}^2}} \\ \frac{x_{vv}}{\sqrt{x_{hh}^2+x_{vv}^2}} & \frac{x_{hh}}{\sqrt{x_{hh}^2+x_{vv}^2}} \end{bmatrix} = \begin{bmatrix} T_{11} & T_{12} \\ T_{21} & T_{22} \end{bmatrix}$$

where each column of $\mathbf{T}$ is an eigenvector of $\mathbf{C}$. $\mathbf{T}$ satisfies $\mathbf{T}^T\mathbf{T} = \mathbf{T}\mathbf{T}^T = \mathbf{I}$ which

[1]The original images from the microwave radar are three-dimensional. In order to obtain a 2D image the data is energy projected on a frontal plane with respect to the position of the objects. More information on energy projection are given in section 3.2.1

means that is an orthogonal matrix. By defining

$$cos(\phi) = \frac{x_{hh}}{\sqrt{x_{hh}^2 + x_{vv}^2}}$$

$$sin(\phi) = \frac{x_{vv}}{\sqrt{x_{hh}^2 + x_{vv}^2}}$$

the eigenvector matrix can be written as a rotation matrix in the following way:

$$\mathbf{T} = \begin{bmatrix} cos(\phi) & -sin(\phi) \\ sin(\phi) & cos(\phi) \end{bmatrix} = \begin{bmatrix} T_{11} & T_{12} \\ T_{21} & T_{22} \end{bmatrix}$$

This can be explained by the fact that PCA[2] finds the most meaningful basis for expressing a set of data. In other words, the new basis, which is found by the transformation $\mathbf{T}$, in the two dimensional case is aligned with the direction of maximum variance of the data. This direction for each pixel is specified by the Polarization Angle[3] :

$$\phi_P = \arctan(\frac{T_{21}}{T_{11}}) - \frac{\pi}{4}$$

The Polarization Angle takes into account how each pixel of the object scatters back the energy, and in which preferred direction, by looking at the relationship between the scattered intensity of the vertical and horizontal polarization data.

(x_{hh}, x_{vv})	ϕ_P
(1,0)	$-\frac{\pi}{4}$
(0,1)	$+\frac{\pi}{4}$
(1,1)	0
(1,0.5)	-0.322
(0.5,1)	+0.322

Table 2.1.: ϕ_P for different values of (x_h, x_v)

[2]For more informations regarding PCA please refer to Appendix A

A SAR measurement of five objects in the free space has been carried out in order to perform a polarization study on the interaction between the EM field and the objects employed in CWD. Also, the measurements are needed to validate Polarization Angle as a shape descriptor. The free space has been simulated by positioning a foam panel ,which appears transparent to microwaves, behind the objects. As shown in Figure 2.2 the set of five objects consisted in:

- A: Ceramic knife
- B: Tester which has the shape and material of a mobile phone
- C: Metallic gun
- D: Bottle of water
- E: Pair of keys

The radar first scanned the target area and received the data in horizontal polarization. Afterwards, it scanned and received the data of the same scene in vertical polarization. The resulting two microwave images are shown in Figure 2.3.

The two sets of data (i.e. HH and VV) are then combined together by computing the Polarization Angle which is shown in Figure 2.4. According to Figure 2.4, all the objects assume an average ϕ_P value equal to -0.7 while their edges present an opposite behavior assuming on average a Polarization Angle value of 0.7.

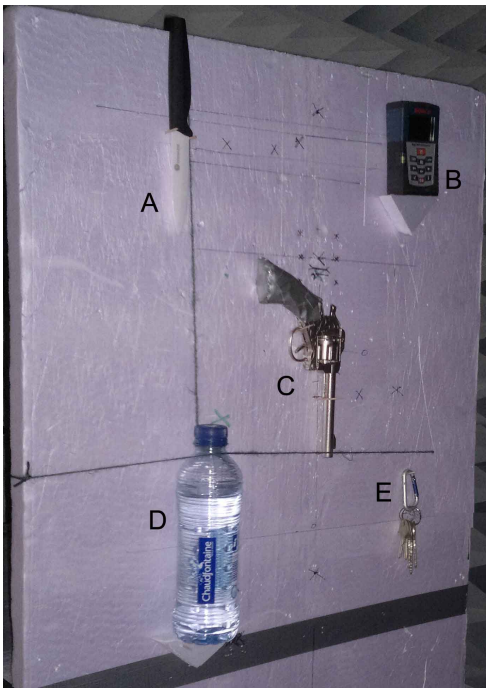

Figure 2.2.: Measuring scenario for experiment 1

According to the above considerations, this first experiment is showing that the edges of the objects are causing diffraction phenomena which are inducing an alteration in the value of the Polarization Angle. This confirms the initial hypothesis of polarization changes due to edge diffraction formulated at the end of section 2.3. Moreover, the background assumes Polarization Angle values between -0.4 and 0.4 allowing to clearly distinguish between background, objects and their edges.

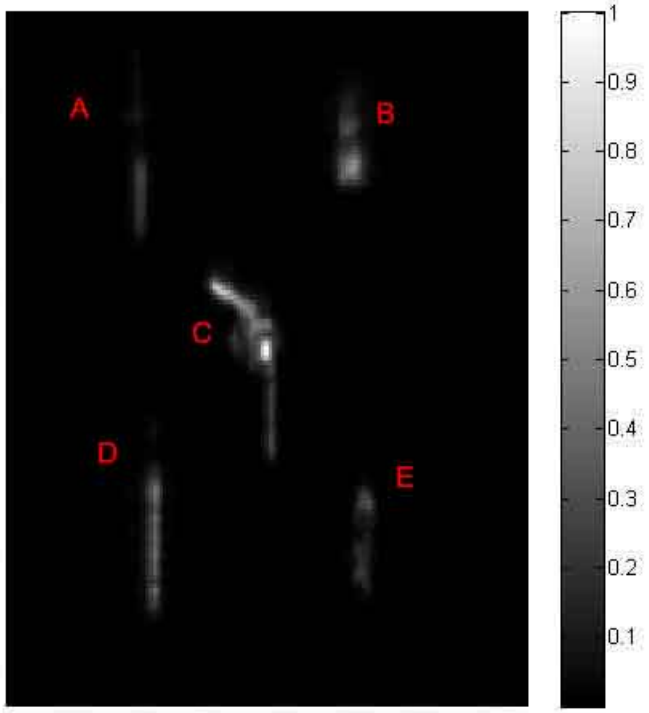

(a)

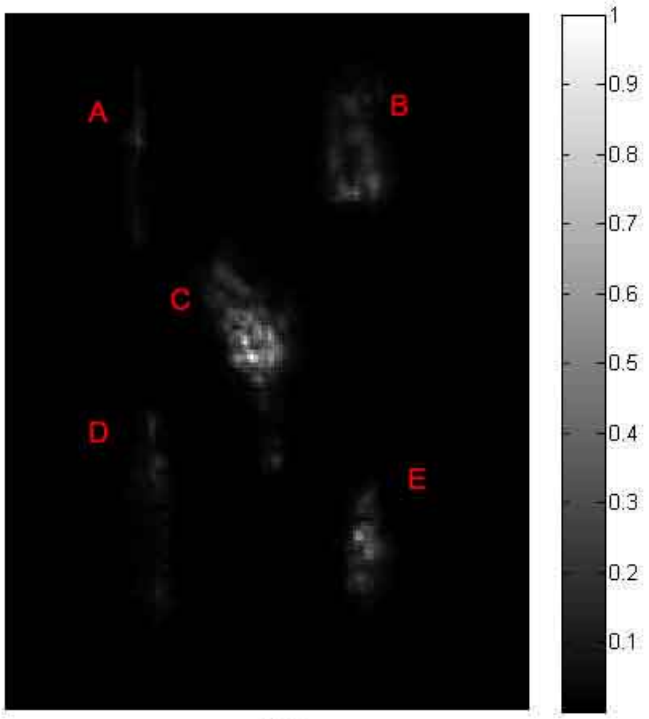

(b)

Figure 2.3.: (a) VV image (b) HH image of the five objects in free space

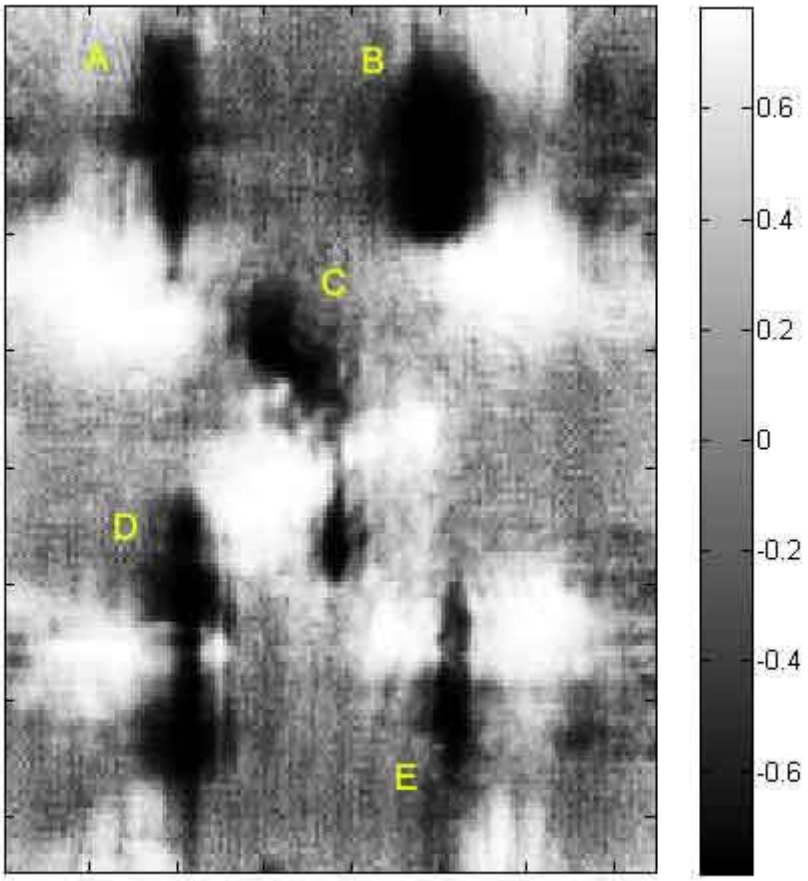

Figure 2.4.: Polarization Angle for the first experiment

A second experiment has been performed by measuring the reflections from a gun and a ceramic knife. In this testing scenario the objects are positioned on a metal plate. The goal of this experiment is to study the polarization phenomena occuring due to the interaction between the objects and the metal plate. According to Figure 2.5(c) the objects, their edges and the background show different Polarization Angle values among each other. In particular from Figure 2.5 it is possible to notice how the trigger and the handle of the gun are causing a polarization shift due to their sharp edges. The values assumed by objects, their edges and by the

background in the two experiments are shown in Table 2.2. By looking at the table, it is possible to state that edges cause polarization shift which is mathematically interpreted as a shift in the value of the Polarization Angle.

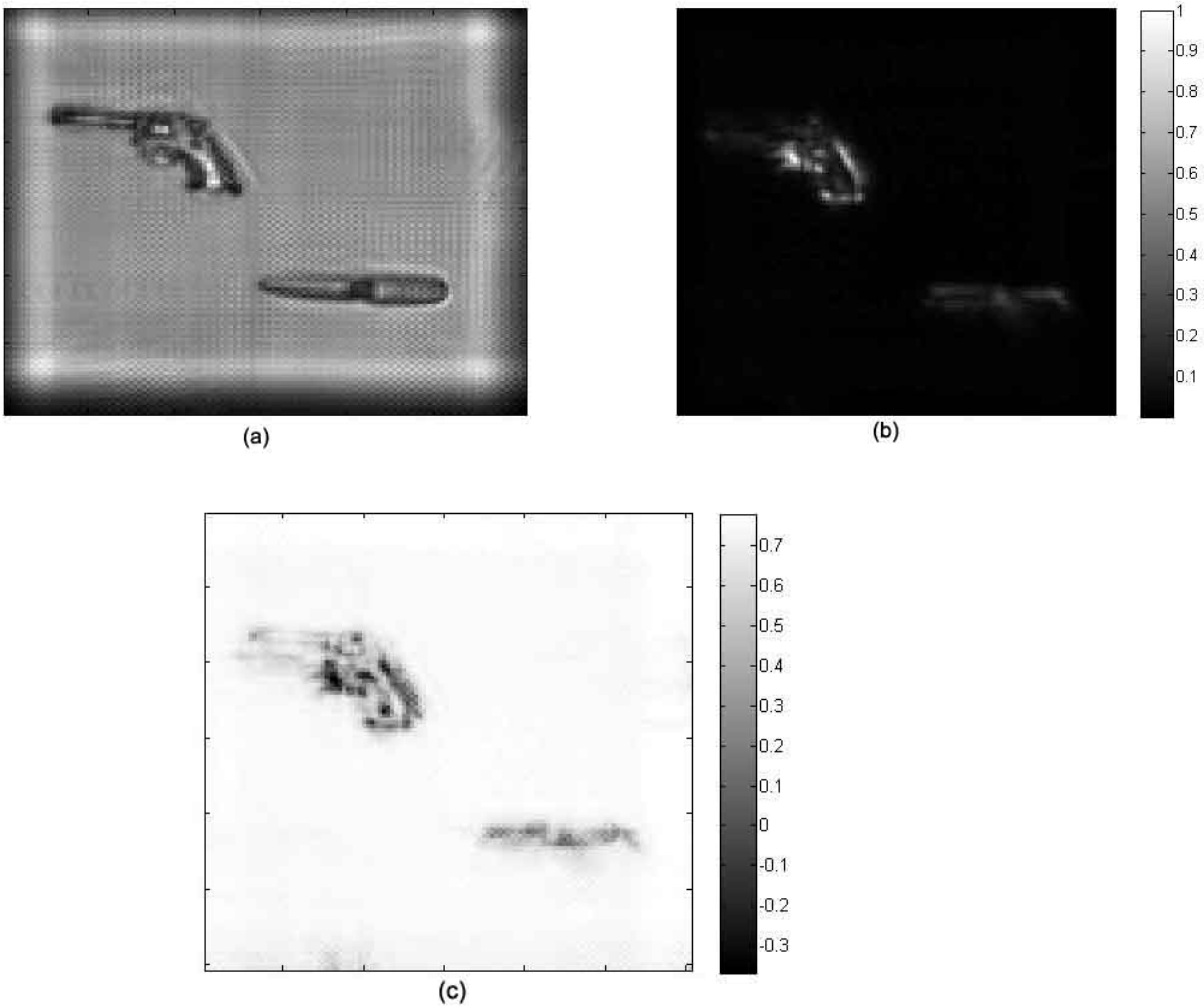

Figure 2.5.: (a) VV data (b) HH data (c) Polarization Angle for the second experiment

Feature (First Experiment)	average ϕ_P	Feature (Second Experiment)	average ϕ_P
Objects	-0.7	Objects	0.5
Edges	0.7	Edges	-0.3
Background (Foam)	0	Background (Metal)	0.7

Table 2.2.: Values of the Polarization Angle for the two experiments

To further investigate polarimetric properties of microwave radar images, the upper chest and head of a mannequin have been scanned by a SAR polarimetric radar. The idea behind this third experiment is to verify whether the shape and material of the mannequin induce polarization changes. As it possible to see in Figure 2.6 the mannequin head and upper chest present negative values of the Polarization Angle while the edges between the mannequin and the background cause a positive shift of ϕ_P. It is important to notice that a shift from negative to positive of the Polarization Angle value can be also found in the eye region due to a corner reflector effect caused by the indentation of that particular area of the body. According to the last experiment, it is possible to deduce that, since the Polarization Angle value across the mannequin is approximately uniform, if an object is placed on the body of the mannequin there must be a shift in the Polarization Angle. This change in the Polarization Angle value is likely to happen at the mannequin-object separation (i.e. edges).

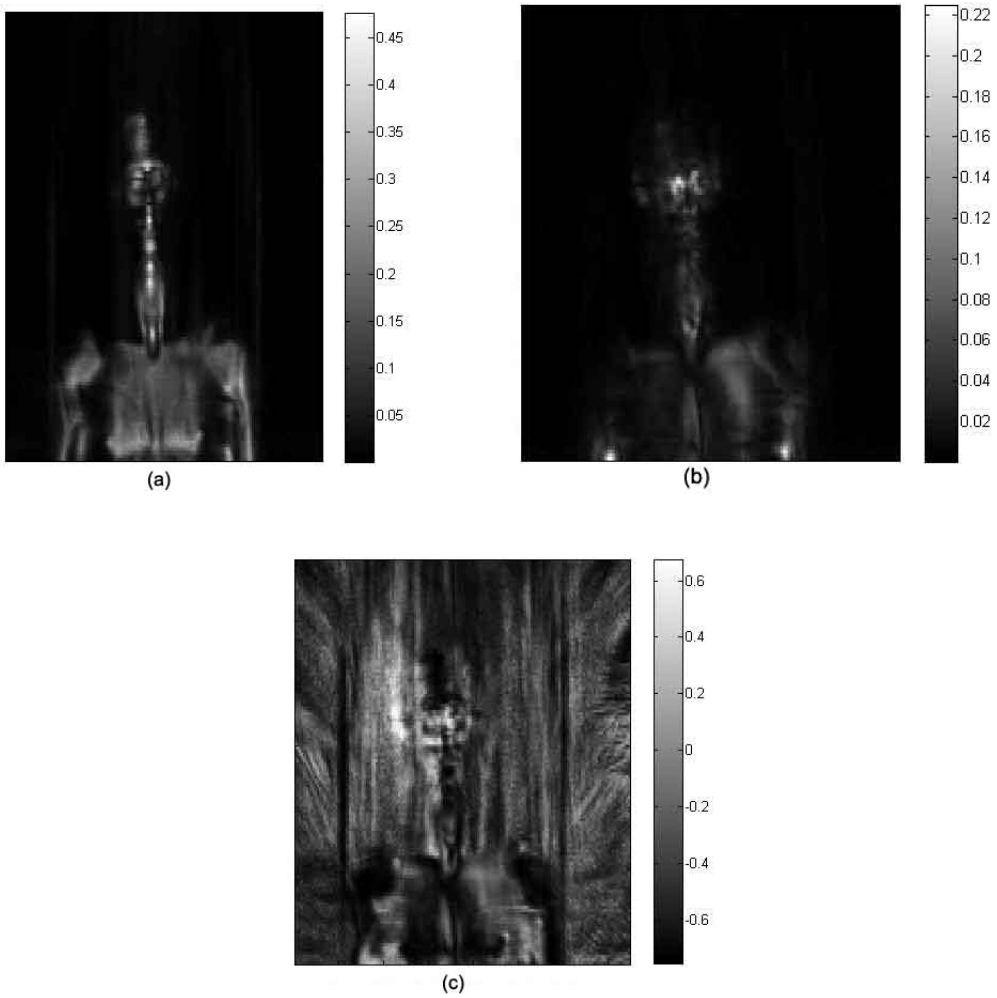

Figure 2.6.: (a) VV data (b) HH data (c) Polarization Angle for experiment 3

The new shape descriptor called Polarization Angle, which has been described in this section, exploits the polarimetric properties of the image to obtain meaningful information regarding edges of objects. The experiments presented in this section showed that edges induce a shift in the Polarization Angle from negative to positive values and viceversa. It is important to notice that objects, their edges and the background assume always different values with respect to each other. Unfortunately, this value is not constant from one measurement to another one (e.g. in the first experiment the gun assumed an average ϕ_P of 0.7 while in the second one the

average was 0.5). This affects the classification capabilities of Polarization Angle since it is not possible to distinguish between different objects. On the other hand, by referring to the shape descriptors general characteristics described in section 2.2, Polarization Angle is achieving invariance to geometrical transformations and abstraction from details. Moreover, some part of the body due to their particular structure are causing a shift in the value of ϕ_P. This makes difficult to distinguish between edges of object and edges caused by indentation of the human body.

Another possible approach, which will be developed in the next section, is to exploit structural informations of the image to obtain a new shape descriptor for concealed weapon detection called Feature Angle.

2.4. Symmetry and Feature Angle

Symmetry is an important mechanism by which structure of objects are identified by the human brain. Man-made object which are needed to be detected in concealed weapon detection can be recognized by the symmetry or partial symmetry that they exhibit. In particular, symmetry found within man made objects is usually related to structural stability. Moreover, phase information plays an important role in human perception of discontinuities (e.g. edges) in images.

By exploiting symmetries is possible to detect concealed object due to the symmetric structures that they produce. It is important to notice that the human body is also symmetric therefore it may be not trivial to distinguish between human body symmetries and man-made objects ones. From these assumptions, an algorithm called phase symmetry is employed in order to extract symmetries from an image. Phase symmetry, which is described in [4], consists of 2D log-Gabor filter banks which are defined by a gaussian amplitude spectrum multiplied by an angular component.

The transfer function for this type of filter can be expressed as:

$$H_{sym}(\omega, \theta) = exp(\frac{-log(\omega/\omega_0)^2}{2log(k/\omega_0)^2} - \frac{(\theta - \theta_0)^2}{2\sigma_\theta^2})$$

Where ω and ω_0 are the frequency range and center frequency. k is a scaling factor, θ_0 the specified filter orientation and σ_θ the standard deviation for the angular component of the gaussian filter. By applying H_{sym} over multiple scales and orientations it is possible to obtain a filter bank representation of of the image. This representation consists of an even $e_{r,n}(i,j)$ and odd $o_{r,n}(i,j)$ symmetric filter outputs. The parameter r represents a specific orientation of the filter while n a specific scale. It is natural to expect points which present high symmetry will be characterized by high magnitudes in the even symmetric filter and by low magnitudes in the odd symmetry filter output. Phase Symmetry at the spatial coordinates of the image (i,j) is defined as:

$$S(i,j) = max\left\{\frac{\sum_{r,n}(|e_{r,n}(i,j)| - |o_{r,n}(i,j)| - T)}{\sum_{r,n} A_{r,n}(i,j) + \varepsilon}, 0\right\}$$

with:

$$A_{r,n}(i,j) = \sqrt{e_{r,n}^2(i,j) + o_{r,n}^2(i,j)}$$

T represents a noise compensation term and ϵ avoids instabilities by zero division when the signal is uniform and no filter response is obtained. It is important to notice that $S(i,j)$ is always normalized between 0 and 1. Before applying phase symmetry the images are preprocessed by applying a Laplacian filter in order to enhance edges[5].

Another important property of phase symmetry is its ability to extract symmetry features of objects under the presence of noise. The syntethic experiment described in [1] shows how phase symmetry is able to extract the symmetry axis of two objects under the presence of gaussian noise conditions in a more efficient way compared to a canny edge detector. The ability to perform under noisy conditions it is a very desiderable quality since microwave images ,which are employed in this thesis for concealed weapon detection, are substantially affected by noise.

After applying the phase symmetry algorithm to the horizontal and vertical polarization data the two images are combined together by selecting the maximum for each pixel by comparing the two polarization images. Let us define $S_m(i,j)$ as the merged image. Then we can define the feature angle as $\phi_F = \arctan\left(S_m(i,j)\right) - \frac{\pi}{4}$. Feature Angle is a shape descriptor which expresses the predominant geometric orientation of an object or of parts of the human body.

The results of applying phase symmetry to experiment 1 of subsection 2.3.1 are shown in Figure 2.7. By comparing Figure 2.7(c) and Figure 2.3 it is possible to notice how phase symmetry is higlighting the structural information of the objects making them easier to be recognized with respect to the unprocessed microwave image of them.

To further explore symmetry properties, the phase symmetry algorithm has been applied to experiment 3 of subsection 2.3.1 which consisted in a scan of the head and upper chest of a mannequin. By inspecting Figure 2.8 it is possible to see that also in this case phase symmetry is highlighting structural information of the image. From the above described experiments, we can expect that by superimposing an object on the mannequin this will cause in the area of superimposition an increase in density and strength of symmetry lines which may indicate the presence of an object. The goal is to mathematically quantify symmetry in a particular region

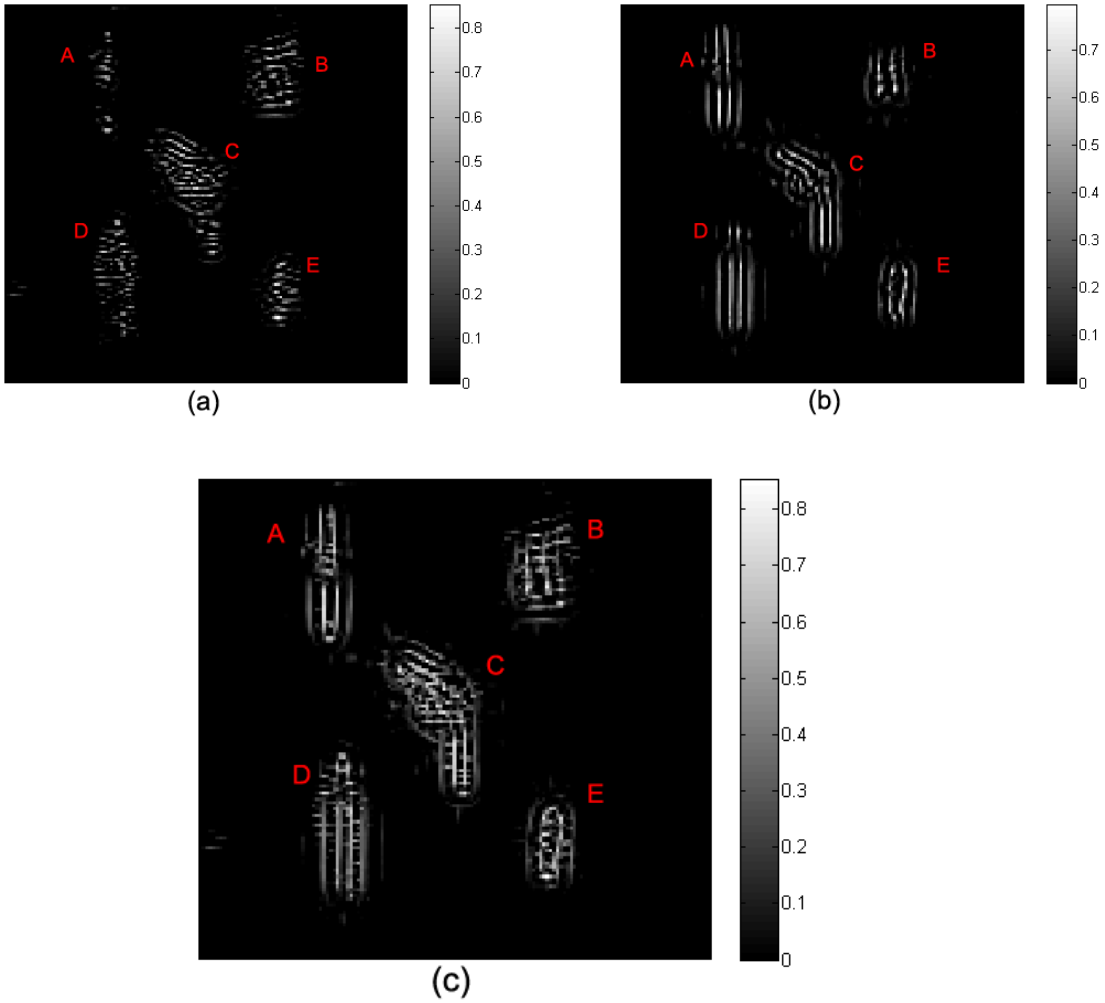

Figure 2.7.: (a)HH data (b)VV data (c) merged image for phase symmetry algorithm applied to experiment 1

of the image. This can be achieved by performing histogram thresholding ,which will be described in subsection 2.7.1, of simmetry lines intensity in a portion of the image.

In this section, it has been shown that it is possible to exploit symmetry to extract and enhance structural information from the image. An internal shape descriptor ,which expresses the predominant geometric orientation of a feature, has been defined as Feature Angle. In order to extract the Feature Angle a symmetry ex-

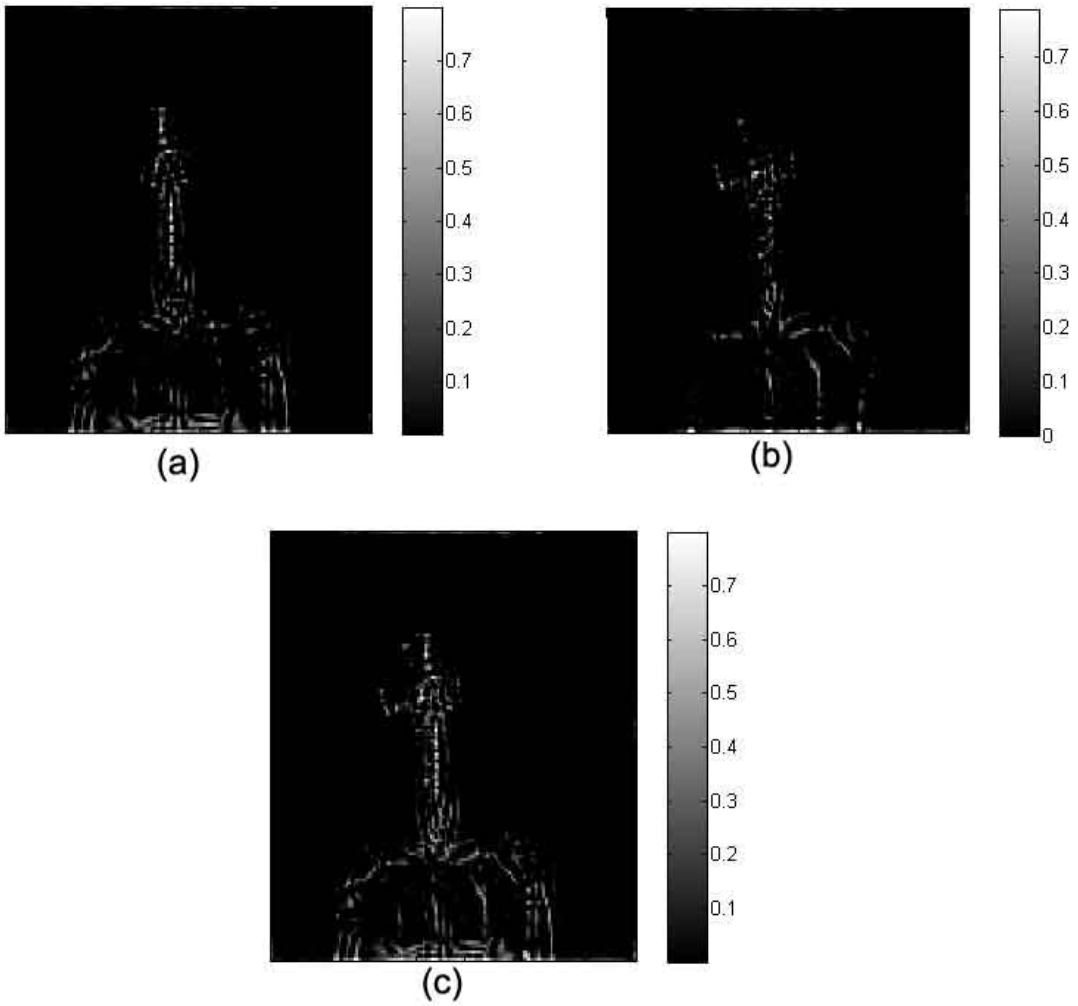

Figure 2.8.: (a) VV data (b) HH data (c) merged phase symmetry data for experiment 3

traction algorithm named Phase Symmetry has been employed. By applying Phase Symmetry to the horizontal and vertical polarization data we can conclude that regions where concealed objects are located are likely to present an increase in density and strength of symmetry lines which can be detected by applying histogram thresholding described in subsection 2.7.1.

2.5. Depolarization Angle

In order to exploit both physical and structural information, Polarization Angle ϕ_P and Feature Angle ϕ_F, which can be classified respectively as an external and internal shape descriptors, are combined together to form a new attribute called Depolarization angle[7] D_p :

$$Dp(i,j) = \begin{cases} \phi_P(i,j)/\phi_F(i,j) & , \|\phi_F(i,j)\| \geq \|\phi_P(i,j)\| \\ \phi_F(i,j)/\phi_P(i,j) & , \|\phi_F(i,j)\| < \|\phi_P(i,j)\| \end{cases} \tag{2.2}$$

It is clear from this definition that $\|Dp\| < 1$ since ϕ_P and ϕ_F are both varying from $-\frac{\pi}{4}$ to $\frac{\pi}{4}$. If D_p value is equal to 1 this indicates a feature exhibiting maximum polarization when the front edge[3] of the Vivaldi Antenna is parallel to the long axis of the feature. If Dp equals to -1 this means that the feature is exhibiting maximum polarization when the front edge of the Vivaldi Antenna is perpendicular to the long axis of the feature. An example for the latter case is shown in Figure 2.9.

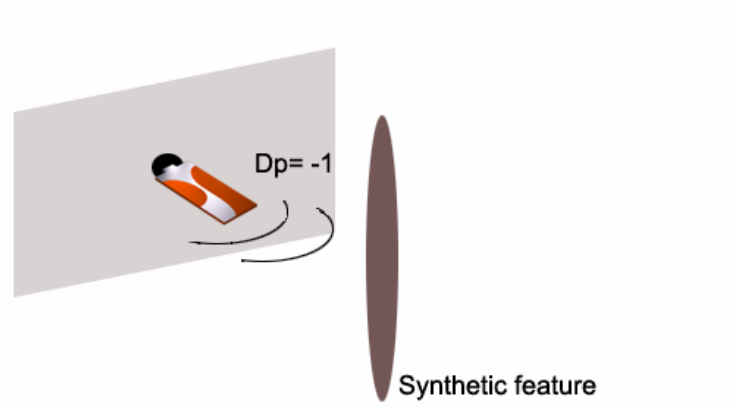

Figure 2.9.: A typical case when $Dp = -1$. The object is exhibiting its maximum polarization in the direction orthogonal to its long axis.

[3]The front edge is considered as the one of the Vivaldi antenna which is the closest in distance to the mannequin

The result of applying equation (1) to the first experiment of subsection 2.3.1 is shown in Figure 2.10. Depolarization Angle is enhancing both structural and polarimetric properties of the combination of the vertical and horizontal unprocessed data image (see Figure 2.3). From the line scan of Figure 2.11, which has been extracted from the central row marked in red in Figure 2.10, it is possible to notice how edges cause a shift from positive to negative (i.e. the deep negative valley in the figure is the gun) in the value of the Depolarization Angle. This shifting property of the Depolarization Angle can be exploited to detect edges of objects. In Figure 2.12 we can see how the mannequin head and upper chest produce a negative Depolarization Angle value while the areas marked as F (head-background separation) and G (eye indentation) are causing a shift in the value of Dp. Therefore Depolarization Angle while improving the detection of edges is inheriting the false alarm issue caused by body indentation of the Polarization Angle described in subsection 2.3.1. The number of false alarms can be greatly reduced by applying histogram thresholding as explained in subsection 2.7.1. By comparing the two above experiments we can state that the background and objects always assume a Dp value which is shifted in sign compared to the edges.

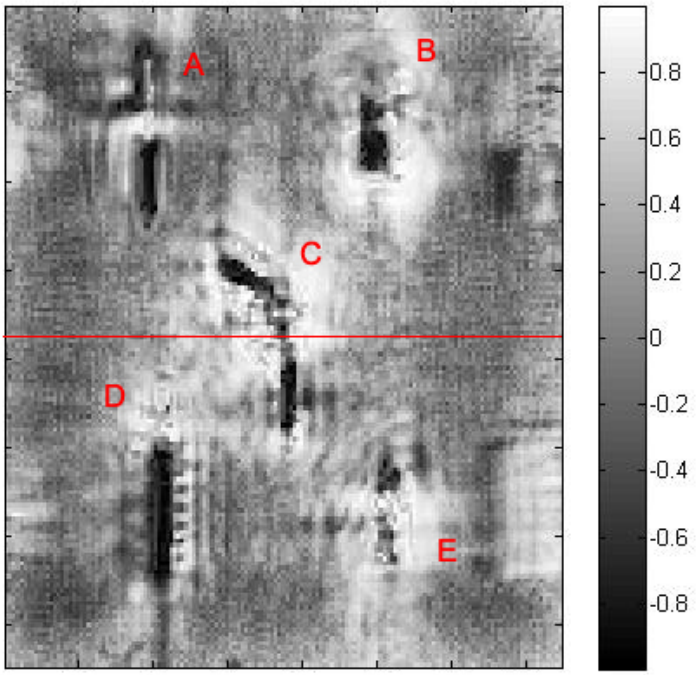

Figure 2.10.: *Dp* for experiment 1 of subsection 2.3.1

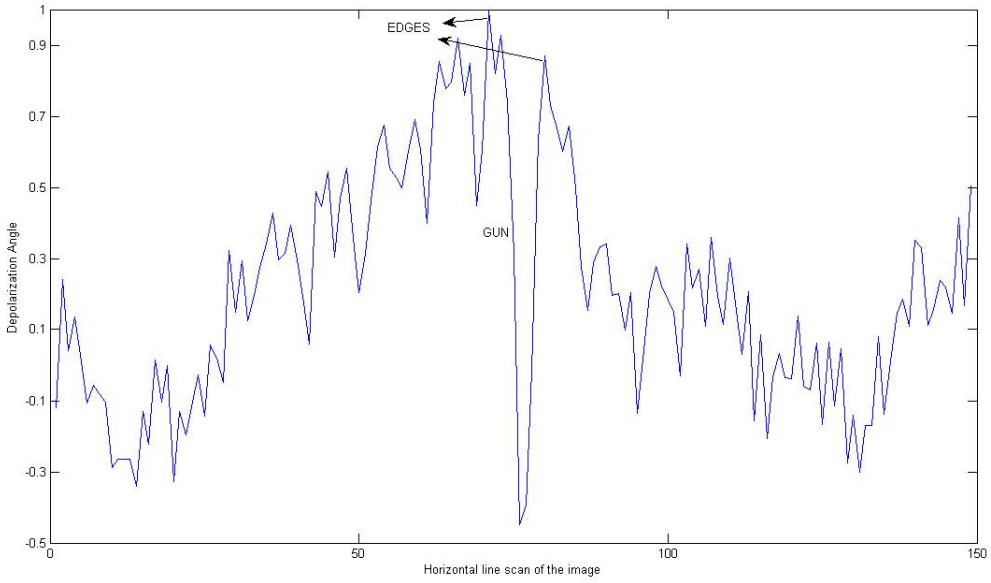

Figure 2.11.: Line scan of Figure 2.10

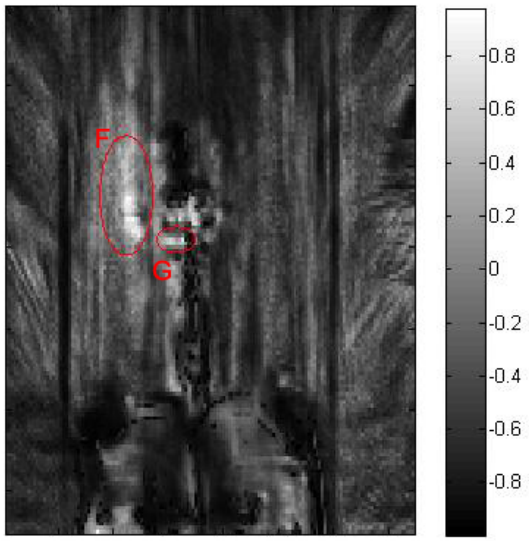

Figure 2.12.: Depolarization Angle value for mannequin head and upper chest

In this section the polarimetric features introduced in section 2.3 are combined with the structural features described in section 2.4. The new shape descriptor which is a combination of Polarization and Feature Angle is called Depolarization Angle. Depolarization Angle allows to detect edges of objects by looking at its value on the edges of objects (e.g. background and objects on average assumes a Depolarization Angle value changed is sign compared to edges). Unfortunately, Depolarization Angle is inheriting the Polarization Angle issue of false alarms caused by body indentation. This issue can be solved by applying histogram thresholding as will be explained in subsection 2.7.1.

The shape descriptor which will be presented in the next section represents a different approach to shape description for concealed weapon detection compared to the ones presented in subsection 2.3.1 and section 2.4. The idea in this case is to try to match an unknown concealed object features set to another set of known features belonging to different objects which are stored in an object library by using only one

polarization data. If the set of features of the unknown object have a match in the library then it means that the unknown object can be detected and classified. In order to do this, a computer vision algorithm named SIFT, which is able to detect and describe local features in optical images by locating pixel intensity maxima and minima will be adapted to microwave imaging radar.

2.6. SIFT Descriptors

What usually happens in airport security is that an operator looks at the image of a person carrying suspicious objects and then attempts to match what he sees in the image with his personal knowledge of objects. The goal of this section is to develop a shape descriptor which takes inspiration from human vision and from the matching process described above. Computer vision is a field that includes methods for acquiring, processing, analysing, and understanding images and, in general, high-dimensional data from the real world in order to produce numerical or symbolic information[8].

Microwave imaging play a key role in detecting object due to the ability of microwaves to penetrate through clothes. On the other hand, microwave images suffer a lack of resolution when compared to optical images. A comparison between an optical and microwave image of a bottle of water is shown in Figure 2.13. Despite the fact that the resolution of the microwave image is way lower than the optical one, the main features of the bottle are still recognizable (e.g. position of edges). In particular the intensity maxima/minima of the bottle image are approximately at the same position in both images. An example of the preservation of maxima/minima is point P1 and P2 in Figure 2.13. The comparison between an optical image and microwave image of a gun (figure Figure 2.14) confirms the fact that the shape is

preserved and the main features of the objects such as the trigger, the handle and the barrel are still clearly recognizable. The property of microwave images of preserving intensity maxima/minima of an image allows to apply computer vision algorithms originally designed for optical images which exploit gradient detection to compare and find matches between two images.

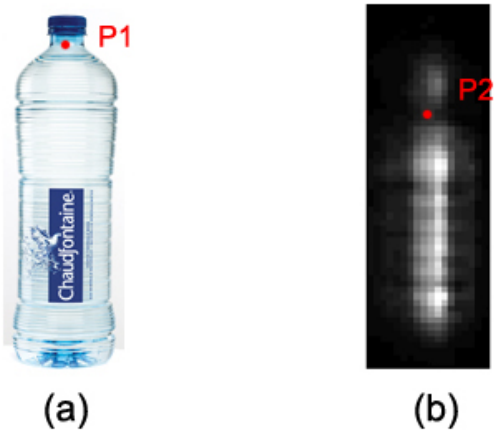

Figure 2.13.: (a) Optical and (b) Microwave image of a bottle of water

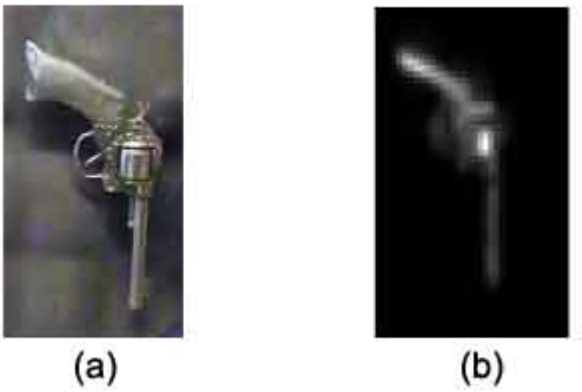

Figure 2.14.: (a) Optical and (b) Microwave image of a gun

A computer vision algorithm named SIFT has been found suitable for microwave

concealed weapon detection due to its peculiar characteristic. SIFT algorithm was first introduced by D.Lowe in 1999. This algorithm is widely used and has proven to be very successful in computer vision to detect and describe local features in optical images. What makes SIFT so noteworthy is its ability to match features between two images with invariance to image scaling and rotation and has shown to be robust with respect to a range of affine distortions, change in 3D viewpoint, addition of noise and change in illumination[9]. Despite not being computationally fast, SIFT has the best performance, when compared to similar feature detection methods such as PCA-SIFT and SURF, in detecting objects when scaling and rotations occurs[10].

In SIFT objects key locations are defined as maxima and minima of the result of difference of Gaussians functions applied in the scale space to a series of smoothed and resampled images[4]. Points with low contrast and edges responses are discarded due to their instability. Once keypoints have been localized, a dominant orientation is assigned to each of them and to the neighbour pixel of the keypoint. Each frame which contains information about a keypoint is characterized by four number which are (x, y) for the position of the frame in the image, σ which is its scale (i.e. smoothing scale) and θ which is the orientation. Each SIFT frame is summarized by a descriptor vector which describes coarsely the appearance of the image patch corresponding to the frame. By matching the SIFT descriptor of the unknown object with the ones stored in the library the algorithm is able to perform image matching and classify concealed objects.

In Figure 2.15 a SIFT feature matching experiment on microwave images has been carried out. The experiment consisted in indentifying a gun among five objects which where the same as experiment 1 of subsection 2.3.1. The matching procedure for this particular experiment presented many false alarms even though the number

[4]For more information regarding SIFT please refer to Appendix C

of correct matching for the gun was superior to the number of false matches with the other objects. In another experiment a gun was positioned on the body of a mannequin and SIFT algorithm was applied. The algorithm correctly identified the gun but there were many false alarms due to indentations of the human body which looked like objects. To reduce the number of false alarms a combination of segmentation and histogram thresholding needs to be applied. This two image processing techniques are described in subsection 2.7.1.

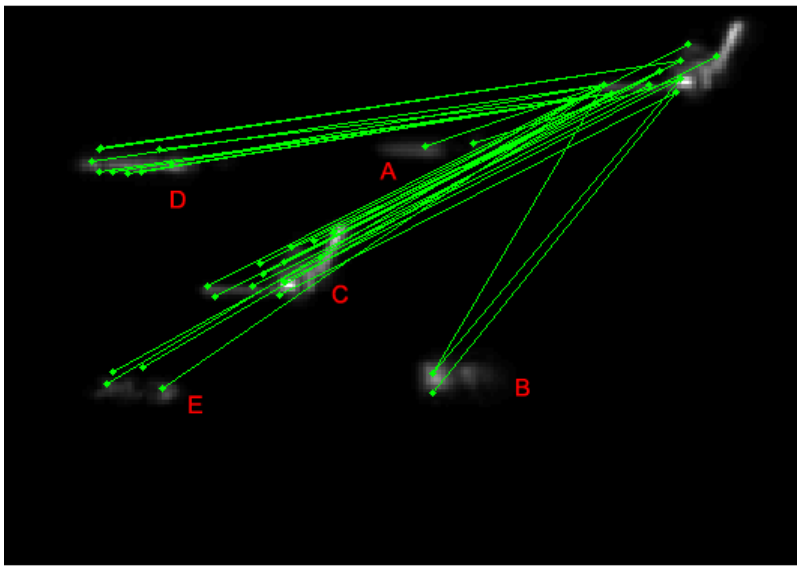

Figure 2.15.: Gradient detection of a gun

The main goal of this section was to find a shape descriptor that allows to perform microwave radar imaging feature matching between an unknown object and a set of object stored in a library by using only one polarization data. We have seen how microwave images differ from optical ones. The lack of resolution of microwave image do not substantially affect the shape and main features of the objects being imaged.

In particular the property of preserving maxima and minima in an image allows to apply gradient detection techniques employed for optical images which allow feature matching. It has been shown in the experiment of Figure 2.15 that a number of false alarms are generated. To reduce the number of false alarms segmentation and histogram thresholding of the image are valuable tools which will be described in section 2.7.

2.7. Shape Descriptors enhancement

In this chapter four new different shape descriptors for microwave radar imaging concealed weapon detection have been described. These descriptors exploit physical and structural information of the image in order to detect objects. In particular Polarization Angle and Feature Angle have been combined together into Depolarization Angle in order to combine the polarimetric and structural data provided by the microwave images. It has been shown in subsection 2.3.1, section 2.4, section 2.5 and section 2.7 that each descriptor is not completely reliable (i.e. it causes false alarms) without some sort of enhancement procedure. This section introduces segmentation and histogram thresholding which are mathematical tools needed in order to enhance the detection capabilities of the shape descriptors described in the previous sections of this chapter.

2.7.1. Segmentation and Histogram Thresholding

Segmentation is the process of partitioning a digital image into multiple segments. It is useful for image analysis since it divides the image into small portions which are more meaningful and easier to analyze. It has been discussed in section 2.6 that the detection of a gun by the means of a SIFT descriptor caused many false

alarms. In order to perform a more accurate detection a prior segmentation of the image before applying the shape descriptor is necessary. In this thesis the segmentation is performed by dividing the image in an overlapping primary and secondary grid as shown in Figure 2.16. The most important factor that affects the segmentation efficiency is the size of the segments. Segmentation efficiency affects detection capabilities of a CWD system. In particular the size of the segments have to be chosen accordingly to the size of the concealed objects that an individual can carry. If the segments are too small the object may be splitted in two different segments which will cause a drop in the detection rate. On the other hand, if the size of the each segment is too large then multiple of objects and too many features of the human body will end up in the same segments. This second hypothesis is also likely to decrease the detection rate.

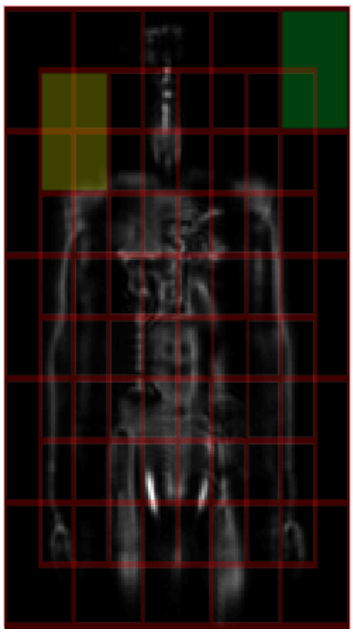

Figure 2.16.: Typical example of primary and secondary grid. The yellow box is an example of a secondary grid segment while the green one of a primary one.

After segmentation, histogram thresholding can be applied to obtain meaningful information regarding the content of a particular segment. An histogram is a graphical

representation of the distribution of a particular set of data. For Symmetry described in section 2.4 the data in which we are interested is the intensity of symmetry lines while for SIFT descriptor of section 2.6 is the pixels intensity. To give a first example on histogram thresholding, many segments for which the SIFT descriptor finds a matching unfortunately do not contain an object but just random background. Histogram thresholding allow us to discard those background segments which are causing false alarms. In the example of Figure 2.17 it is possible to see how a segment containing a concealed (upper part of the image) shows an intensity histogram richer in high intensity values when compared to a background segment. Therefore we can discriminate between segments containing a suspicious object or background by looking at the high intensity values bins of an histogram. The same process can

Shape Descriptor	Flaws	Solution
Depolarization Angle	False alarms (body indentations)	Histogram thresholding (Simmetry lines intensity)
SIFT Descriptors	False alarms (body indentations)	Segmentation and histogram thresholding (Pixel intensity)

Table 2.3.: Shape Descriptors flaws and solution

be repeated for the symmetry lines described in section 2.4. In this case a portion of the merged symmetry image S_m is extracted and histogram thresholding is applied to that particular portion looking for intensity of symmetry lines greater than a certain threshold. The values assumed by the thresholds and how segmentation and histogram considerations are implemented will be described in chapter 4 and 5. A summary of the shape descriptors flaws and solution is shown in Table 2.3.

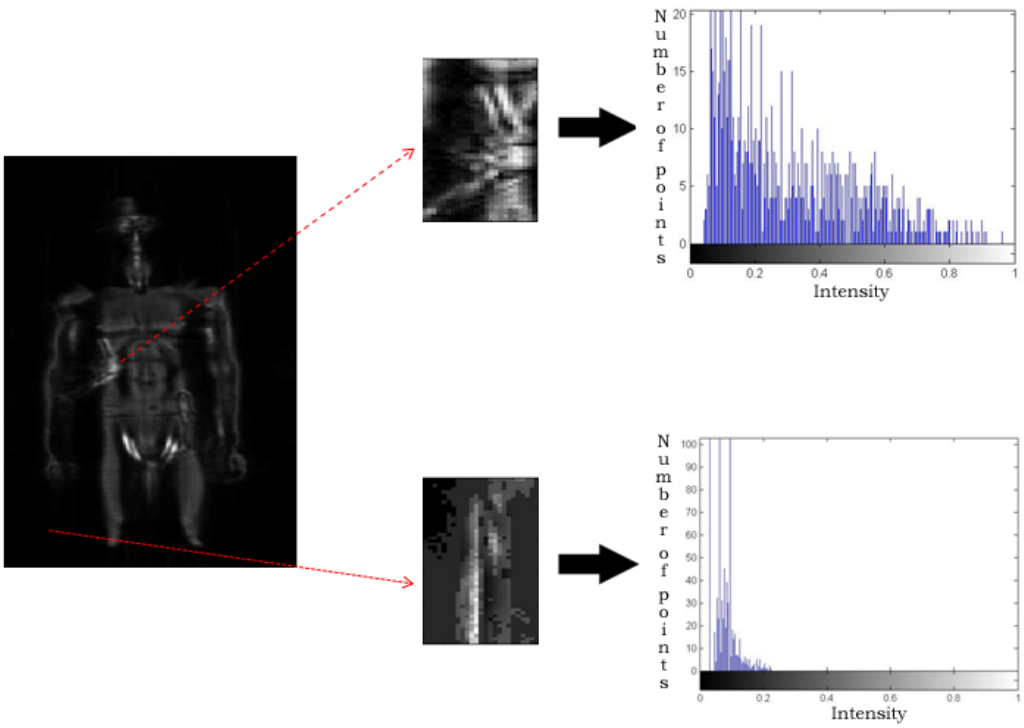

Figure 2.17.: Histogram thresholding example

2.8. Conclusions

This chapter was dedicated to shape descriptors. As said in section 2.2, shape descriptors are mathematical functions which are applied to an image and produce numerical values which are representative of a particular characteristic of that image. These numerical values can then be processed in order to provide some information about the objects which are concealed.

For the purpose of this thesis, four new shape descriptors for microwave radar imaging of CWD has been introduced. In section 2.3 physical phenomena such as reflection, diffraction and scattering which affect the polarization of a microwave have been studied in order to obtain meaningful information regarding concealed objects. The result of this physical analysis is an external shape descriptor called Polar-

ization Angle described in subsection 2.3.1 which has been found, by performing a series of experiments, to be able to detect edges of concealed objects by exploiting polarimetric properties of the combined vertical and horizontal polarization data. Furthermore, in section 2.4 an analysis on structural and symmetry information contained in a microwave radar image lead to the formulation of an internal shape descriptor named Feature Angle. Polarization and Feature Angle are then combined together in section 2.5. The result of this combination is shape descriptor named Depolarization Angle which can be exploited to detect edge of objects in a more reliable way compared to Polarization Angle since it contains also structural information of the image. As explained in section 2.5 indentation of the human body are causing a shift in the Depolarization Angle which is equal to the one produced by edges of actual objects. In order to discriminate between actual objects and indentation of the human body histogram thresholding is required which is explained in subsection 2.7.1.

In section 2.6 a shape descriptor inspired by human vision and brain's associative properties is introduced. The main idea was to try to match an unknown concealed object features set to another set of known features belonging to different objects which are stored in an object library by using only one polarization data. After a comparison study between optical and microwave images it has been found that they share in common the same position of pixel intensity maxima and minima in the image despite their consistent difference in resolution (i.e. microwave images have a poorer resolution compared to optical ones). Therefore it appeared as a feasible approach to apply a computer vision algorithm employed on optical images to the field of microwave imaging. The algorithm which resulted to be the more suitable to be applied to microwave image was SIFT. The experiments in section 2.6 showed that the algorithm was able to correctly match between an concealed object in a

scene with the same one in the library. Unfortunately, many false alarms where present due to specific parts of the human body which where interpreted as objects. Segmentation and histogram thresholding are two mathematical tools described in section 2.6 which can be employed in this particular case to reduce the false alarm rate.

The shape descriptors which have been analyzed and synthesized in this chapter (e.g. Depolarization Angle and SIFT descriptors) along with the enhancing techniques presented in section 2.7 will be employed in the following chapters to design two novel robust microwave radar imaging concealed weapon detection algorithms.

Bibliography

[1] ”Digital Image Processing Algorithms and Applications”, Ioannis Pitas, Wiley-Interscience; 1 edition (February 4, 2000)

[2] ”Physics of Waves”, William C. Elmore, Dover Publications (October 1, 1985)

[3] P. N. Mahob and J. P. Castagna, “Avo hodograms and polarization attributes”, Leading Edge, vol. 21, no. 1, pp. 18-27, Jan. 2002

[4] Symmetry and Asymmetry from Local Phase, P.Kovesi, Tenth Australian Joint Converence on Artificial Intelligence, 1997

[5] R.C. Gonzalez and R. E. Woods, Digital Image Processing, 3rd edition, Nj: Prentice - Hall, 2002.

[6] Böniger, U.; Tronicke, J.; , "Symmetry based 3D GPR feature enhancement and extraction," Ground Penetrating Radar (GPR), 2010 13th International Conference on , pp.1-5, 21-25 June 2010 doi: 10.1109/ICGPR.2010.5550155

[7] Boniger, U.; Tronicke, J.; , "Subsurface Utility Extraction and Characterization: Combining GPR Symmetry and Polarization Attributes," Geoscience and Remote Sensing, IEEE Transactions on , vol.50, no.3, pp.736-746, March 2012 doi: 10.1109/TGRS.2011.2163413

[8] Tim Morris (2004). Computer Vision and Image Processing. Palgrave Macmillan

[9] Lowe, David G. (1999). "Object recognition from local scale-invariant features". Proceedings of the International Conference on Computer Vision. 2. pp. 11501157.

[10] A Comparison of SIFT, PCA-SIFT and SURF", L.Juan, O.Gwon, International Journal of Image Processing (IJIP), Vol. 3, No. 4. (2009), pp. 143-152

3. Depolarization Analysis

"*Symmetria est in rebus*"

Aristotle

3.1. Overview

The main objective of this thesis report is to develop a novel CWD method which is able to detect concealed objects carried by an individual in a low contrast environment such as the microwave radar imaging one. A novel CWD method called Depolarization Analysis is presented in this chapter. Depolarization Angle, which has been described in section 2.5, represents the core of the hereby presented method. Therefore the presented algorithm exploits and combines physical and geometric features of the target which are provided by a dual polarization SAR to achieve object detection. The method is divided in two processing blocks which are named respectively Depolarization unit and Detection unit. In section 3.2 the processing blocks which form the Depolarization unit shown in Figure 3.1 are described in details. This unit has the main task of computing the Depolarization Angle. It has been discussed in section 1.5 how the Depolarization Angle is affected by false alarms and how it is possible to reduce them by applying histogram thresholding. In section 3.3 the processing blocks enclosed in the detection unit needed to reduce the false alarm

rate are discussed. Conclusions are presented in section 3.4.

Figure 3.1.: Block diagram of the algorithm for Depolarization analysis

3.2. Depolarization unit

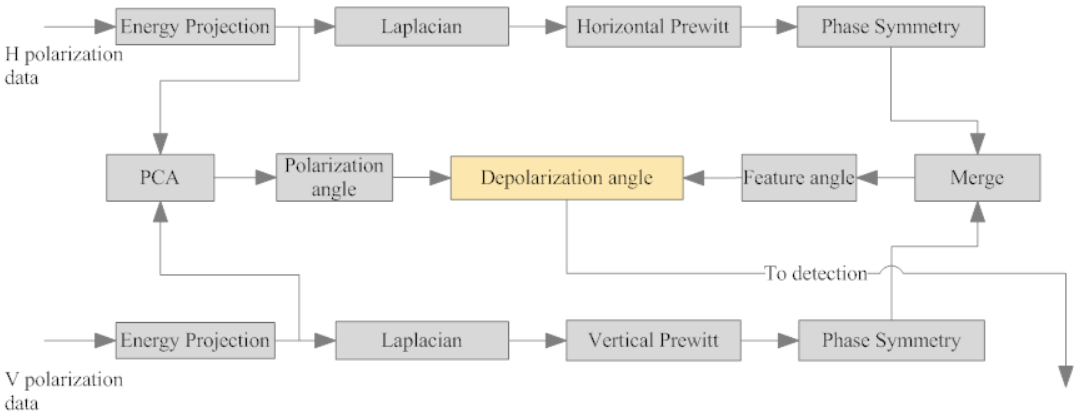

Figure 3.2.: Depolarization unit block diagram

The Depolarization unit is the first building block of the algorithm and its final purpose is to compute the Depolarization Angle. It can be divided in two parts. After an initial energy projection described in subsection 3.2.1 for both polarization data which transforms the 3D volumetric scalar data into a 2D image, there are two processing paths for each polarization image[1, 2]. One path is dedicated to compute the Feature Angle by a cascade of image processing filters (i.e. Laplacian, Prewitt and Phase symmetry) described in subsection 3.2.2 and subsection 3.2.3. The other processing path described in subsection 3.2.4 computes the Polarization Angle by performing PCA. The Polarization and Feature Angles are then combined together into a new attribute called Depolarization Angle which is described in

subsection 3.2.5. Depolarization Angle is then sent to the Detection unit for further processing.

3.2.1. Energy Projection

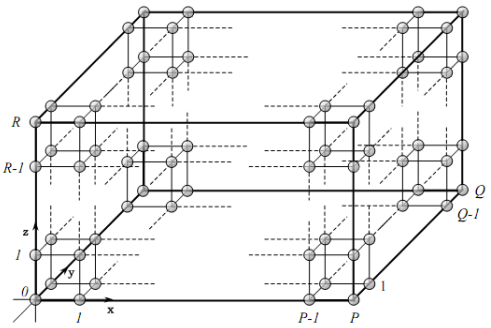

Figure 3.3.: Grid arrangement

Let us define $\mathbf{I} \epsilon \mathbb{C}^{\mathbb{P}\times\mathbb{Q}\times\mathbb{R}}$ as the complex matrix containing the 3D volumetric scalar data of the mannequin being measured by the radar[1] . Accordingly to the grid arrangement of Figure 3.3 we can define each point in $\mathbf{I}$ as $I(x_p, y_q, z_r)$ with $p = 1, 2, ..P$, $q = 1, 2, ..., Q$ and $r = 1, 2, ..., R$. Being the axis of the mannequin image oriented as in Figure 3.4, the matrix $\mathbf{I}$ is energy projected along the y dimension in the x-z plane by performing $I(x_p, z_r) = \sum_{q=1}^{Q} \|I(x_p, y_q, z_r)\|^2 \, \forall \, p,\, r$. There are two reasons behind the choice of projecting the image in a 2D plane. The first one is that well known 2D image processing algorithms can be applied. The second one is related to the choice of the x-z plane as projection plane. This plane, according to the axis orientation in Figure 3.4 , is of specular simmetry for the mannequin body which allows to make symmetry considerations. Moreover, the approach of applying image processing algorithms to several (i.e. the number of slices is Q) x-z plane energy slices proved to be unsuccessful due to the fact that each object, due

[1]For more informations regarding the measurement setup please refer to appendix B

to its three dimensional nature, is contained in many slices and phase symmetry algorithm requires the entire 'energy information' of the concealed object to work.

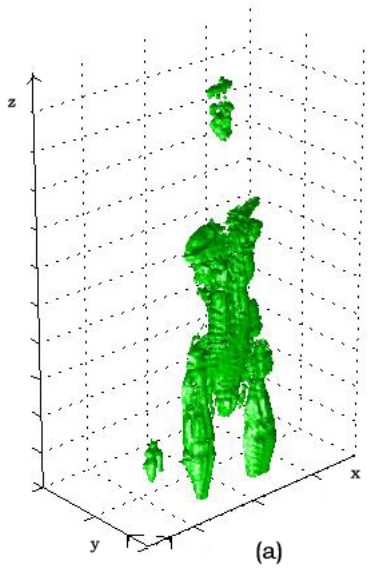

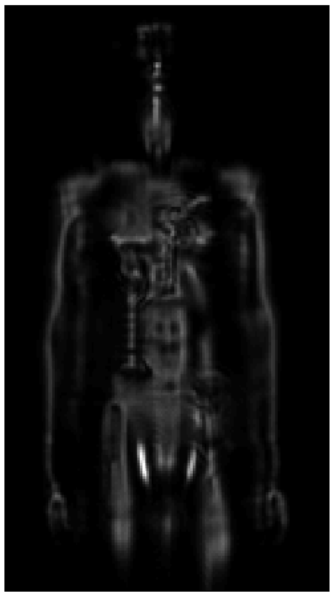

(b)

Figure 3.4.: (a) A typical 3D volumetric scalar measurement of a mannequin. Radar is transmitting and receiving in vertical polarization (b) Energy projection in the x-z plane

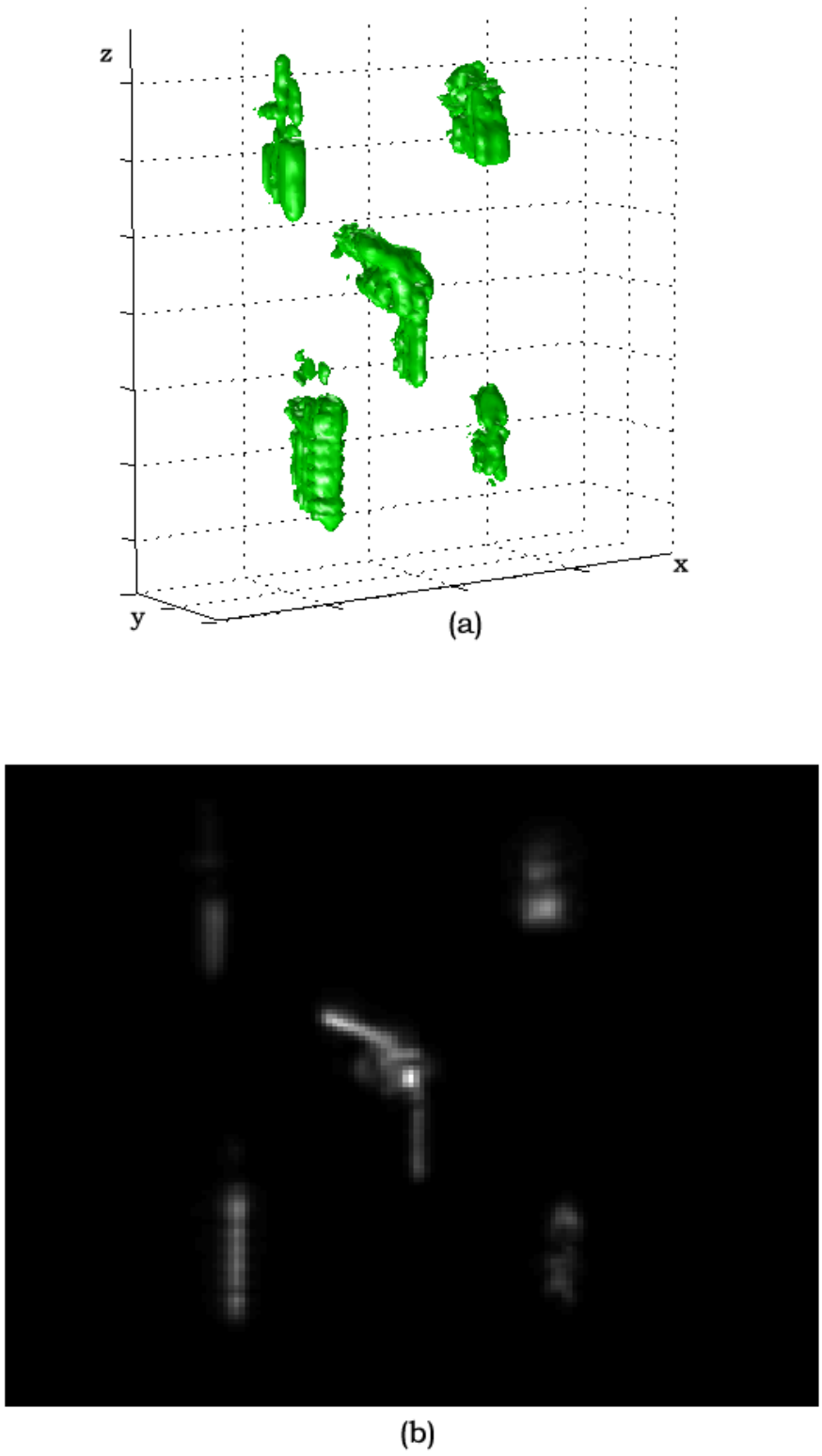

Figure 3.5.: (a) 3D volumetric scalar measurement of five objects in the free space. Radar is transmitting and receiving in vertical polarization. (b) Energy projection in the x-z plane

3.2.2. Image filtering

Let us define $I_H(x_p, z_r)$ as the image matrix containing the projected horizontal polarization data and as $I_V(x_p, z_r)$ the one containing the vertical polarization one. In order to enhance edges of the image, both components are convolved with a Laplacian 3x3 filter of the type $\nabla^2 = \frac{4}{\alpha+1}\begin{bmatrix} \frac{\alpha}{4} & \frac{1-\alpha}{4} & \frac{\alpha}{4} \\ \frac{1-\alpha}{4} & -1 & \frac{1-\alpha}{4} \\ \frac{\alpha}{4} & \frac{1-\alpha}{4} & \frac{\alpha}{4} \end{bmatrix}$. The value of α, which controls the shape of the Laplacian, has been set to 0.9 since it offered the best tradeoff between edge enhancing and noise. To further enhance edges depending on the polarization the Laplacian filter is combined with a Prewitt operator sensitive to the horizontal direction when it is applied to $I_H(x_p, z_r)$ and with a Prewitt operator sensitive to the vertical one when it is being applied to $I_V(x_p, z_r)$.

3.2.3. Phase Symmetry and Feature Angle

After the image processing steps described in subsection 3.2.2, the horizontal filtered image $I_f^{(H)}(x_p, z_r)$ and vertical one $I_f^{(V)}(x_p, z_r)$ are then processed with a Phase Symmetry filter H_{sym} with the following parameters :

- Number of wavelets scales = 5
- Number of orientations = 6
- Wavelenght of smallest scale filter = 12
- Scaling factor between successive filters = 2.1
- $\epsilon = 10^{-4}$
- T (i.e. noise compensation term) is computed by using the median of the smallest scale filter response. This is due to the fact that the smallest scale

filters spend most of their time responding to noise, and only occasionally responding to features.

This values have been chosen since they offer the best tradeoff between noise reduction and symmetry enhancement. An example is shown in Figure 3.6.

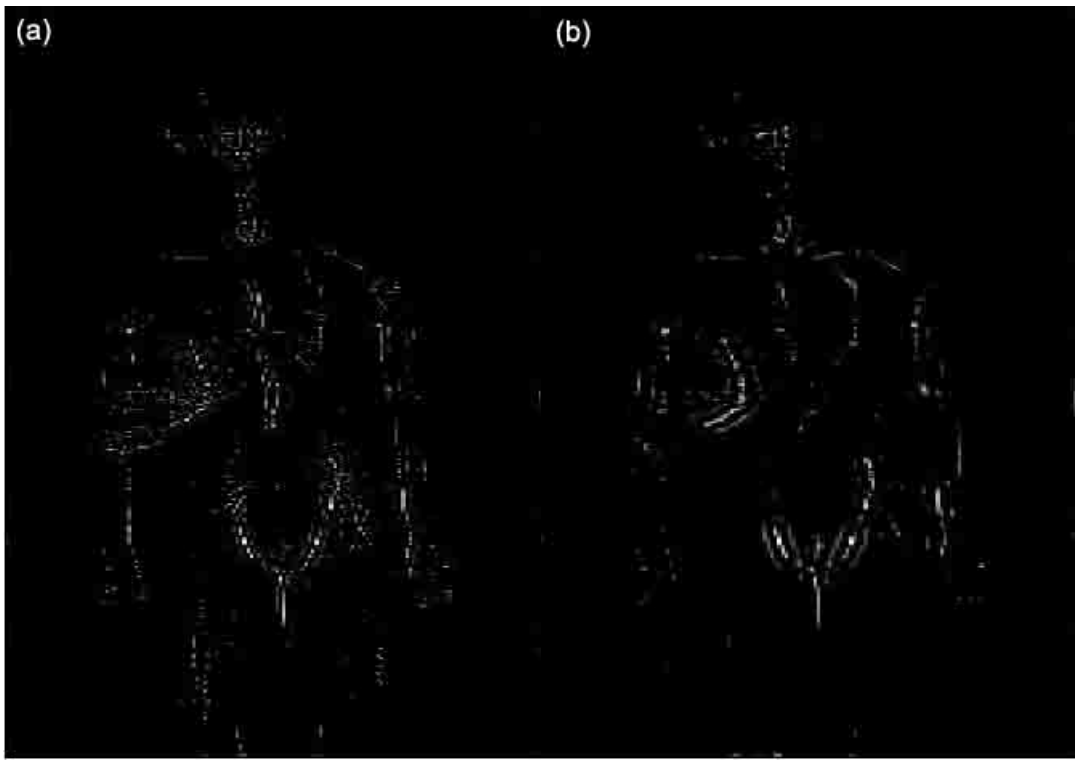

Figure 3.6.: (a) Wavelenght of smallest scale filter = 3 (b) Wavelenght of smallest scale filter = 12 . In both cases the number of wavelets scales is equal to 5 and the number of orientations is equal to 6

Let us denote as $S_H(x_p, z_r)$ the output of the Phase Symmetry filter when applied to $I_f^{(H)}(x_p, z_r)$ and as $S_V(x_p, z_r)$ when applied to $I_f^{(V)}(x_p, z_r)$. Subsequently, $S_H(x_p, z_r)$ and $S_V(x_p, z_r)$ are then merged by the following rule:

$$S_m(x_q, z_r) = \begin{cases} S_H(x_q, z_r) & , S_H(x_q, z_r) \geq S_V(x_q, z_r) \\ S_V(x_q, z_r) & , S_H(x_q, z_r) < S_V(x_q, z_r) \end{cases}$$

The reason why S_V and S_H are merged is to highlight the objects on the mannequin and to ensure maximum information from both components. This is based on the assumption that concealed objects should present many symmetry lines in many directions compared to the human body since they can be considered as a combination of many geometric shapes (e.g. a gun can be considered approximately as a combination of two rectangles). As we can see in Figure 3.7(c) the marked areas are rich of symmetry lines and may underline the presence of an object. Unfortunately not only objects, marked in red, are detected but also human body symmetries which are marked in yellow. The feature angle $\phi_F(x_q, z_r)$ is defined as $\phi_F(x_q, z_r) = \arctan\left(S_m(x_q, z_r)\right) - \frac{\pi}{4}$. In a way, the feature angle expresses the predominant geometric orientation of an object or of parts of the human body.

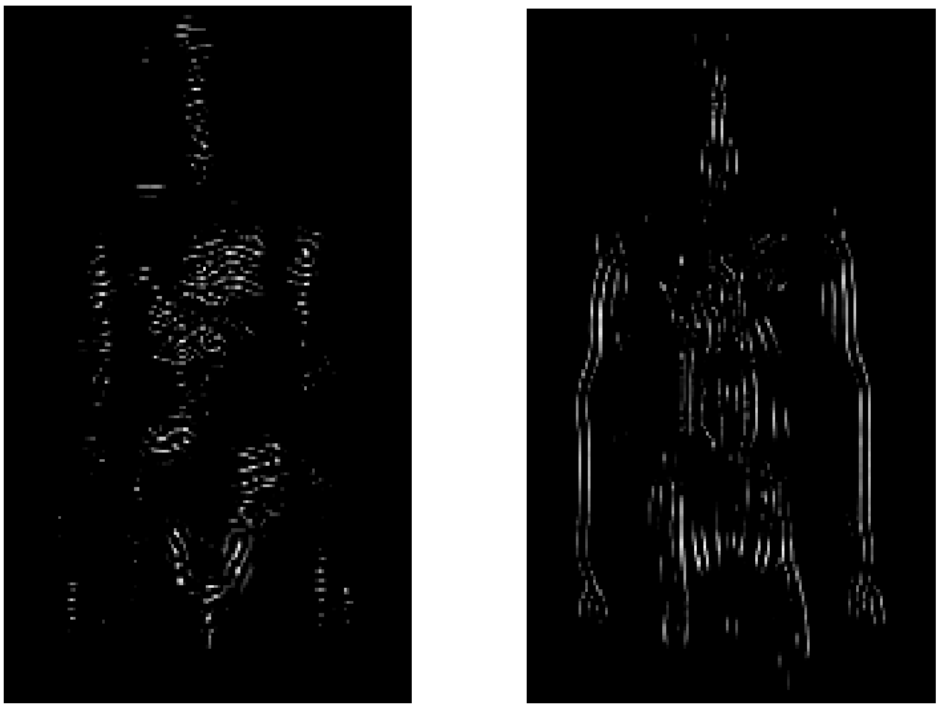

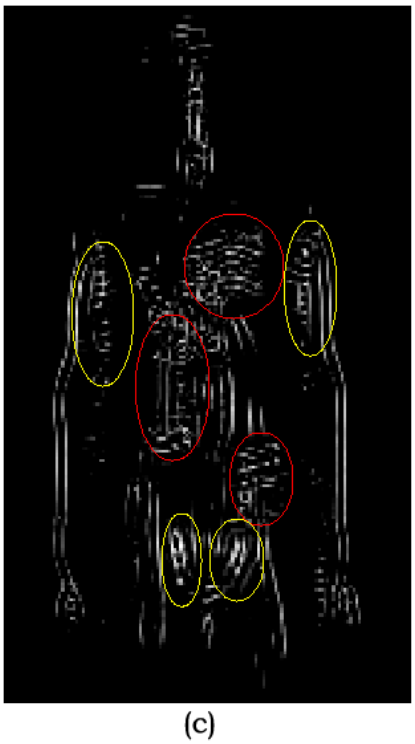

Figure 3.7.: (a) S_H (b) S_V (c) S_m for a mannequin with concealed objects

3.2.4. PCA and Polarization Angle

The Polarization Angle, which has been described in section 2.3.1, quantifies the scattering properties of an object and the dominant polarization characteristic from a dual polarization SAR. Polarization Angle is computed by the algorithm by performing PCA as:

$$\phi_P = \arctan(\frac{T_{21}}{T_{11}}) - \frac{\pi}{4}$$

Where T_{21} and T_{11} are the elements of one of the two eigenvectors of the pixel intensity covariance matrix. As it is possible to see in Figure 3.8 and according to the considerations of section 2.3.1 edges of the objects which are marked in red, and edges of the mannequin which are marked in blue, present Polarization Angle values which are switched in sign compared to the rest of the image. This is caused by diffraction phenomena due to the interaction of the microwave field with the edges. In order to extract edges from the image, the Polarization Angle and the Feature Angle respectively quantifying polarimetric and structural data of the image are then combined togheter to form the Depolarization Angle.

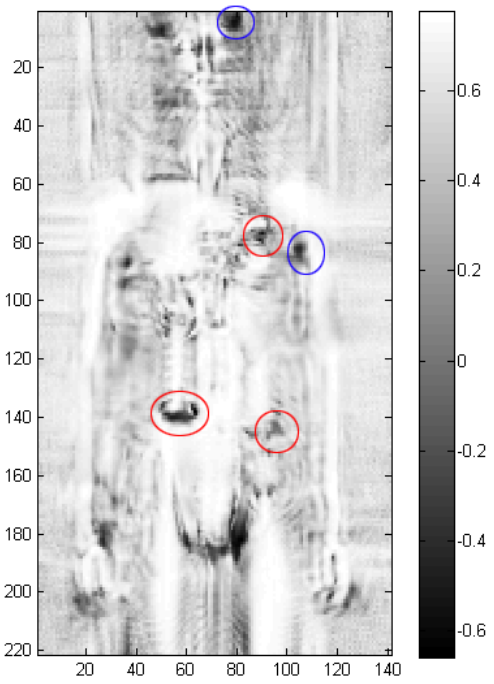

Figure 3.8.: Polarization angle for a mannequin carrying concealed objects

3.2.5. Depolarization Angle

Depolarization Angle, as explained in section 1.5, is a combination of the Polarization and Feature Angle and it is computed by performing:

$$Dp(i,j) = \begin{cases} \phi_P(i,j)/\phi_F(i,j) & , \|\phi_F(i,j)\| \geq \|\phi_P(i,j)\| \\ \phi_F(i,j)/\phi_P(i,j) & , \|\phi_F(i,j)\| < \|\phi_P(i,j)\| \end{cases}$$

Where (i,j) are the coordinates of the pixels of the image. As it possible to see in Figure 3.9 and, as explained in the previous chapter, Depolarization Angle is able to highlight the edges of objects. In particular by looking at the line scan of Figure 3.10,

the edges of the bottle, which is located on the upper right part of the chest of the mannequin, present an higher value of the Depolarization Angle compared to the rest of the image. Unfortunately, not only the edge of the objects but also indentations of the human body, produce a shift in the value of the Depolarization Angle. An example of this phenomenon is shown in the line scan of Figure 3.11. From this figure we can see how a left arm indentation causes a shift in the Depolarization Angle value from negative to positive which is greater than the one caused by the cap of the bottle but still significantly lower compared to the edge of the gun. In order to separate the Depolarization Angle shifts caused by indentation of the human body from the one of actual object histogram tresholding is required. This procedure will be described in the following section.

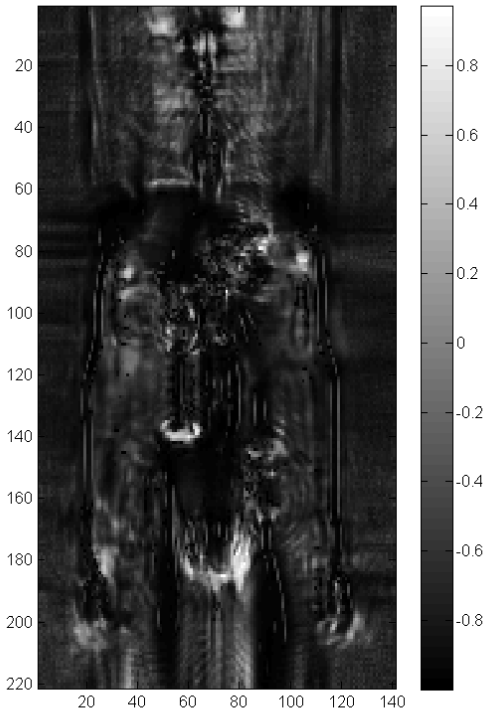

Figure 3.9.: Depolarization angle for a mannequin carrying concealed objects

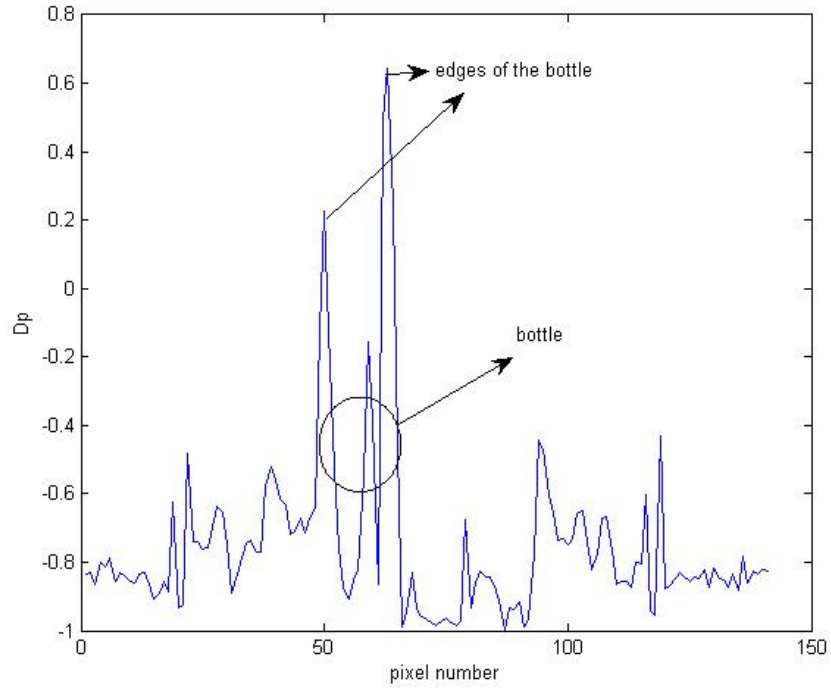

Figure 3.10.: Scan of row 137 of Figure 3.9

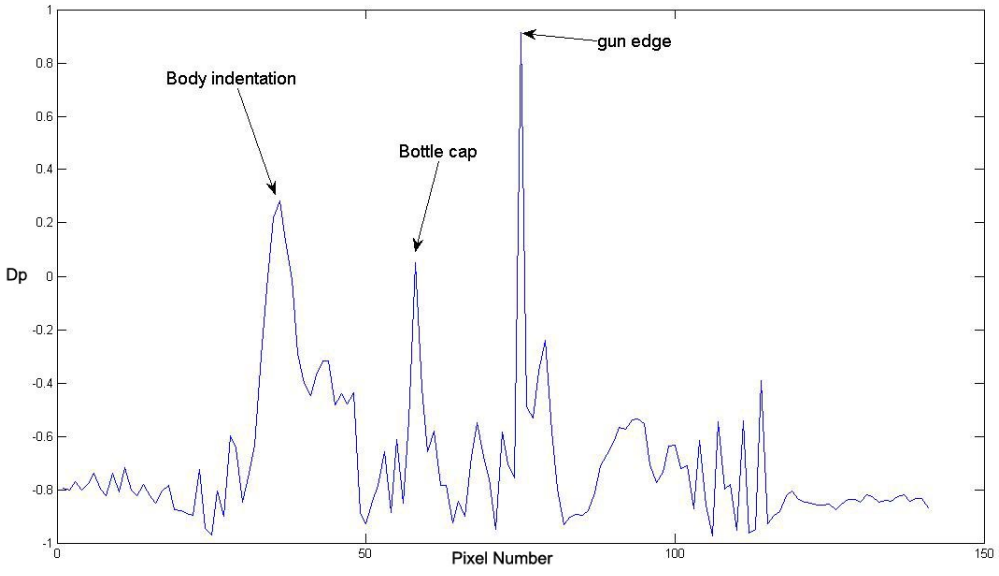

Figure 3.11.: Scan of row 93 of Figure 3.9

3.3. Detection unit

Once Depolarization angle has been computed, it has to be exploited in order to highlight the objects on the mannequin. The Detection unit is the part of algorithm in charge of doing that. As shown in Figure 3.12 , the Detection unit is divided in four parts. The Threshold selector unit described in subsection 3.3.1 works on the assumption that interesting objects on the mannequin have similar Depolarization Angle values. After a threshold selection, symmetry considerations within the image are taken into account by the Symmetry Verification, Inset Inspection and Specular Symmetry verification units described respectively in subsection 3.3.2, subsection 3.3.3 and subsection 3.3.4 in order to reduce the number of false detections before output.

Figure 3.12.: Detection unit block diagram

3.3.1. Threshold selector

We have seen that Depolarization Angle assumes particular values on the edges of objects of interest. Objects employed in concealed weapon detection always present a complex scattering response which is difficult to interpret as a consequence of their complex geometrical structures. A possible solution to interpretate the scattering response is to decompose the object under analysis into a combination of simpler shapes for which the response is known. In the literature, no theorical studies have been performed on the scattering response of objects which are typically employed in concealed weapon detection and their depolarization properties. Due to the above considerations, an experimental approach to extract meaningful range of values of

the Depolarization Angle is employed in this thesis. Let us define the average value of the Depolarization Angle of the image as μ. It has been experimentally verified in this thesis that by applying the following adaptive thresholds, which depends on the value of μ, we can extract concealed objects edges from the image:

$$D(x_q, z_r) = \begin{cases} 1 & if\ Dp(x_q, z_r) \geq 0.8\, and\, \mu < 0 \\ 0 & if\ Dp(x_q, z_r) < 0.8\, and\, \mu < 0 \end{cases}$$

$$D(x_q, z_r) = \begin{cases} 1 & if\ Dp(x_q, z_r) \leq -0.8\, and\, \mu > 0 \\ 0 & if\ Dp(x_q, z_r) > -0.8\, and\, \mu > 0 \end{cases}$$

Where $D(x_q, z_r)$ is defined as the detection image. In other words, concealed objects due to their sharper edges compared to the background are producing a shift in Depolarization Anglue for which $|Dp| > 0.8$.

3.3.2. Symmetry Verification

The threshold selection procedure described in subsection 3.3.1 is not sufficient to guarantee that all the points with a Depolarization angle value exceeding the threshold of 0.8 are actual objects due to human body indentations. According to section 2.4, Phase Symmetry is capable of revealing structural information of the image by highlighting symmetry lines which are typical of human made objects.
Therefore it appears natural to do a pixel by pixel comparison of $S_m(x_q, z_r)$ and $D(x_q, z_r)$ by applying the following rule:

$$D(x_q, z_r) = 1\, if\, S_m(x_q, z_r) = 1$$

Therefore if symmetry lines, which can underline the presence of an object, are present in a particular region of the image it means that the detected points, in the same region, via Depolarization Angle thresholding (i.e. $D(x_q, z_r)$) are potentially correct otherwise they are discarded.

3.3.3. Inset Verification

After Symmetry verification a further inspection is required to reduce the false alarm points in $D(x_q, z_r)$. The detected points in $D(x_q, z_r)$ which are spatially close in the image are merged together by perfoming morphological dilation with a disk of radius 4. Dilation is needed in order to compute the centroid for each of these agglomerate of detected points. For each centroid, an inset is built around it which it has the size of 10 pixels by 10 pixels. The size of the inset has been chosen in order to cover an image area consistent with the average size of the objects involved in concealed weapon detection. This set of insets (i.e. one for each centroid) are drawn on the image $S_m(x_q, z_r)$. For each inset a Contrast Limited Adaptative Histogram Equalization[4] is performed in order to improve the local contrast of the image without over amplifying noise. After computing CLAHE each inset histogram[2] is inspected in order to look for symmetry lines with values greater of a certain threshold (i.e. the 'stronger' is the line the more likely is that is belonging to an object). The threshold has been experimentally found to be effective when it is set to 0.8. Furthermore the presence of a greater density of symmetry lines in an inset may also indicate the presence of an object. An example of this procedure is shown in Figure 3.13 and Figure 3.14. In this example it is possible to see how the histogram of inset 2 (Figure 3.14(b)) which represents a gun contains symmetry line values greater than 0.8 while inset 1 (Figure 3.14(b)) that represents part

[2]For more information regarding histogram thresholding please refer to section 2.7.1

of the background only contains simmetry lines intensity values ranging from 0 to 0.6. The two insets are referring to Figure 3.13. Candidate points (i.e. the remaining centroids which are not discarded) are then sent to the specular symmetry verification unit for further investigations.

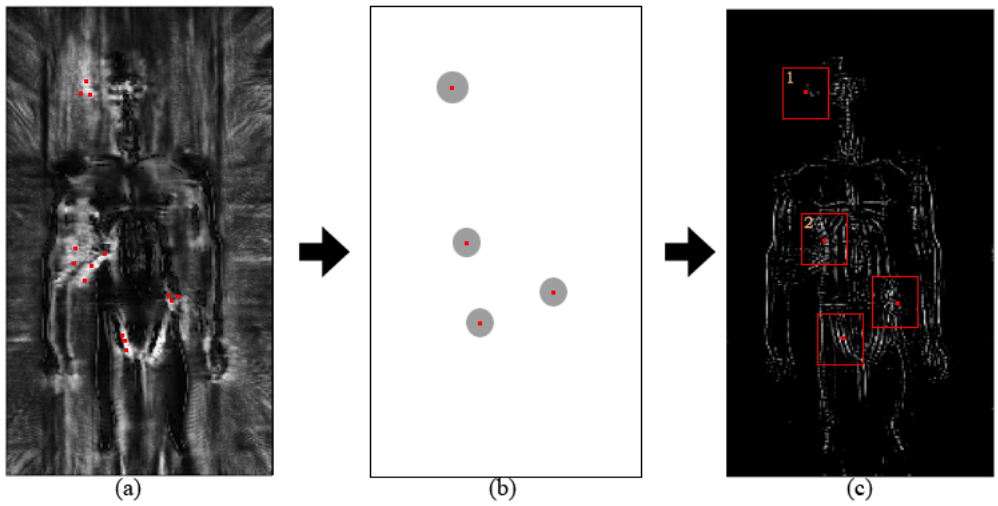

Figure 3.13.: Inset Verification procedure. (a) Detected points over Depolarization Angle (b) Dilation and centroids positions (c) Inset for each centroid over S_m

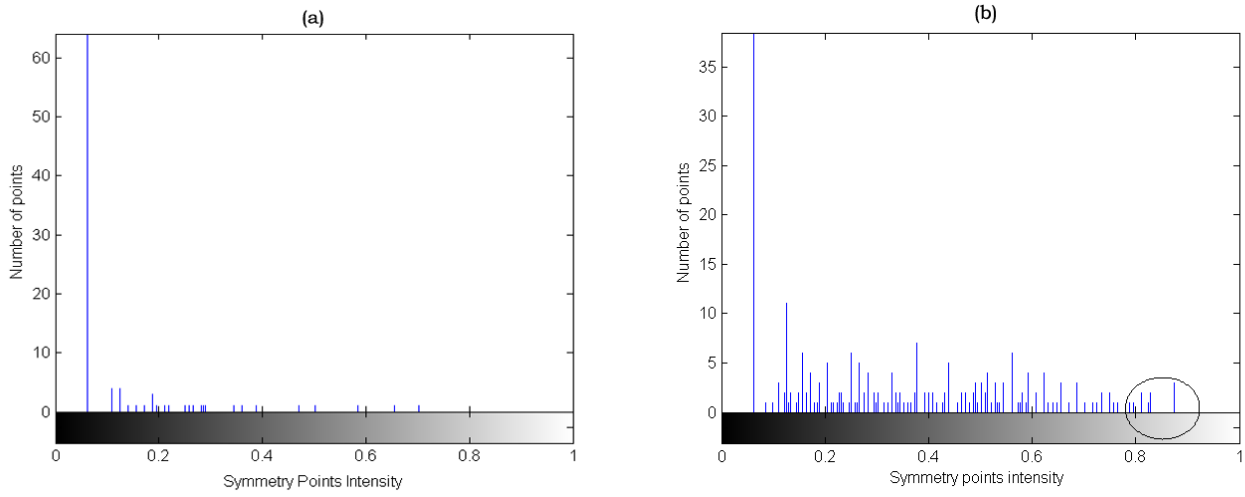

Figure 3.14.: (a) Histogram for inset 1 for Figure 3.13 (b) Histogram for inset 2 for Figure 3.13

3.3.4. Specular Symmetry Verification

This final stage before final output has the task to eliminate points which present a specular symmetry with respect to the center of the image (i.e. the mannequin is centered). This procedure is based on the assumption that in most cases only detection points caused by the human body and not by the objects present this type of symmetry. Therefore two points $(x1, y1)$ and $(x2, y2)$ are discarded if

$$d1 \cong d2 \, and \, y1 \cong y2$$

with $d1 = \sqrt{(x1)^2 + (y1)^2}$ and $d2 = \sqrt{(x2)^2 + (y2)^2}$.

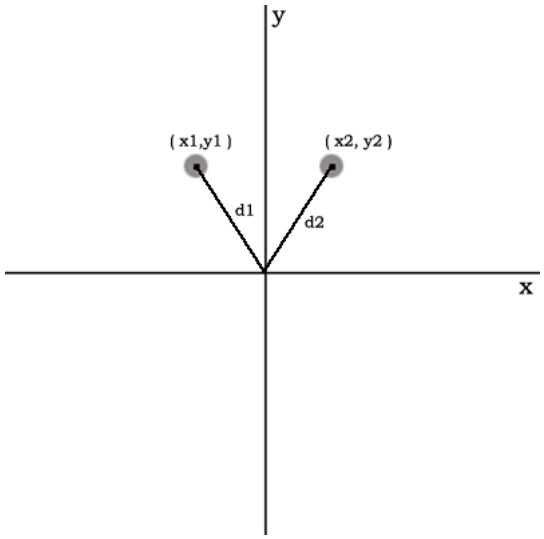

Figure 3.15.: Specular symmetry setup

3.4. Conclusions

The main idea behind this work is to combine the physical and simmetry informations of the target (i.e. a mannequin with concealed weapons on its body) which are provided by a dual polarization imaging SAR. The physical informations are ex-

tracted from the polarization-dependent scattering properties of the target while the simmetry properties are extracted from the structural information provided by both VV and HH data sets. In order to extract the physical information, a Polarization Angle is defined which is computed by performing Principal Component Analysis. To extract the structural and symmetry properties under the form of an attribute called Feature Angle, an imaging processing filter known as Phase Symmetry is employed. The Polarization Angle and Feature Angle are then combined together in a new attribute called Depolarization Angle. By exploiting the properties of the Depolarization Angle it is possible to detect objects.

In order to get meaningful information from the Depolarization Angle and to discard false alarm points additional symmetry considerations and thresholding procedures are required. This tasks are performed by the processing block named as Detection unit in Figure 3.1. It has been experimentally verified that a particular range of values (i.e. $|Dp| > 0.8$) of the Depolarization Angle can be considered as a robust descriptor for the detection of objects. Moreover, a key role for successful detection is played by the thresholds described in subsection 3.3.1 and in subsection 3.3.3 which allow the method to locate the objects by lowering the false alarm rate. It has be seen in subsection 3.3.2 and subsection 3.3.3 that symmetry analysis of the image plays a major role in identifying the objects and discarding false alarm points before output. Practical results of this algorithm will be presented in chapter 5.

Bibliography

[1] Boniger, U.; Tronicke, J.; , "Subsurface Utility Extraction and Characterization: Combining GPR Symmetry and Polarization Attributes," Geoscience and Remote Sensing, IEEE Transactions on , vol.50, no.3, pp.736-746, March 2012

[2] Böniger, U.; Tronicke, J.; , "Symmetry based 3D GPR feature enhancement and extraction," Ground Penetrating Radar (GPR), 2010 13th International Conference on , pp.1-5, 21-25 June 2010 doi: 10.1109/ICGPR.2010.5550155

[3] Kovesi, P.: Symmetry and asymmetry from local phase. In: Proc. Tenth Australian Joint Converence on Articial Intelligence (1997), pp. 24.

[4] Rajesh Garg, Bhawna Mittal, Sheetal Garg, “Histogram Equalization Techniques For Image Enhancement”, IJECT Vol. 2, Issue 1, March 2011

4. SIFT Analysis

"*Symmetria est ante res*"

Plato

4.1. Overview

After Depolarization Analysis which has been described in chapter 2, this chapter of the thesis is dedicated to the development of an another novel concealed weapon detection method called SIFT Analysis. Depolarization Analysis exploited physical and geometric information of the image provided by a dual polarization SAR radar in order to detect objects. The fact that Depolarization algorithm needs a dual polarization radar to work makes it more expensive and technically complex from the point of view of the antenna than a single polarization one. In this chapter, a novel concealed weapon detection algorithm that uses only the vertical polarization data to detect concealed objects will be presented.

The main idea behind the algorithm, as explain in section 2.6, is to compare the microwave image of a specific object, which is stored in an item library, with the image of the mannequin carrying concealed harmful and harmless objects and look for correlations.

A block diagram of the proposed algorithm is shown in Figure 4.1 and in figure

Figure 4.2 . This chapter is divided in the following way. First energy projection and image segmentation will be described in section 4.2. After segmentation a three step detection procedure which is based on SIFT, histogram thresholding and correlator is explained in section 4.3, section 4.4 and in section 4.5. Finally the segment which is considered as the one containing the object under analysis is chosen by forming a Ranking and Global Ranking Matrix which are described respectively in section 4.5 and section 4.6.

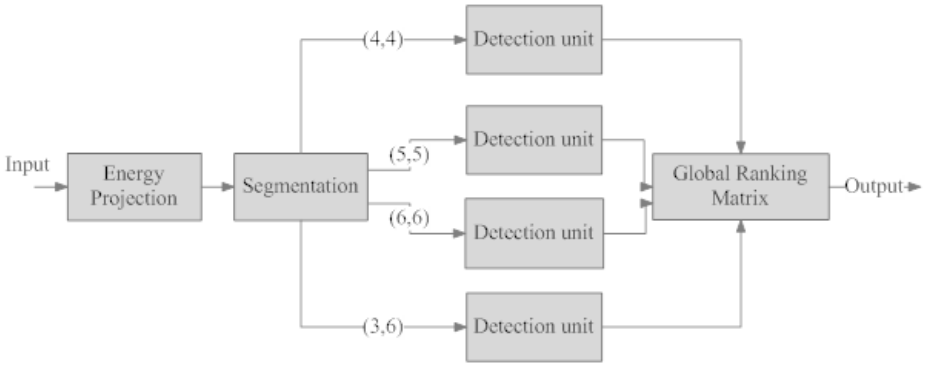

Figure 4.1.: SIFT Analysis block diagram

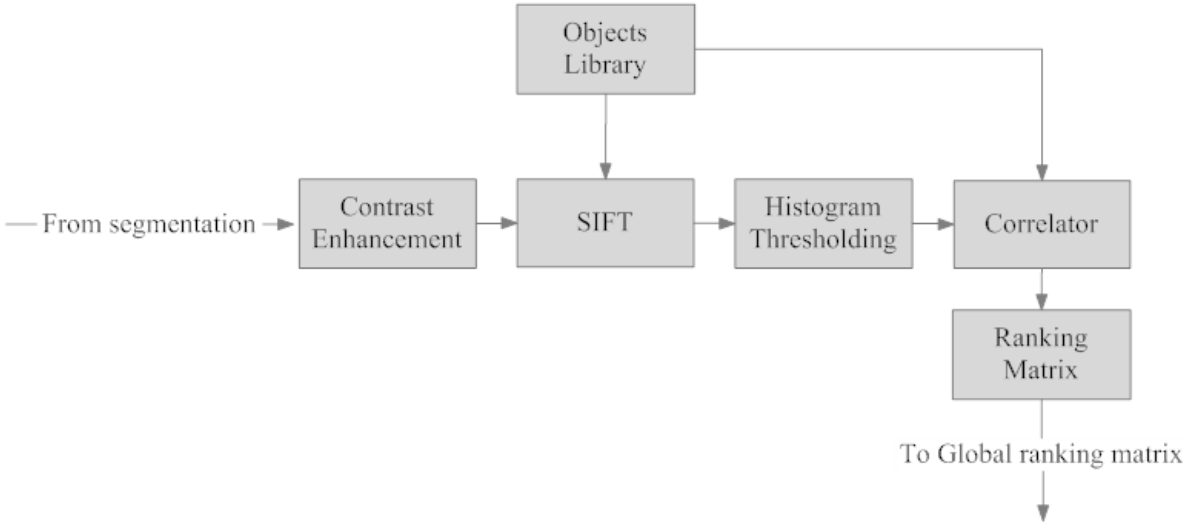

Figure 4.2.: Detection unit block diagram

4.2. Energy Projection and Image Segmentation

Following the exact same approach described in subsection 1.2.1, the 3D volumetric scalar data of the mannequin, defined by the matrix $\mathbf{I} \epsilon \mathbb{C}^{\mathbb{P}\times\mathbb{Q}\times\mathbb{R}}$, being measured by the radar is projected in a 2D plane by performing $I(x_p, z_r) = \sum_{q=1}^{Q} \|I(x_p, y_q, z_r)\|^2 \, \forall \, p, \, r$ with $p = 1, 2, ..., P$ and $r = 1, 2, ..., R$. The reason behind the projection of the 3D volumetric scalar data in a 2D plane is to make the application SIFT algorithm possible.

Since the three step detection unit based on SIFT, Histogram thresholding needs small portions of the image to work and correctly locate objects, after energy projection the image $I(x_p, z_r)$ is sent to the segmentation unit. This unit segments the image accordingly to a partially overlapping with each other primary and secondary grid.

The primary grid gives the following segments:

$$I_{ij}(x_p, z_r) \; for \; i = 0, 1, ...k_x - 1 \; j = 0, 1, .., k_z - 1$$

Within each segment we have the points with the following index values $p = i \cdot N_x + 1, i \cdot N_x + 2, ..., (i+1)N_x$ and $r = j \cdot N_z + 1, j \cdot N_z + 2, ..., (j+1)N_z$. Moreover, k_x and k_z are the integer segmentation parameters (i.e. the total number of image segments is $k_x k_z$) . The stepsizes are $N_x = \left\lfloor \frac{P}{k_x} \right\rfloor$and $N_z = \left\lfloor \frac{R}{k_z} \right\rfloor$. Secondary grid segments are described by the following equations:

$$I_{mn}(x_p, z_r) \; for \; m = 0, 1, ...k_x - 2 \; n = 0, 1, .., k_z - 2$$

With $p = \frac{N_x}{2} + m \cdot N_x, \frac{N_x}{2} + m \cdot N_x + 1, ..., \frac{N_x}{2} + (m+1) \cdot N_x$ and $r = \frac{N_z}{2} + n \cdot N_z, \frac{N_z}{2} + n \cdot N_z + 1, ..., \frac{N_z}{2} + (n+1) \cdot N_z$. Regarding the choice of the values of k_x and k_z, the algorithm takes under consideration four possible combinations

which are considered meaningful for detection. Since the pair (k_x, k_z) governs the shape of the segment it is important to select pair values which are able to create segments which are large enough to fully include inside them all the possible objects which are stored in the library. According to this, the chosen combinations for the segmentation parameters are $(k_x, k_z) = \{(4,4), (5,5), (6,6), (3,6)\}$ .Therefore at the output of the segmentation unit there are 4 primary grids and 4 secondary grids which are processed in parallel as shown in Figure 4.1. Such a high number of generated segments from a single image it is likely to guarantee that the object will be fully contained in at least one of them since there is the possibility that, for a chosen segmentation, an object may end up half in one segment and half in another one which can lead to misdetection.

After segmentation, each segment is contrast enhanced by performing a contrast limited adaptative histogram equalization [1]. CLAHE differs from ordinary histogram equalization by operating in small regions of the image, called tiles, rather than the entire image. Each tile is contrast enhanced so that the histogram of the output region matches the histogram of a uniform distribution. The neighboring tiles are then combined using bilinear interpolation to eliminate artificially induced boundaries. Compared to AHE, CLAHE do not have the tendency of overamplifying noise in relatively homogenous regions of the image while highlighting the details. As it is possible to see in Figure 4.3 traditional histogram equalization deteriorates the quality of the image while CLAHE is enhancing the contrast bringing out more details from the image without overamplifying noise.

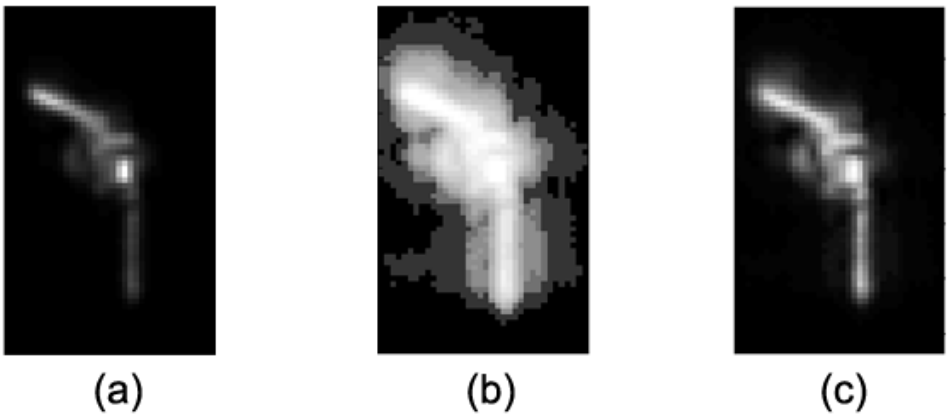

Figure 4.3.: (a) Gun with no histogram equalization (b) Gun with histogram equalization (c) Gun with Contrast Limited Histogram Equalization

4.3. SIFT and Objects Library

SIFT performs consistently on feature detection and matching local features in the image and it has been introduced in section 2.6. These features are used for detecting objects in the image by identifying stable points in scale space in order to create image keys. The SIFT function $S\{\cdot\}$, as described in [2], returns a matrix $\mathbf{F}$ containing the SIFT[1] frame (i.e. maxima/minima of the Difference of Gaussians (DoG) that occur at multiple scales) and a 128x1 matrix $\mathbf{D}$ containing their descriptors. For each segment we are interested in the descriptors matrix which is computed by performing on each segment $S\{\, I_{ij}(x_p, z_r)\,\}$ or $S\{\, I_{mn}(x_p, z_r)\,\}$ if the segments belongs to the secondary grid. This procedure is done for every pair (k_x, k_z) chosen in section 4.2.

For each item $Obj(x_p, z_r)$ (e.g. guns, keys, mobile phone) stored in the object library ,in the form of a microwave image, the descriptors have been previously computed by performing $S\{\, Obj(x_p, z_r)\,\}$. Following the same approach described at the end of section 4.2, each object in the library has been contrast improved by perfoming CLAHE. The main SIFT parameters which gave optimal results were:

- Number of octaves: $\lfloor log2(min\{M, N\}) - 2 \rfloor$ where M and N are respectively the number of rows and column of the image.
- Number of levels: 3
- Base smoothing σ_o: 2.01
- Number of spatial bins: 4
- Number of orientation bins: 8
- Threshold : 0.0067 (i.e. Maxima of the DOG scale space below this threshold are ignored).

[1]For more information regarding SIFT please refer to appendix C

Once descriptors for the segment under analysis have been computed they are compared with the ones for each object in the library in order to estimate the pairs of matching features in the image. This feature matching is done through a Euclidean-distance based nearest neighbor approach. Let us denote as α the number of matching features between a segment and a particular object. All the segments for which $\alpha > 0$ are sent to the histogram thresholding unit. It is intuitive to state that the greater is α the more likely is that the segment under analysis contains the target object due to the greater number of matching features. If $\alpha = 0$ for all the segments it means that the object is not present or it has not been detected.

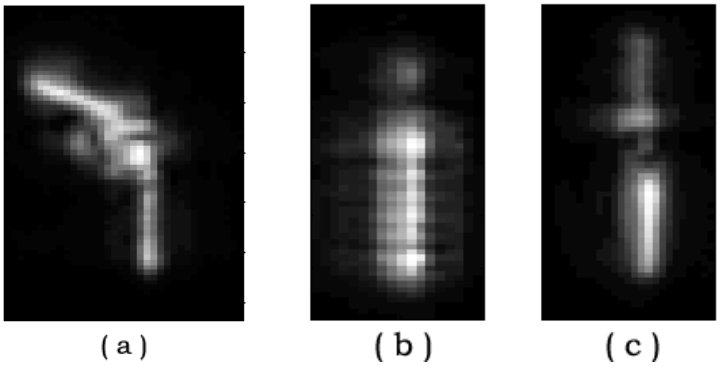

Figure 4.4.: An example of sample objects in the library. (a) gun (b) bottle (c) ceramic knife

4.4. Histogram thresholding

Candidate segments, which are determined by SIFT, where the target is likely to appear are sent to histogram thresholding unit for further investigation. Many segments for which $\alpha > 0$ unfortunately do not contain an object but just random background. Histogram thresholding is a really valuable tool that allow us to discard those background segments which are causing false alarms. For each candidate segment, an image intensity histogram with 1024 bins is computed. The number

of bins have been set to 1024 in order to guarantee sufficient accuracy. Since all the segments intensities are normalized between 0 and 1, it has been verified experimentally that segments with a concealed object must contain histogram with pixel intensities greater than 0.8. Finally, all the segments for which $\alpha > 0$ not containing intensity values greater than 0.8 in the histogram are discarded. The remaining segments (i.e. the ones for which $\alpha > 0$ and containing histogram intensity values greater than 0.8) are sent to the correlator.

4.5. Correlator and Ranking Matrix

In order to reduce the false alarm rate all the segments that verified the histogram thresholding and SIFT matching conditions are sent to a correlator for further investigations. The correlator computes $CP(x_p, z_r) = I_{ij}(x_p, z_r) \star Obj(x_p, z_r)$ or $CS(x_p, z_r) = I_{mn}(x_p, z_r) \star Obj(x_p, z_r)$ if the segment belongs to a secondary grid. Subsequently, a correlation coefficient denoted as β is computed as $\beta = \sum_{p=1}^{P} \sum_{r=1}^{R} CP(x_p, z_r)$ or $\beta = \sum_{p=1}^{P} \sum_{r=1}^{R} CS(x_p, z_r)$ depending on the grid. The value β has been defined in such way in order to guarantee a partial rotational invariance of the correlator.

At this point, there are two values denoted as α and β available in order to estimate the segment which is likely to contain the object under analysis. This two values are combined together into a new variable denoted as Score:

$$S = \beta(1 + \alpha) \tag{4.1}$$

Equation (1) weights between the correlation coefficient which usually varies between 10^3 and 10^4 and the number of matching features which usually varies between 1 and 20.

Subsequently, for each segmentation parameters (i.e. k_x and k_z) a Ranking Matrix is defined. The segments included in this matrix are the ones for which $\alpha > 0$ (i.e. the number of matching features of the segment with a specific object is greater than 0) and which also fulfilled the histogram thresholding requirement of having intensities greater than 0.8 in their histogram. Only the segment which present the greatest value of S is sent to a so called Global Ranking Matrix for final output decision. The Ranking Matrix is ordered in such a way that $S_1 > S_2 > ... > S_K$ and its size is Kx8 where K is the number of candidate segments. An example on how a ranking matrix looks like is shown in Table 4.1.

S	α	β	P/S	i	j	m	n
S_1	α_1	β_1	P	1	2	-	-
S_2	α_2	β_2	S	-	-	1	3
S_3	α_3	β_3	S	-	-	3	1
S_4	α_4	β_4	P	3	3	-	-

Table 4.1.: Example of a Ranking matrix for a fixed value of the segmentation parameters. P=Primary grid segment, S=Secondary grid segment.

4.6. Global Ranking Matrix

The Global Ranking Matrix has the task to choose the segment which it is considered as the one containing the object $Obj(x_p, z_r)$ under consideration. For each of the four possible value choices defined in section 4.2 of the pair of segmentation parameters k_x and k_z the two segments with the highest value of S are stored in a newly defined Global Ranking Matrix . The GRM selects the segment which presents the highest value of S among all the possible segmentations (i.e. (k_x,k_z) pairs). Moreover, the GRM size is always a 4x10 matrix with $S1 > S2 > .. > S_4$. An example of how the GRM looks in practice is shown in Table 4.2. Finally, the selected segment (i.e. the one with the greatest Score value) is sent to the output since it is considered as the

one containing the object.

S	α	β	P/S	i	j	m	n	k_x	k_z
S_1	14	10^5	P	1	2	-	-	4	4
S_2	16	10^4	S	-	-	2	2	3	6
S_3	12	10^3	P	3	3	-	-	5	5
S_4	7	10^2	S	-	-	2	1	6	6

Table 4.2.: Example of a Global Ranking Matrix. P=Primary grid segment, S=Secondary grid segment.

4.7. Conclusions

This chapter introduced a new concealed weapon detection method, named as SIFT Analysis, tailored for the radar microwave imaging environment. The main idea behind the proposed method is to compare the microwave image of a series of harmful and harmless contained in an object library with the image of a mannequin carrying those objects on its body. After an initial image projection of the 3D volumetric scalar data of the mannequin a procedure of image segmentation is performed. The segmentation is done in such a way that at the output of the unit has a total number of 8 different segmentations grids which are available for further investigations. Such number of segmentation grids is needed in order to improve the detection probability (i.e. the object on the mannequin is more likely to fall entirely in just one segment). Each segment is then processed by the SIFT unit which looks for the number of SIFT matching features α between a specific object and the segment under analysis. SIFT has been employed since it is a computer vision algorithm that has the ability to match features between two images with invariance to image scaling and rotation and has shown to be robust with respect to a range of affine distortions, change in 3D viewpoint, addition of noise and change in illumination. SIFT processing is then followed by an histogram thresholding unit which discards segments that are consid-

ered false alarms by doing histogram intensities considerations which are described in section 4.4. The candidate segments which are not discarded by the histogram thresholding unit are then sent to a correlation unit for further verification. For each segment a correlation coefficient β is computed. The correlation coefficient is weighted over α by the Score variable defined as $S = \beta(1 + \alpha)$. The information about the candidate segments for each segmentation and their Score values are then combined together in a Ranking Matrix. Only the segment which present the highest value of S for each possible segmentation is sent to a Global Ranking Matrix which decides the final output by selecting the segment with the highest value of the Score parameter. Experimental results of this method will be described in Chapter 5.

Bibliography

[1] Zuiderveld, Karel (1994), "Contrast limited adaptive histogram equalization", Graphics gems IV, Academic Press Professional, Inc., pp. 474485

[2] An implementation of the SIFT detector and descriptor - Vedaldi - 2007

5. Experimental Results and Comparative Analysis

"*Symmetria est* in mente"

Kant

5.1. Overview

This chapter contains the results and comparative analysis of the Depolarization and SIFT methods developed respectively in Chapter 3 and Chapter 4. To establish the validity and reliability of the two algorithms a measurement campaign has been carried out. Since concealed weapon detection finds one of its main application in airport security, a mannequin with various concealed object under its jacket has been deployed for the radar measurements[1]. The measurements have been performed in the DUCAT room of the Delft University of Technology by the means of a polarimetric SAR providing both HH and VV data. Regarding the choice of the concealed objects, a representative set of common harmful and harmless items which an individual may carry at an airport security checkpoint have been chosen. The object set consisted in a gun, a ceramic knife, a pair of keys, a mobile phone and a

[1]For more information regarding the measurements setup please refer to appendix B

bottle of water. It is important to notice that each object have been selected because it differs from the others in size, shape or material. This choice have been made in order to widely and accurately test the detection and classification capabilities of Depolarization and SIFT algorithms. The results of the application of Depolarization Analysis to the set of microwave images of the mannequin with different concealed objects on its body will be shown in section 5.2. Subsequently, in section 5.3 results of application of SIFT analysis to the images will be presented which is followed by a comparative analysis of the two methods in section 5.4. Finally, section 5.5 contains the conclusions of the chapter.

5.2. Depolarization Analysis Results

In this section, results regarding Depolarization Analysis will be presented and discussed. As explained in Chapter 3, this method exploits and combines both sets of polarization data (i.e. HH and VV) provided by the polarimetric radar in order to achieve concealed weapon detection by the means of a novel attribute called Depolarization angle. The Depolarization angle described in section 2.5 is a combination of the Polarization and Feature angles which are described in section 2.3.1 and section 2.4. Polarization Angle is the expression of a physical phenomenon which is scattering, while Feature Angle is the expression of symmetries in the image.

In order to perform the simulations, Depolarization Analysis has been algorithmically implemented in MATLAB R2010b. The main computational steps included the calculation of the main mathematical quantities of the method which are, as said before, the Polarization Angle, the Feature Angle and the Depolarization Angle. Furthermore extra processing time is needed in order to compute the algorithm steps that are included in the Detection Unit (see section 3.3). The average compu-

tational time needed to detect objects on a mannequin is about 8 seconds on a 2.00 Ghz Intel Core DUO CPU with 2 GB of RAM.

The measurements campaign which has been briefly in section 5.1 , consists of five cases (scenarios):

1. Mannequin with a concealed gun and a ceramic knife located respectively in the upper right part of the torso and upper left part of the leg under a cotton jacket.

2. Mannequin with a concealed gun and a ceramic knife under a cotton jacket. The gun is located on the upper right part of the torso but it is rotated compared to test case 1 while the knife is positioned on the lower left part of the leg.

3. Mannequin with a concealed gun and a pair of keys under a cotton jacket. The gun and the pair of keys are located respectively in the upper right part of the torso and in the lower left part of it.

4. Mannequin with a concealed gun and a mobile phone under a cotton jacket. The gun and the mobile phone are located respectively in the upper right part of the torso and in the lower left part of it.

5. Mannequin with a concealed bottle of water, a knife, a gun and a mobile phone under a cotton jacket. The bottle of water and the gun are located respectively in the upper right and in the upper left part of the torso. The knife is located on the upper part of the right leg while the mobile on the upper part of the left leg.

For each test scenario VV and HH polarization data have been collected. The scan area for all the measurements was 74x100 cm^2 with steps between the consequent positions of the antennas of 1 cm (75x101 points). The 3D images produced by

the radar had a size of 149x201x81 points. This is due to the fact that the spacing employed for the image is of 0.5 cm. Therefore the number of points in width and height are doubled compared with the one of the raw data. In depth, the number of points in the 3D image depends on the interpolation factor that has been used for the IFFT from frequency to time domain.

The test case 1 checked the capabilities of Depolarization Analysis to detect and classify a metallic dangerous object of medium dimensions represented by a revolver gun and a dielectric object of medium dimensions represented by the ceramic knife. After an initial energy projection in the frontal with respect to the mannequin plane, the horizontal and vertical polarization data are processed with a Laplacian and subsquently with a Prewitt filter. The Prewitt filter is enhancing edges depending on the initial polarization of the data (e.g. vertical polarization data edges are enhanced with a vertical prewitt filter). It is clear from the encircled areas of Figure 5.1 (a) and (b), which are respectively the barrel and the handle of the gun, that the features pointing in the horizontal direction are enhanced by the prewitt horizontal filter and the ones oriented in the vertical direction by the vertical prewitt filter.

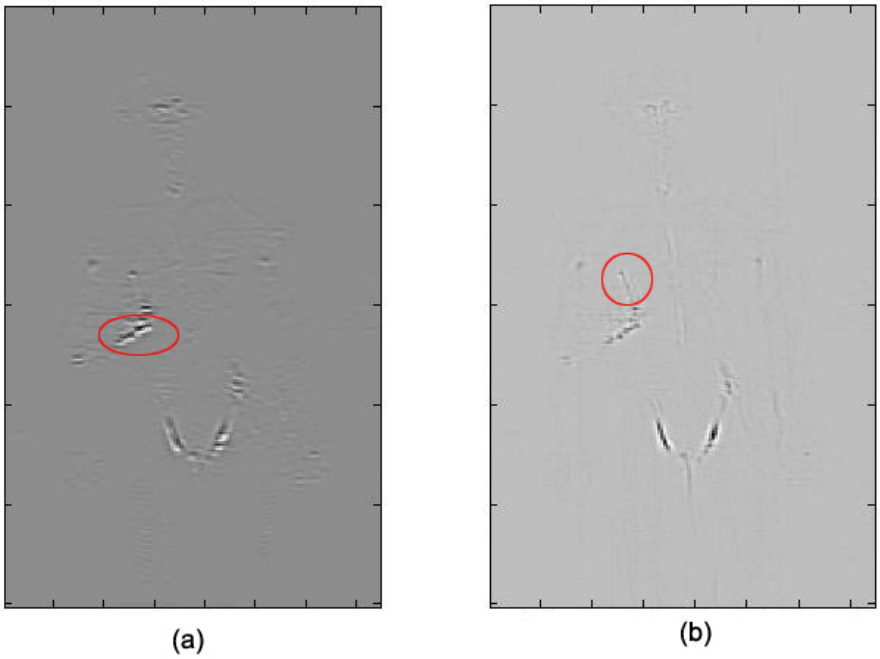

Figure 5.1.: (a) Horizontal Polarization Data (b) Vertical Polarization Data after Laplacian and Horizontal/Vertical Prewitt filters

We can see in Figure 5.3 the images of horizontal and vertical polarization data for this test case along with the images of the Polarization and Feature Angle which are needed for computing the Depolarization Angle. As we can see from Figure 5.3(c) and (d) even before computing the Depolarization Angle, the visual perception of the weapons on the mannequin has already improved compared to the original data.The Polarization Angle highlights very clearly the edges of the objects and in particular the ones of the gun. This can be explained by the fact that reflections from sharp edges cause a shift in the Polarization Angle compared to the background (i.e. the mannequin). On the other hand, Feature Angle is highlighting the symmetric features of the objects and especially the gun position on the upper right part of the torso. In fact, the body areas of the mannequin where the objects are located are showing a greater density and a greater variability in the direction of symmetry lines

compared to the rest of the mannequin. After computing the Polarization and Feature angles, the Depolarization Angle is computed and an example of this is shown in Figure 5.4 for the test case 1. As explained in section 3.3.1, the threshold which is considered meaningful for detecting an object has been set to 0.8 or -0.8 depending on the average Depolarization Angle value of the image. The Depolarization Angle histogram for test case 1 is shown in Figure 5.2.

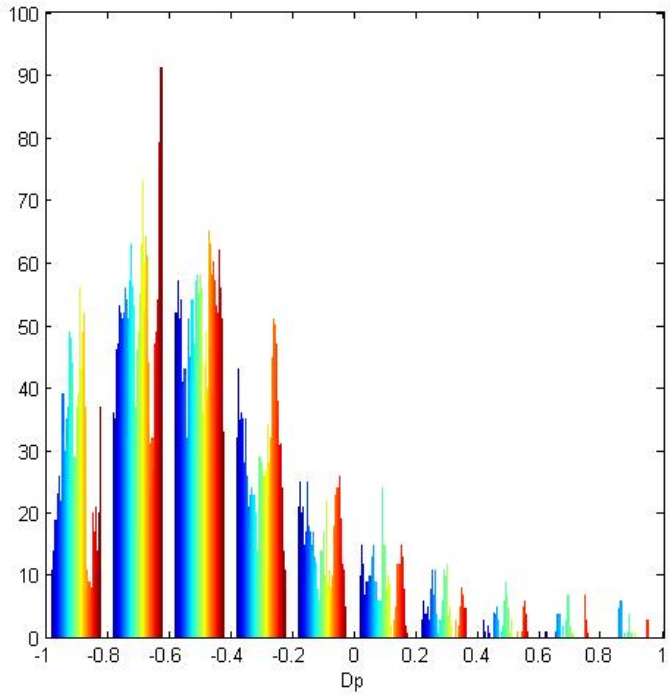

Figure 5.2.: Depolarization Angle histogram when the average Depolarization Angle value is negative

By inspecting Figure 5.4 it is clear that not only objects, but also some part of the background, like the one encircled in Figure 5.4, falls in that particular threshold causing false alarms. As said in Chapter 3, the Detection Unit has the purpose to reduce the number of false alarm points by performing symmetry verifications on the image which are described in section 3.3.2, 3.3.3 and 3.3.4. Among all the Depolarization Angle values which exceed the threshold, in Figure 5.5 the red en-

circled areas are the one detected by the detection unit. The usefulness of this unit is clearly shown in Figure 5.6 where the final output for the test case 1 is presented and which shows detection spots belonging only to the gun or the knife respectively achieving a perfect detection. From this test case we have seen how Depolarization Analysis is capable of correctly detecting objects and how it is possible to reduce the false alarm rate by the mean of the detection unit.

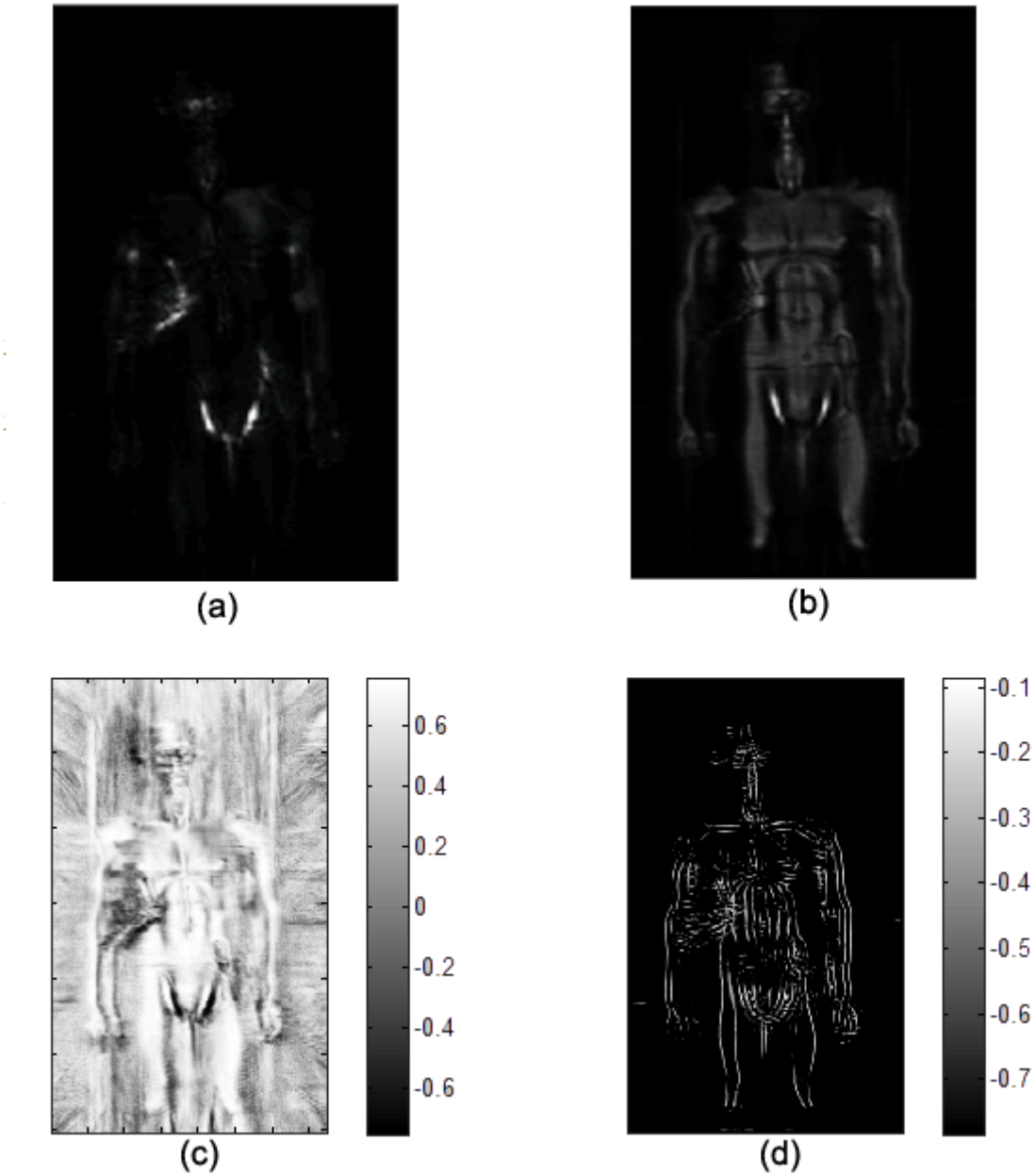

Figure 5.3.: (a) Horizontal polarization data (b) Vertical Polarization data (c) Polarization angle (d) Feature angle for test case 1

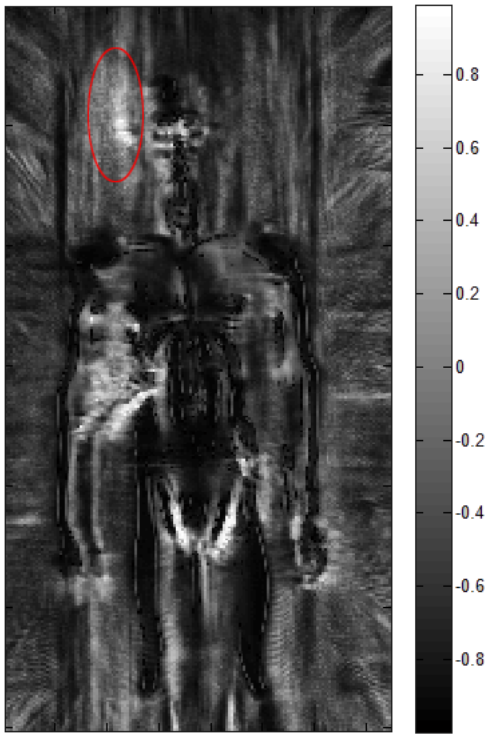

Figure 5.4.: The Depolarization Angle for test case 1

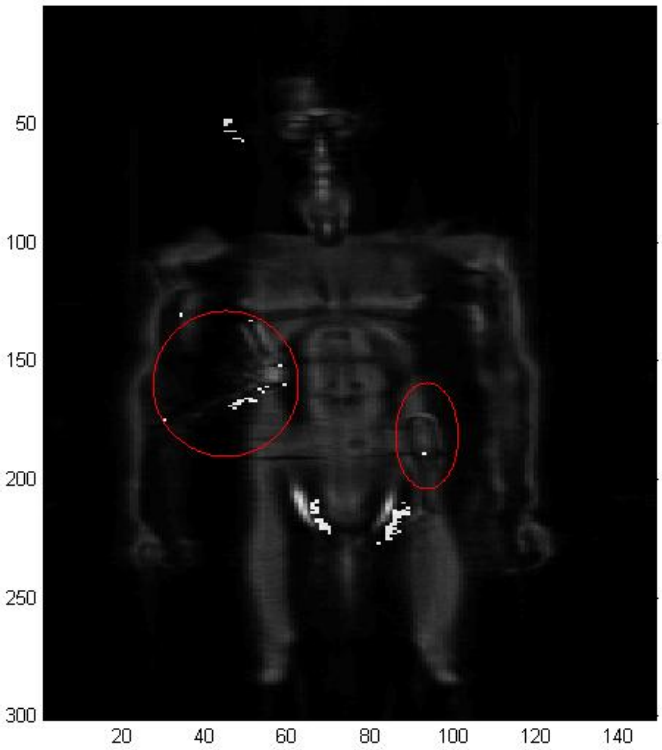

Figure 5.5.: Mannequin image with values for which Dp>0.8 marked in white. Red circles are the points detected by detection unit.

Figure 5.6.: Image processing chain output for test case 1

The test case 2 is a slight variation of test case 1 which assessed if the algorithm is able to detect objects when a rotation occurs. In Figure 5.7 the output for this test case is shown along with the optical image of the mannequin with weapons on its body. As we can see, the algorithm clearly detected the gun and the ceramic knife which is marked by points A and B in Figure 5.7, representing respectively the handle and the tip of the knife. Points C (abdomen-torso separation) and D (neck indentation) in Figure 5.7 represent two false alarms due to strong reflections from body areas of the mannequin that, due to their particular shapes, cause a corner reflector effect that makes them assume a Depolarization Angle value similar to the one of the objects.

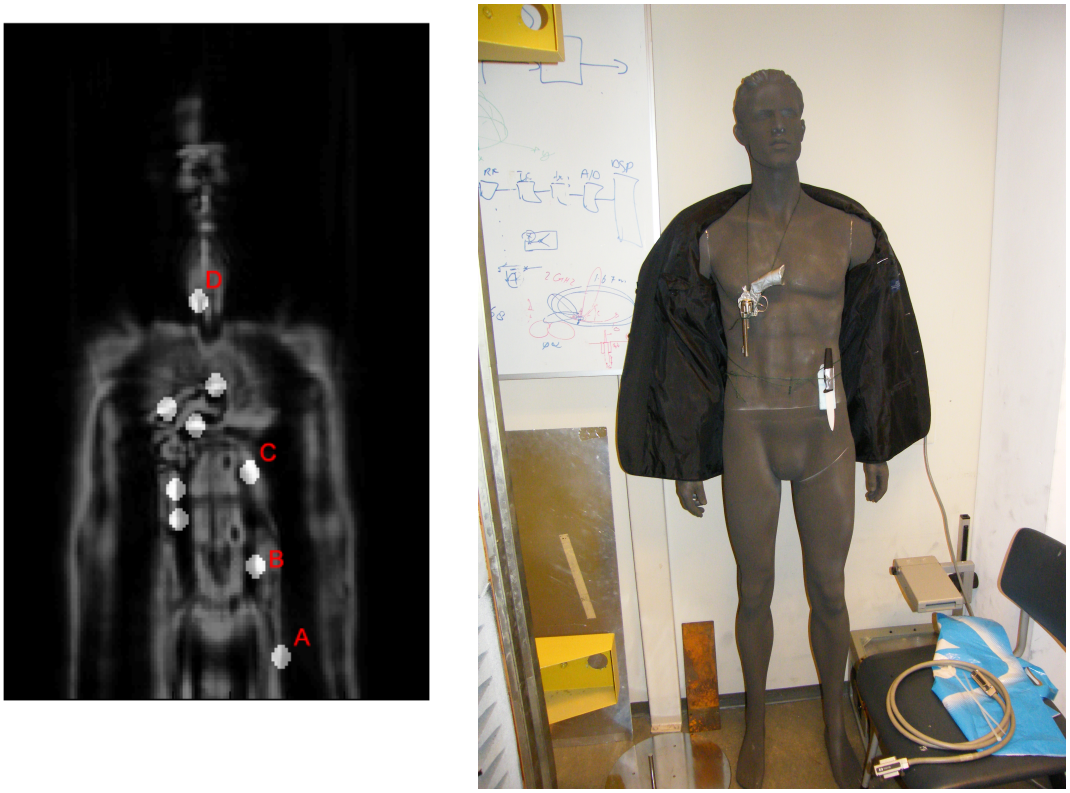

Figure 5.7.: Output for Test Case 2 (left) and Optical image of the mannequin for Test Case 2 (right)

The test case 3 and test case 4 verified how the algorithm responds in an almost similar test scenario as test case 3. In these experiments the gun is kept at the same place as in test case 2 while in test case 3 the knife has been replaced by a pair of keys and subsequently by a mobile phone in test case 4. These two experiments, for which the output is shown in Figure 5.8, demonstrate that Depolarization Analysis is capable of detecting a small metallic object (i.e. keys) which is marked as A and B in the left figure and small metal-dielectric objects (i.e. mobile phone) which is marked as E in the right figure. Is it possible to see in Figure 5.8 that the gun is consistently detected in both experiments. Moreover, the same issue of false alarm, which was present in the test case 2, due to corner reflector effect from indentation in some parts of the human body is also appearing in these experiments

especially in arm, neck and groin area (points respectively marked as C, D, F and G in Figure 5.8). False alarms which are caused by the head of the mannequin are of very little concern and therefore discarded due to the fact that is almost impossible that a concealed object would be carried in that body region.

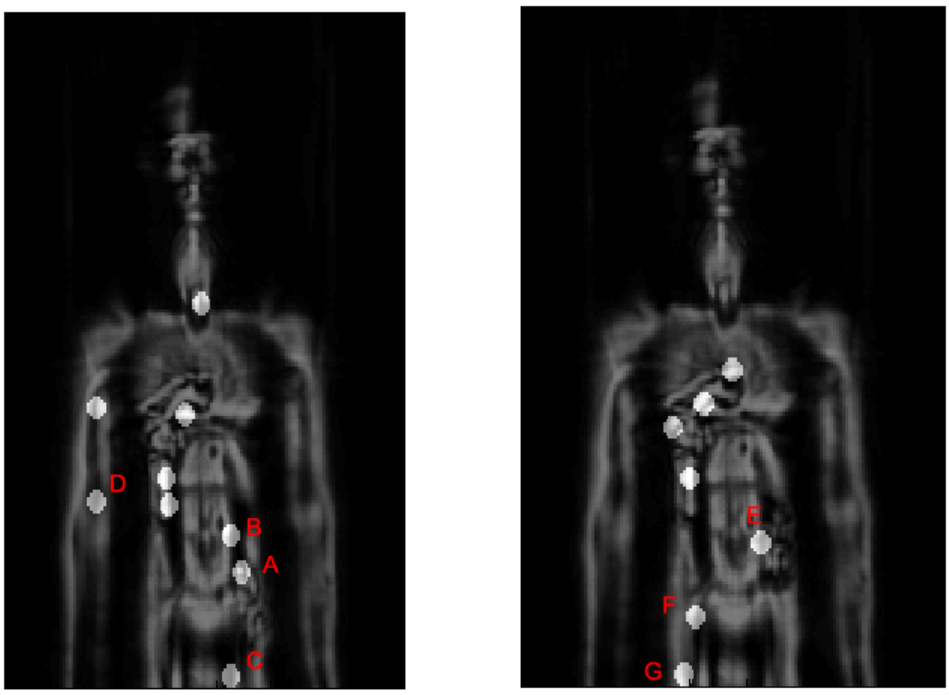

Figure 5.8.: Output for Test Case 3 (left) and output for Test Case 4 (right)

The main purpose of test case 5 was to verify if the Depolarization algorithm is capable of detecting a gun in a different position compared to the other four test cases along with a medium size dielectric object which is a bottle of water. In this test case also a mobile phone and a knife are present. According to the results shown in Figure 5.9 the algorithm is capable to clearly detect the gun and the bottle of water (point marked as A in figure Figure 5.9). The knife, which is positioned on the upper right leg of the mannequin, is not detected. This happened not due to an

algorithm limitation but due to the fact that it was positioned near the edge of the antenna aperture which made it not clearly visible in the radar image. Furthermore, this time the algorithm failed to detect the mobile phone and a false alarm, marked as B in Figure 5.9, is present in the groin area of the mannequin.

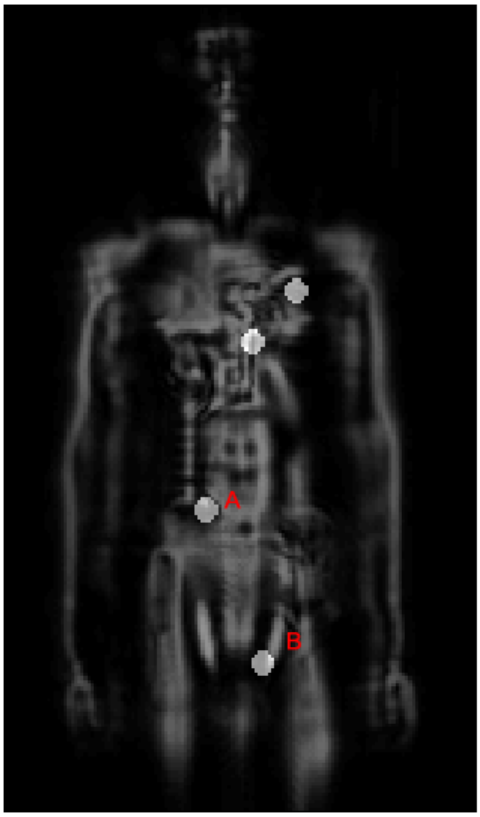

Figure 5.9.: Output for test case 5

From the described results we can state that, apart from minor false alarm rates due to indentation of specific areas of the human body which (i.e. groin,arm and neck), the Depolarization Analysis was capable to detect objects which differ from each other in shape, size and material without the need of any form of segmentation but only exploiting the data provided by the dual polarization radar with a success

rate of 10 out of 11 trials. Furthermore, the experimental results of the concealed gun show that detection capabilities are invariant to the position of the object on the mannequin.

It is important to underline that the algorithm was not able to classify object. This can be explained by the fact that the majority of objects present similar Depolarization angle values.

5.3. SIFT Analysis Results

After describing in section 5.2 the results of Depolarization Analysis, this section is dedicated to the results of SIFT Analysis. As explained in Chapter 4, the main elements of this algorithm are the segmentation unit, the three step detection procedure composed by SIFT, a correlator and histogram thresholding and a Ranking Matrix for final output decision. SIFT Analysis is a method that has its core in the SIFT algorithm which allows to extract interesting points of an object by providing a mathematical description of it (i.e. feature description) and then try to match this feature description to the one of a different image (i.e. the matching is successful if the image contains the same object). In order to start the matching procedure, an object library in the form of microwave images containing harmful and harmless object, have been build. The chosen objects set, which is particularly suitable for aiport security applications, consisted in a gun, a ceramic knife, a mobile phone, a pair of keys and a bottle of water. This objects were SAR scanned in an anechoic chamber simulating the free space. Moreover, the object library is also needed for the operations of the correlation unit described in section 4.5. After the object library have been built a measurement campaign have been carried out in order to provide the images of the mannequin with the concealed objects. The following

test cases have been performed in order to evaluate the automatic detection and classification performances of the method:

1. Mannequin with a concealed gun and a ceramic knife located respectively in the upper right part of the torso and upper left part of the leg under a cotton jacket.

2. Mannequin with a concealed gun located in the right part of the torso under an heavy winter jacket

3. Mannequin with a concealed bottle of water, a knife, a gun and a mobile phone under a cotton jacket. The bottle of water and the gun are located respectively in the upper right and in the upper left part of the torso. The knife is located on the upper part of the right leg while the mobile on the upper part of the left leg.

4. Mannequin with a concealed gun and a mobile phone under a cotton jacket. The gun and the mobile phone are located respectively in the upper right part of the torso and in the lower left part of it.

5. Mannequin with a concealed gun and a pair of keys under a cotton jacket. The gun and the pair of keys are located respectively in the upper right part of the torso and in the lower left part of it.

Moreover, the algorithm as introduced and described in Chapter 4 has been implemented in MATLAB R2010b. The main computational steps involved the calculation of the segmentation branches and of the three step detection procedure (i.e. SIFT, Correlator and Histogram thresholding). The average computational time needed to detect objects on a mannequin is about 6 seconds on a 2.00 Ghz Intel Core DUO CPU with 2 GB of RAM. This slightly longer computational time compared to Depolarization Analyis is due to the multiple segmentations (refer to

section 4.2 for more information) that requires only by itself 10 seconds to run. It is clear that a tradeoff between robustness and computational time has to be taken under consideration. An increase in number of segmentations will increase detection rate (i.e. the object is more likely to entirely fall in one segment) but at the cost of an higher computational time.
SIFT analysis developed in Chapter 4 claimed to be robust in indentifying object in low contrast condition. In particular an object included in the library can be matched, if present, on the mannequin even under different scaling, orientation and also affine distortions and illumination changes. The measurement setup previously described has been specifically designed to test these capabilities.

Test case 1 assessed the ability of SIFT Analysis to detect a gun and a ceramic knife. Compared to Depolarization Analyis, SIFT is not exploiting any physical property of the object therefore the material is not relevant but only the size and the position over the mannequin. As shown in Figure 5.10 the method is able to recognize the gun. In particular, in the top box of Figure 5.10 (a) the matching between the segment considered as the one containing the target and the object in the library (located in the right part of the box) is shown. As we can see from this box, even under a 3D rotation of the weapon the algorithm is capable of associating correctly the points belonging to the barrell of the gun. The final output for the gun of test case 1 is shown in Figure 5.10 (b). Another example of successful gun detection is shown, for test case 2, in Figure 5.11. It is important to state that the detection is sensitive to the number of segmentations. The SIFT algorithm was not recognizing the gun in test case 1 if more than two parallel segmentations were used due to false alarms caused by parts of the mannequin's body. Regarding the ceramic knife, it is not possible to detect it. The same happens for the ceramic knife in test case 3, for the mobile phone of test case 3 and 4, for the pair of keys of test case 5 and for the

gun of test case 3 and 4. This can be explained by the fact that radar measurements can distort the geometry of objects due to interference patterns that arise between the items and the mannequin.

For its intrinsic nature SIFT algorithm is likely to find feature points in high-contrast regions of the image such as objects corners.

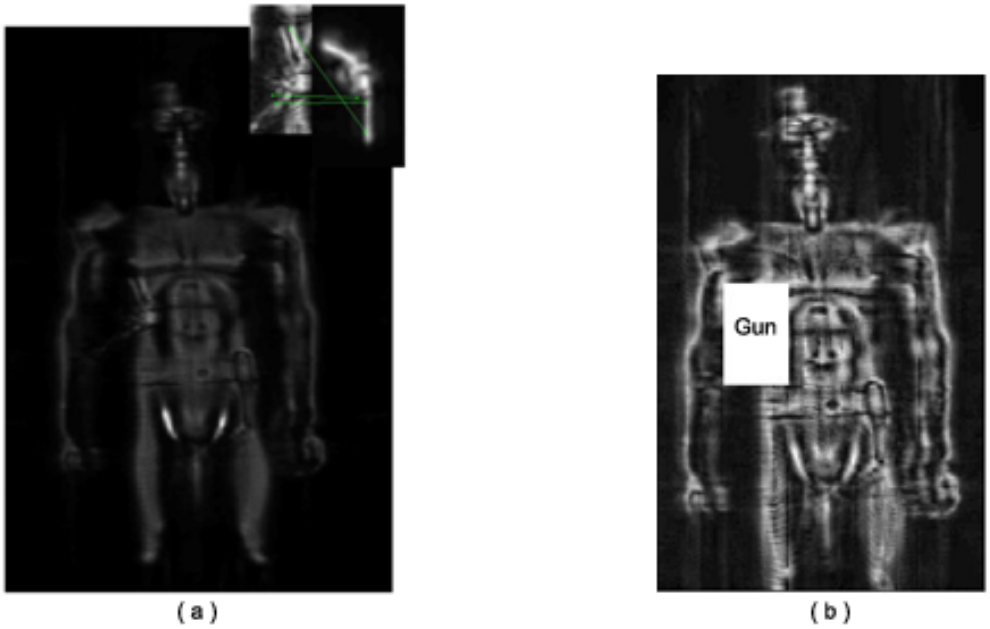

Figure 5.10.: (a) Measured Mannequin for Test Case 1 (b) Output for Test Case 1

Furthermore, in comparing two images it is important that the relative position between the object features in the library and the object features, when the same item is positioned on the body of the mannequin, should not change. Therefore feature matching would not typically work if any change in the object internal geometry happens between two images which is the case in microwave images due to the above described interference phenomena. To make this clear let us consider the syntethic example in Figure 5.12. As it possible to see in Figure 5.12 (a) and in Figure 5.12 (b) a change in the object geometry due to interference and noise will

cause 4 out of 6 features to be different causing the detection to fail. It's important to notice that SIFT algorithm has been developed for optical images where the problem of geometric distortion due to interference is not as prominent as in the microwave ones.

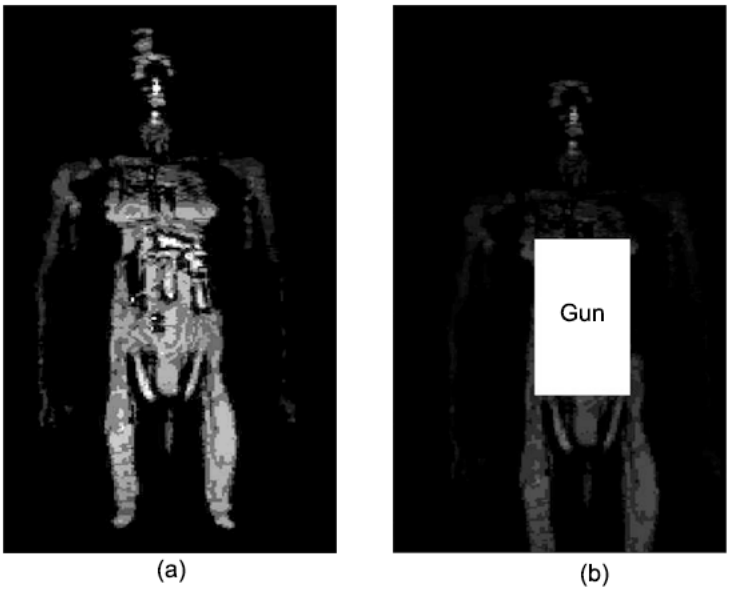

Figure 5.11.: (a) Measured Mannequin for Test Case 2 (b) Output for Test Case 2

Figure 5.12.: Syntethic example of image distortion. (a) Distorted object on the mannequin (b) same object in the library

Finally, test case 5 have been designed to test the capabilities of the SIFT Analysis to properly work when a multitude of objects are present in the same image. As it is possible to see in Figure 5.13 the algorithm is successful to uniquely detect both guns and bottle of water but fails to detect the knife and mobile phone. In this case the misdetection of the knife can be attributed to the fact that the object is not clearly visible in the radar image due to its position near the antenna aperture edge and not to the geometric distortion due to interference.

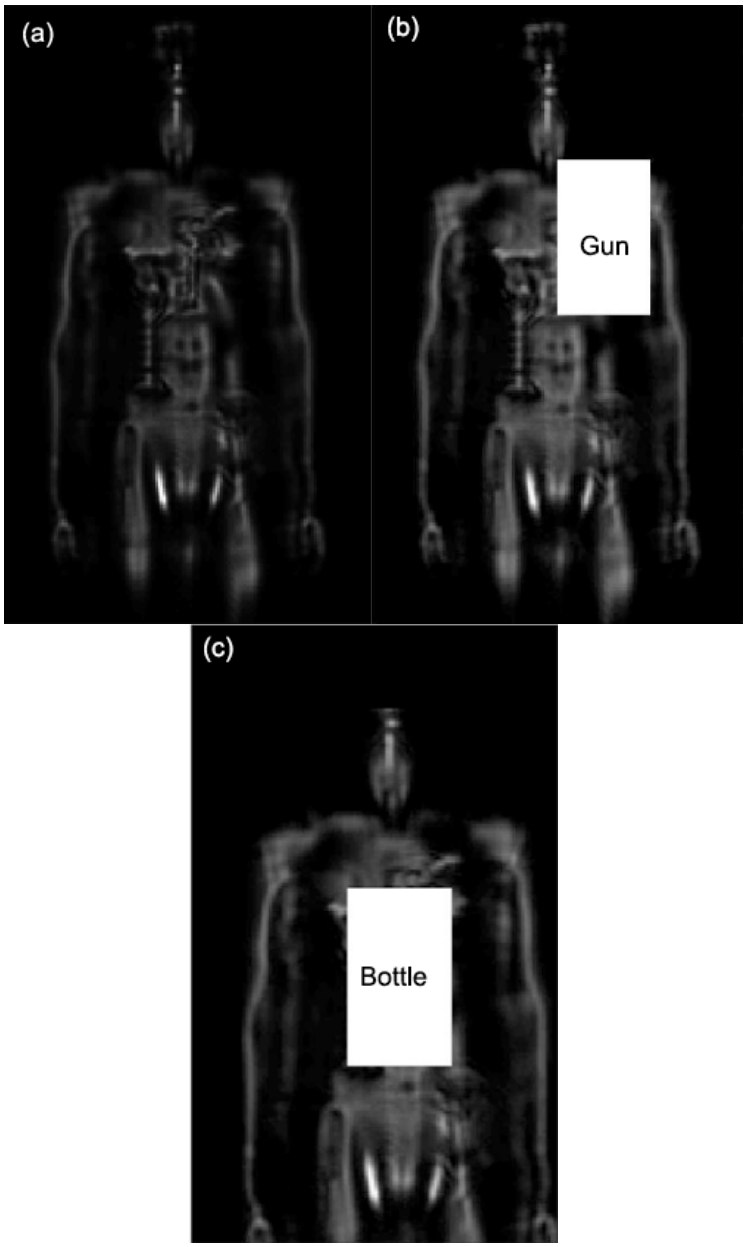

Figure 5.13.: (a) Measure Mannequin for Test Case 3 (b) Output for gun recognition (c) Output for bottle recognition

According to the above presented results, SIFT Analysis is capable of detecting and classifying a concealed gun on a mannequin under different experimental conditions (i.e. change in position, scale and orientation of the object) which is one of the thesis research objectives. Furthermore, a bottle of water was detected in a single

experiment. At the current implementation the algorithm proved not to be reliable and robust since it failed to detect different objects such as a pair of keys and a mobile phone. Moreover, the detection of the gun proved to be partially robust since was only detected three times out of five experimental trials.

5.4. Comparative Analysis

Depolarization and SIFT Analysis represent two different approaches to concealed weapon detection. The first one (i.e. Depolarization Analysis) exploits both physical and geometrical properties of objects, which can be retrieved by the radar to robustly detect objects in a microwave image. On the other hand, SIFT Analysis is inspired by typical optical imaging matching procedures which relies only on the geometric shape of the objects. According to what it has been shown in section 5.2 and section 5.3 the following considerations can be done:

- Depolarization Analysis is only capable of detecting objects while SIFT Analysis is capable of both detecting and classifying them. However, Depolarization is more consistent than SIFT. In particular SIFT method fails to detect keys, knifes and mobile phones due to geometric distortions in the image while Depolarization is able to detect all of them.
- Depolarization Analysis does not require segmentation while SIFT do. The ability of an algorithm to work without a segmentation procedure is likely to increase its detection rate while keeping the computational costs low.
- Depolarization Analysis does not require an object library to work. This means that *a priori* knowledge of the entire set of objects that an individual may carry is not required, making the algorithm versatile and more efficient. On the other hand, SIFT do require an object library to classify objects but at

the price of being less versatile.

- Depolarization Analysis requires both polarization data (i.e. VV and HH) in order to work while SIFT Analysis requires only the vertical polarization data. The fact that SIFT does not require a dual polarization antenna makes it more likely to be practically applied in surveillance systems due to the lower price and technological complexity of the antenna system.
- Depolarization Analysis and SIFT Analysis are both affected by false alarms caused by indentations of the human body which appear as objects in the microwave radar image.

A summary of the above considerations is shown in Table 5.1.

Method	Detection	Classification	Polarization	Segmentation	Object Library
Depolarization	yes	no	dual	no	no
SIFT	yes	yes	single	yes	yes

Table 5.1.: Comparative Analysis between the two proposed methods

5.5. Conclusions

This capter was dedicated to the assessment of the performance of the concealed weapon detection methods developed in Chapter 3 (i.e. Depolarization Analysis) and Chapter 4 (i.e. SIFT Analysis). In order to do so, a measurement campaign was carried out in the anechoic chamber of the Delft University of Technology. In the measurement campaign described in section 5.1 a mannequin with different harmful and harmless concealed objects has been scanned by a SAR radar. The

measurements have been carefully planned in order to evaluate the performance of the algorithms under different circumstances such as different position, material and size of the objects which were positioned on the mannequin. Subsequently, the obtained microwave images were processed by the means of MATLAB code implementing Depolarization and SIFT analysis respectively.

Depolarization analysis results are presented in section 5.2 and they show that this method is capable of robustly detecting a variety of objects (i.e. a gun, a pair of keys, a mobile phone, a ceramic knife and a bottle of water) which differ from each other for shape, size and material with a 90% success rate. Moreover, detection has proven to be invariant with respect to the position of the object on the mannequin. Despite the good detection performances, there are some false alarms caused by indentation of the human body from the arm, neck, abdomen and groin area. These body indentations, due to their particular interaction with the eletromagnetic energy radiated by the radar, assume a value of the Depolarization Angle which is similar to the one of actual objects. Therefore it is important to choose an appropriate threshold for the Depolarization Angle which has experimentally found to be effective when set to 0.8.

In section 5.3 SIFT analysis results are presented. From the experimental results SIFT method was able to detect and classify a concealed gun (success rate was three out of five test cases) under different measurement conditions such as rotation, scaling and different position of the object. In addition to this, a bottle of water was detected in a single trial. The method was not consistent in detecting a pair of keys, a mobile phone or a knife due to the geometric object distortions described in section 5.3. These distortions are caused by the interference patterns due to the interaction between the mannequin and the objects positioned on it. The choice

of segmentation parameters (i.e. k_x and k_z) is really important since it affects the detection rate. If the segments size are too small the object may be splitted in two different segments which will cause a drop in the detection rate. On the other hand, if the size of the each segment is too large then multiple of objects and too many features of the human body will end up in the same segments. This second hypothesis is also likely to decrease the detection rate.

Finally, in section 5.4 a comparative analysis between the two methods is presented. Referring to Table 5.1 we can state that Depolarization Analysis is able to detect object but not to classifying them while SIFT method also has the possibility to identify them. Also, Depolarization Analysis proved to be more versatile than SIFT analysis due to the fact that it does not need a segmentation procedure or an object library to work. It is important to notice that Depolarization Analysis requires a dual polarization radar to work while SIFT Analysis does not making the latter method more likely to be applied in the field due to the lower price and complexity of the antenna system. We have seen how both methods are affected by false alarms caused by the human body. As shown in Table 5.2 body indentations are showing Depolarization Angle values on edges similar to the ones of actual objects.

Feature	$max\{\|Dp\|\}$
Bottle	0.83
Gun	0.96
Knife	0.81
Keys	0.99
Mobile	0.94
Body indentations	0.92

Table 5.2.: Maximum value for the Depolarization Angle for different features edges

An important role is this phenomenon is played by the resolution of the image. Microwave radar image do not offer a good resolution compared to the millimeter

and optical ones. By increasing the number of points in the image the objects are more detailed and the same happens with the anatomical details of the mannequin. Moreover, the number of indentations of the human body in the radar microwave image increases with the resolution. From the above considerations we can conclude that a higher resolution improves the details of the object allowing to better detect edges but at the same increases the rate of false alarms due to the increased number of indentations that look like object in the radar image. On the other hand, a coarser resolution compared to the microwave range is likely to reduce the number of indentations but at the same time it smoothes the edges of the image decreasing the detection rate.

6. Conclusions and Recommendations

6.1. Overview

This chapter concludes the thesis. The main objective of this thesis was to design novel robust image processing algorithms for the detection and classification of concealed weapons. Automatic weapon detection is an important part of every surveillance system. In the particular case of the body scanners at airports privacy concerns prevent showing high-resolution body images to the security operators and thus limiting application of the body scanners. By replacing the airport security operator with an automatic detection system this type of privacy concerns will no longer be present. In section 6.2 a summary of the developed methods is presented and the results will be compared to the research objectives stated in Chapter 1. In section 6.3 the scientific contributions made by this project are described. Finally, in section 6.4 a series of recommendations for further research are presented.

6.2. Conclusions

Two algorithms have been developed in the thesis for the automated target detection in the 3D high-resolution microwave images. The proposed algorithms are specifically tailored for working on images of humans (mannequin) produced by a microwave imaging radar and they are validated by MATLAB simulations and experiments.

The first method, which was developed in Chapter 3, is called Depolarization Analysis. This method exploits polarization properties of the radar (i.e. HH and VV data is retrieved by a SAR dual polarization radar) and geometric symmetry features of the combined image (i.e. the vertical polarization produced image is combined with the horizontal produced one) to create a novel shape descriptor called Depolarization Angle. Depolarization Angle can be considered as the ratio between the Feature and the Polarization angle which are respectively an internal and external shape descriptors introduced in chapter 2. In particular PCA and Phase symmetry algorithms play a major role in the processing stage by extracting respectively the Polarization Angle and the Feature Angle. It has been shown in section 2.3.1 and section 5.2 that Polarization Angle highlights very clearly the edges of the objects while the Feature Angle enhances the symmetry features of them. By selecting an appropriate threshold for the Depolarization Angle and by doing filtering, as explained in section 3.3, based on histogram thresholding and symmetry considerations it is possible to drastically reduce the false alarm rate and detect concealed objects in the image.

A measuring campaign of a mannequin carrying different concealed harmful and harmless for safety objects has been carried out in order to assess the validity and reliability of the algorithm. The campaign has been designed in such a way that the capabilities of the algorithm to detect objects with different shape, size, mate-

rial and position over the mannequin have been tested. Results of the measuring campaign, which are described in Chapter 5, show that Depolarization Analysis is capable of detecting various objects which included a gun, a pair of keys, a mobile phone, a ceramic knife and a bottle of water in ten out of eleven cases. Moreover, the results have shown that a minor number of false alarm points are present. This false alarms are originated by indentations of the human body that, due to their particular shapes, cause a corner reflector effect that make them assume a Depolarization Angle value similar to the one of the actual objects. Experimental results of the concealed gun show that detection capabilities are invariant to the position of the object on the mannequin. It is important to underline that the algorithm is not able to classify objects which can be explained by the fact that the majority of objects present similar Depolarization Angle values. In conclusion, Depolarization Analysis accomplished the thesis objective of reliably detecting objects but failed in the task of classifying them.

The second method, which was developed in Chapter 4, is called SIFT analysis. The research approach in this case, as explained in section 2.6, was to develop a detection and classification method for CWD inspired by computer vision algorithms used to detect and describe local features in images. The main task of the developed method consists in comparing a set of harmful and harmless objects stored in a library with a mannequin carrying a combination of them and see if the objects are correctly classified. The SIFT algorithm has been chosen to be the core of this detection method due to its capability to match features between two images with invariance to image scaling and rotation and robustness with respect to a range of affine distortions, change in 3D viewpoint, addition of noise and change in illumination. It is important to notice that SIFT has been developed for working with optical images and the application to the microwave range represents a challenge by

itself. SIFT analysis, apart from its main core which is the SIFT algorithm, also includes a segmentation unit which it is needed for increasing detection rate and a two step detection procedure formed by a Correlator and Histogram Thresholding which is needed to reduce the false alarm rate. A global ranking matrix, which it is introduced in section 4.6, finally declares which segment is considered as the one containing the object under test by producing a mathematical quantity called Score which takes under consideration the number of matching features α and the correlation value β for each candidate segment. In order to test the detection and classification capabilities of the algorithm a measuring campaign similar to the one of Depolarization Analysis have been carried out. From the results presented in section 5.3 is it possible to conclude that SIFT Analysis was able to detect and correctly classify a concealed gun three out of five cases and a bottle of water in another experiment. The algorithm proved to be not consistent in detecting a pair of keys, a mobile phone and a ceramic knife due to geometric distortions of objects caused by interference patterns that arise between the concealed items and the mannequin. Due to the above explained geometric distortions the matching between the library object and the correspondent object on the mannequin would not work due to displacement of the feature points from one image to another. In conclusion, SIFT Analysis partially accomplished the thesis objective of detecting and classifying objects but did not reach the objective of having a low false alarm rate.

From the Comparative Analysis in section 5.4 we can state that Depolarization Analysis proved to be way more robust than SIFT in detecting objects even though the algorithm is not able to classify them. Furthermore, Depolarization Analysis do not require an object library in order to work making it more versatile and efficient than SIFT. On the other hand, SIFT analysis can classify objects and it

does not require a dual polarization radar setup to work (i.e. a HH or VV image is sufficient for the algorithm to recognize the object). The fact that SIFT analysis does not require a dual polarization radar makes it more likely to be applied in airport security where a single polarization radar is usually on duty. Finally, no segmentation is needed in the case of Depolarization Analysis compared to SIFT making it more computational efficient and more likely to have an higher detection rate.

6.3. Summary of Contributions

As said in section 6.2 this thesis presents and discusses two novel algorithms, named as Depolarization and SIFT analysis, for concealed weapon detection.

Depolarization analysis is a new procedure inspired by a previous work on GPR buried pipes detection by Boniger and Tronicke. Furthermore, the algorithm proposed in Chapter 3 is a completely new method for concealed weapon detection. Due to this, the author of this thesis is reasonably sure of future prosperous development which are not known at the moment for this technique.

SIFT analysis takes its inspiration from object recognition method employed in the optical range. The approach proposed in Chapter 4 has never been employed before in concealed weapon detection.

Moreover, we can divide the scientific contributions according to Depolarization and SIFT method. For Depolarization analysis the following contributions are made:

- *Novelty*: Depolarization analysis is a new concealed weapon detection method that can detect concealed objects in a low contrast environment such as the microwave imaging one.

- *Novelty*: Successful application of Principal Component Analysis and of Phase Symmetry algorithm for the first time to the field of concealed weapon detection.
- *Novelty*: The algorithm does not require an object library. It is important to mention that this algorithm is not capable of classifying object but only to detect them.
- The algorithm does not require a segmentation of the image. This leads to a more reliable detection and a lower computational time.

For SIFT analysis the following contributions are made:

- *Novelty*: The SIFT Analysis is a new concealed weapon detection method which can detect and classify different concealed objects in a low contrast environment such as the microwave one under a wide spectrum of geometric transformation.
- *Novelty:* Application of an optical image matching algorithm (i.e. SIFT) to radar microwave imaging concealed weapon detection
- The algorithm requires a single polarization to work

6.4. Recommendations

Based on the results achieved by this project, the following recommendations for further research are given:

- In SIFT analysis some objects are still not recognized or detected with a high false alarm rate. Therefore the algorithm needs to be further developed in order to improve detection. As said in section 5.3 geometric distortions of the image will cause the algorithm to not detect objects. It is also true that

microwave produced image of objects do not have a fine resolution but some parts of the scanned object are always recognizable and represent an invariant feature. Let us consider the gun in figure 4.4 (a) as an example. As we can see from the image, the handle and the barrel of the gun are more defined in details than the rest of the object and the same is always true when the gun is on top of the mannequin. Therefore, by associating to SIFT another pattern matching algorithm which it is specifically tailored to detect those clearly recognizable parts of the gun, false alarm rate can be decreased. The same procedure can be applied to all the others objects in the library.

- Reduce the false alarm rate in Depolarization Analysis. As explained in section 5.2 some very specific parts of the human body produce an object like Depolarization angle value due to a corner reflector effect. By broadening the measurement campaign will be possible to deeper analyze this phenomenon and confirm the hypothesis that those reflection are always from the same specific parts of the body and therefore can be treated as systematic errors.

- Increase the variety of test concealed objects. In this research the algorithms have been tested to work only with 5 objects which where a gun, a ceramic knife, a bottle of water, a mobile phone and a set of keys. Objects which can be useful to detect are plastic explosives and more in general dangerous or restricted items which are likely to be taken on board of a flight.

- Try to apply Depolarization Analysis and SIFT analysis to other frequency ranges. In particular the millimiter wave range and X-ray range may be very suitable for the proposed algorithms due to the superior resolution compared to microwave range imaging.

- Project the data in different directions. Since the SAR radar which has been employed in this thesis is producing 3D images, in order to enhance detection

of extra objects it is possible to project the data in different directions from the one that has been chosen in this research project.

A. PCA

Principal component analysis is a valuable data analysis tool which has the goal of identifying the most meaningful basis, which is a linear combination of the original basis, to represent a data set. Let $\mathbf{X}$ be a m x n matrix representing the original data set . Each row element represents a physical quantity (i.e. measurement type) while each column an experimental trial. To give an example, if we were measuring voltage and current over a resistor at N different time intervals the matrix would be $\mathbf{X} = \begin{bmatrix} V(t_1) & V(t_2) & \cdots & V(t_N) \\ I(t_1) & I(t_2) & \cdots & I(t_N) \end{bmatrix}$. Let us define Y as the matrix $\mathbf{Y} = \mathbf{TX}$. Where $\mathbf{Y}$ is a new representation of the data set and $\mathbf{T}$ the matrix transformation that allows to express $\mathbf{X}$ in a more meaningful basis. Looking closer at $\mathbf{T}$ we can state that the rows are a set of new basis vectors for expressing the columns of $\mathbf{X}$ and ,from a geometric point of view, $\mathbf{T}$ is a strech and rotation of $\mathbf{X}$. We can now define the covariant matrix $C_X = \frac{1}{n} X X^T$ with the following properties :

1. The diagonal terms are the variances of a particular measurement type.
2. The off-diagonal terms are the covariance between different measurement types.

For the previous example the covariance matrix is

$$C_X = \frac{1}{n} \begin{bmatrix} \sum_{i=1}^{N} V^2(t_i) & \sum_{i=1}^{N} V(t_i) I(t_i) \\ \sum_{i=1}^{N} V(t_i) I(t_i) & \sum_{i=1}^{N} I^2(t_i) \end{bmatrix}$$

We assume that the data has high SNR. Therefore principal components with larger associated variances represent interesting structure while the others represents noise. The goal of PCA is to find an orthornal matrix $\mathbf{T}$ in $\mathbf{Y} = \mathbf{TX}$ for which C_Y is a diagonal matrix (i.e. $\mathbf{Y}$ is decorrelated) . We call the rows of $\mathbf{T}$ as the principal

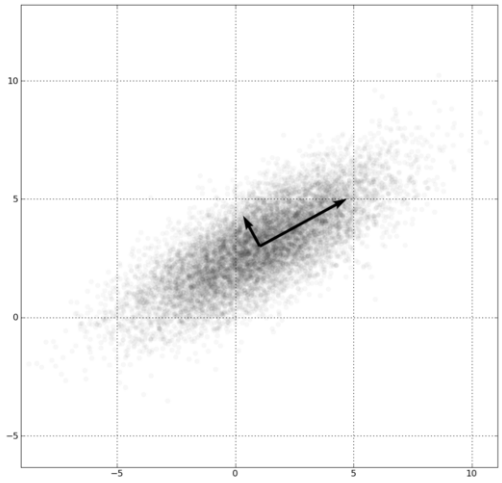

Figure A.1.: PCA of a multivariate Gaussian distribution centered at (1, 3) with a standard deviation of 3.

components of $\mathbf{X}$. It can be easily demonstrated that ,in order to diagonalize C_Y, each row of $\mathbf{T}$ has to be an eigenvector of C_X and $\mathbf{T}$ has to be orthonormal. To compute PCA of a data set $\mathbf{X}$ it is necessary to subtract off the mean from each measurement type and then compute the eigenvectors of $C_X$which in turns are the rows of $\mathbf{T}$. The approach described above represents the solution of PCA using eigenvector decomposition. As we can see in Figure A.1 the new basis, for the multivariate gaussian in figure, located by PCA is oriented along the direction where the variance of the data is maximized.

B. Measurements Setup

The measurements campaign needed to validate the methods developed in Chapter 3 and 4 was carried out in the anechoic chamber (DUCAT) of the IRCTR at Technical University of Delft.

The technical details of the deployed SAR radar shown in Figure B.1 are the following:

- The operating frequency range was set from 4 to 20 Ghz
- The employed antennas are two Vivaldi type ones
- The power transmitted by the radar was of 4 dBm
- The effective aperture of the radar was 75 cm in width and 1 meter in height
- The distance between the two feeding points of the antenna was 5.5 cm
- The distance between the antenna and the target mannequin was set 50 cm
- The cable used to connect the vector analyzer to the antenna where two Sucoflex-100 cables of 2 meters lenght which provide optimal perfomances up to 50 Ghz.
- The network analyzer employed to collect the data is an AGILENT E8364B shown in Figure B.4. For more technical details regarding the network analyzer refer to http://cp.literature.agilent.com/litweb/pdf/5988-7988EN.pdf

Measurements have been performed on a mannequin shown in Figure B.2 which was hiding different objects under a cotton jacket. The chosen items were a gun, a ceramic knife, a bottle of water, a pair of keys and a mobile phone. The selection of object is considered as a representative sample of a variety of dangerous or restricted items that an individual can carry at an airport security checkpoint.

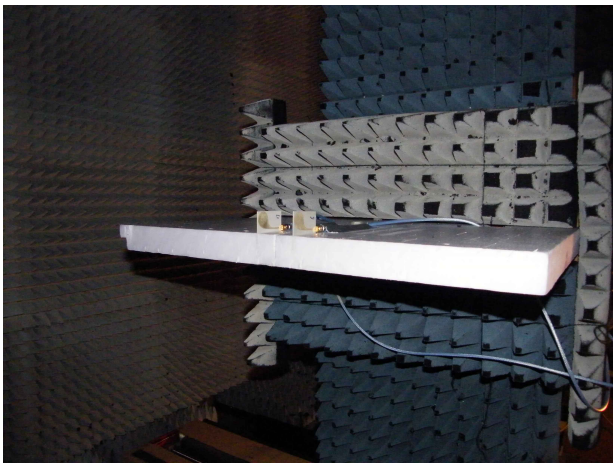

Figure B.1.: SAR antenna

Figure B.2.: Mannequin which has been employed in the measurements

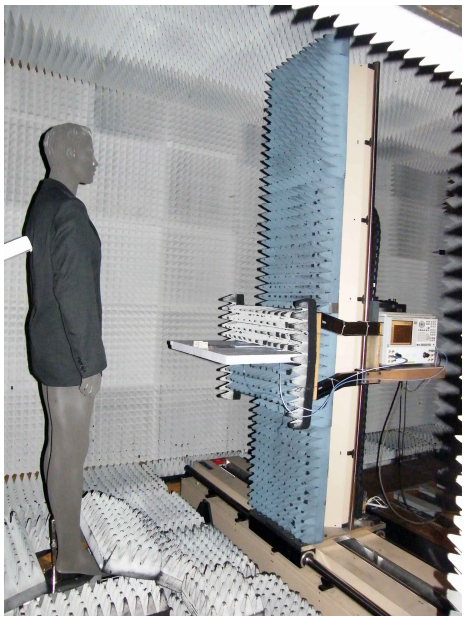

Figure B.3.: Mannequin positioned in the anechoic chamber

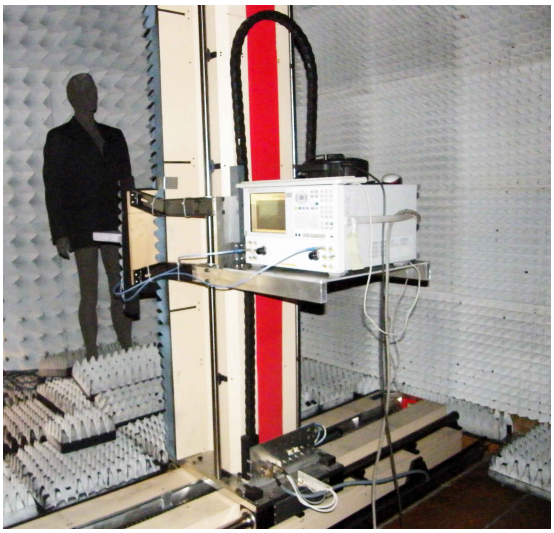

Figure B.4.: Mannequin positioned in the anechoic chamber with the AGILENT E8364B network analyzer clearly visible in the front

C. SIFT

Matching features from one image to another is a common problem in computer vision. Unfortunately images are not always the same in scale, orientation and illumination. SIFT algoritm has the ability to match features between two images with invariance to image scaling and rotation and has shown to be robust with respect to a range of affine distortions, change in 3D viewpoint, addition of noise and change in illumination.

The first step of the algorithm is to create an internal representation of the original image $I(x, y)$ to ensure scale invariance. In order to create a scale space the original image is progressively blurred out by convolving it with a Gaussian blur operator described by :

$$G(x, y, \sigma) = \frac{1}{2\pi\sigma^2} e^{-(x^2+y^2)/2\sigma^2}$$

Where σ is the scale parameter. The scale parameter in a way controls the amount of blur applied to the image.
The blurred image is defined as:

$$L(x, y) = I(x, y) * G(x, y, \sigma)$$

Let us assume that the blurring in a particular image is σ. Then the amount of blur

in the next image will be $k\sigma$ where k is a constant. A set of progressively blurred images forms an octave. The number of blur levels has been found to be effective when set to 5. Subsequently, three more octaves are formed by reducing the original image in the previous octave to half its size and performing for each octave the blurring procedure again. Therefore the number of octaves is set to four. After the scale space of the image $I(x, y)$ have been generated by the procedure described above, the blurred images are used to generate another set of images called the Difference of Gaussians (DoG). The DoG images represent a smart way of approximating the Laplacian of Gaussian (LoG) operations which are computationally intensive.

To calculate the DoG images the difference between two consecutive scales images is computed (i.e. $L(x, y, k\sigma) - L(x, y, \sigma)$). The procedure of computing the DoG image is shown Figure C.1. As said before DoG is approximating the LoG operation which is represented by $\nabla^2 G(x, y)$. In order to obtain scale invariance the LoG operator shall be multiplied by σ^2. It has been found that the DoG operations are already performing implicitely the multiplication by σ^2 therefore achieving scale invariance.

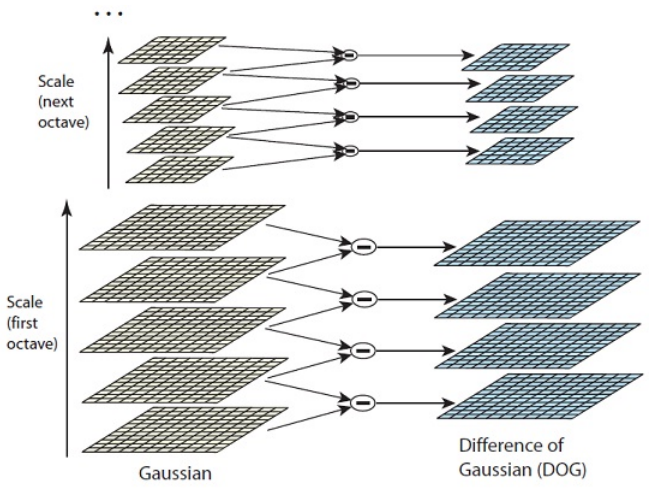

Figure C.1.: DoG calculations

After the DoG images are computed for each consecutive scale images for every octave, the next step is to find keypoints. Keypoints are located by a two step

procedure consisting in finding first the maxima/minima of DoG and then by finding subpixel maxima or minima. The first step of the procedure is performed by iterating through each pixel and check all its neighbours and see if that pixel is a maxima or a minima. The check is performed by comparing the current image to the one above and below at the same octave as shown in Figure C.2. The pixel marked as x in Figure C.2 is considered a keypoint if it is the greatest or least of all 26 neighbours.

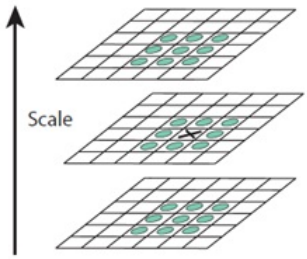

Figure C.2.: Maxima/Minima of DoG

Subpixel maxima or minima are then found by performing a Taylor expansion of the scale-space function of the image around the approximate keypoint:

$$\mathbf{D}(\mathbf{x}) = \mathbf{D} + \frac{\partial \mathbf{D}^T}{\partial \mathbf{x}}\mathbf{x} + \frac{1}{2}\mathbf{x}^T\frac{\partial^2 \mathbf{D}}{\partial \mathbf{x}^2}\mathbf{x}$$

The subpixel values are calculated in order to increase the chance of matching and stability of the algorithm.

By this procedure a lot of keypoints are generated. The ones lying on edges of the image or not having enough contrast are discarded. Edges are evaluated by computing for each keypoint two perpendicular gradients and check for their magnitude. The ones with small gradient magnitudes are discarded. Low contrast feature are discarded by performing intensity thresholding for each pixel.

Once keypoints have been computed an orientation needs to be assigned to each one of them. This is needed in order to achieve rotation invariance. For each keypoint

gradient magnitude and orientations are calculated the following way :

$$m(x,y) = \sqrt{(L(x+1,y) - L(x-1,y))^2 + (L(x,y+1) - L(x,y-1))^2}$$

$$\theta(x,y) = arctan((L(x,y+1) - L(x,y-1))/(L(x+1,y) - L(x-1,y)))$$

The magnitude and orientation are calculated for all the pixels around the keypoint. Then a histogram is created in which the 360 degrees of orientation are divided into 36 bins. For each pixel under analysis the relative orientation $\theta(x,y)$ weighted by its magnitude $m(x,y)$ is stored in the relative "angular degree" bin of the histogram. Once the procedure has been done for every pixel surrounding the keypoint the algorithm assigns an orientation to the keypoint based on the peak of the histogram. If there are multiple peaks in the histogram they are all converted into new keypoints. At this point scale and orientation invariance is achieved for every keypoint.

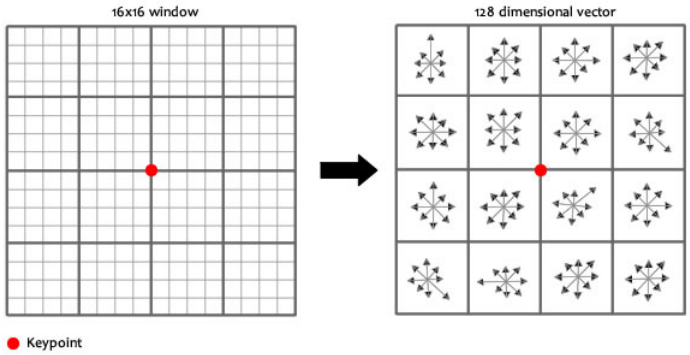

Figure C.3.: SIFT Descriptor

Subsequently, the next goal is to create a unique identifying mark which is called descriptor for each keypoint. In order to do so a 16 x 16 window ,which is broken into sixteen 4x4 windows, is created around the keypoint. Within each 4x4 window, gradient magnitudes and orientations are calculated and put into an 8 bin histogram . As explained before the "amount of orientation" added to the bin depends on the

magnitude of the gradient and, in this case, also on the distance from the keypoint. The distance weighting is achieved by applying a gaussian window to the magnitude of orientations. The above procedure is repeated for all the 16 pixels around the keypoint. Since each histogram contains 8 bins and since this procedure is repeated for 16 times (i.e. number of neighbouring pixels) the descriptor vector describing the keypoint contains 128 elements. The keypoint is uniquely identified by the 128x1 descriptor vector.

Glossary

AHE: Adaptive Histogram Equalization

CLAHE: Contrast Limited Adaptive Histogram Equalization

CWD: Concealed Weapon Detection

CWDS: Concealed Weapon Detection System

GPR: Ground Penetrating Radar

GRM: Global Ranking Matrix

MM: Millimeter

PCA : Principal Component Analysis

PCA-SIFT: Principal Component Analysis Scale Invariant Feature Transform

SAR: Syntethic Aperture Radar

SIFT: Scale Invariant Feature Transform

SURF: Speeded Up Robust Feature